Interactions between magmas and host sedimentary rocks: a review of their implications in magmatic processes (magma evolution, gas emissions and ore processes)

Giada Iacono-Marziano

UNIVERSITE D'ORLEANS

ECOLE DOCTORALE
ENERGIE, MATERIAUX, SCIENCES DE LA TERRE ET DE L'UNIVERS

Institut des Sciences de la Terre d'Orléans

Giada IACONO MARZIANO

Habilitation à Diriger des Recherches

Soutenue le 17 Septembre 2020

Interactions between magmas and host sedimentary rocks: a review of their implications in magmatic processes (magma evolution, gas emissions and ore processes)

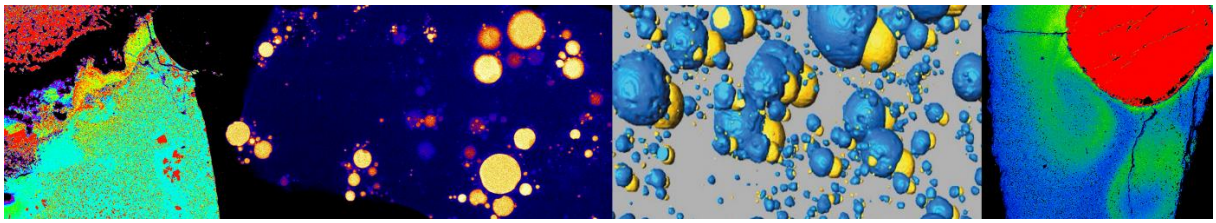

JURY :

Sarah-Jane BARNES	**Professeur (Université du Québec à Chicoutimi)**	**Rapporteur**
Marie EDMONDS	**Professeur (University of Cambridge)**	**Rapporteur**
Fidel COSTA	**Professeur (Earth Observatory of Singapore)**	**Rapporteur**
Catherine CHAUVEL	**Directrice de Recherche (IPGP)**	**Examinateur**
Caroline MARTEL	**Directrice de Recherche (ISTO)**	**President du jury**
Stanislas SIZARET	**Professeur (Université d'Orléans)**	**Examinateur**

Abstract

High temperature interactions between magmas and volatile-rich sedimentary rocks, usually referred as assimilation, may have variable consequences for magmatic processes depending on the nature of the sedimentary rocks. This manuscript reviews the assimilation mechanisms for carbonate, evaporitic and carbonaceous rocks and the magmatic processes that are directly impacted by these interactions.

A first, poorly studied consequence of magmatic assimilation, which is however potentially important, is on magma emplacement mechanism. The nature of the sedimentary rocks is likely to play a role in the formation and propagation of sill-like structures, therefore controlling magma intrusion in sedimentary basins. This in turn may favour the interaction of the magma with the sedimentary rocks that are more easily intruded.

When the magma volume is high, as in the case of large igneous provinces, magmatic intrusion into sedimentary rocks may produce extensive degassing. The assimilation and, to a larger extent, the thermal metamorphism of volatile-rich sedimentary rocks may indeed cause significant gas release with noteworthy environmental consequences (e.g. greenhouse effect and mass extinction). At the scale of a single volcano, the addition of external volatiles due to magma-sediment interactions can enhance degassing and/or modify the eruptive behaviour.

The effect of assimilation on the redox conditions of the magma and therefore on ore forming processes is also extremely important, although much less investigated. Significant modifications of the magma redox state can trigger the segregation/crystallization of magmatic phases that are generally uncommon or represent accessory phases (like native iron, sulfide melt or oxide minerals), possibly forming world class ores. Furthermore, magma-sediment interactions may produce magmatic-hydrothermal fluids enriched in metals and metalloids, but this field is almost unexplored.

Least but not last, the assimilation of volatile-rich sedimentary rocks can modify the composition of the magma, significantly in some extreme cases and not only in terms of volatile content. Assimilation of carbonate rocks produces silica undersaturated, alkali-rich magmas, while the effect of carbonaceous and evaporitic rocks is almost uninvestigated.

The manuscript deals with four rock types (carbonate, sulfate, chloride-bearing and carbonaceous rocks); case studies are presented for each rock type to illustrate how magma-sediment interactions affect the different magmatic processes.

Table of contents

1. Introduction

High temperature interactions between magmas and host rocks are usually referred as assimilation. With the exception of magmatic ore geology, assimilation processes are commonly considered as marginal in magma evolution, possibly due to the difficulty of modelling open-system processes in evolving magma bodies. Rigorous thermodynamic models, accounting for mass and enthalpy balance, allow to simulate the impact of assimilation on trace element and isotopic composition of the magma (Bohrson & Spera 2001, 2003; Spera & Bohrson 2001, 2002), and more recently also on its major element composition (Bohrson et al. 2014). However, the diversity of crustal contaminants that a magma may assimilate from the lower to the upper crust can significantly increase the complexity of the modelling (e.g. Fowler et al. 2004).

Recent studies however show that the assimilation of volatile-rich sedimentary rocks in particular may have important consequences for magma degassing, ore formation or even magma differentiation. Sedimentary rocks can indeed be extremely rich in volatiles (i.e. CO_2 in carbonates, SO_2 in sulfates, C-H species in carbonaceous rocks, and Cl in salts), and therefore play a crucial role in magmatic degassing. CO_2 released by interaction with crustal carbonates is for instance likely to represent a significant fraction of the present-day global carbon emissions at volcanic arcs (Mason et al. 2017; Aiuppa et al. 2017). Thermal devolatilization occurring during contact metamorphism of sedimentary host rocks engenders massive release of fluids (e.g. Aarnes et al. 2010, 2011a,b) at relatively low temperatures (i.e.<800°C), but magmatic assimilation can also contribute additional volatiles (e.g. Iacono-Marziano et al. 2007, 2009, 2012a,b; Troll et al. 2012; Carter & Dasgupta 2015, 2016, 2018). When high volumes of magma are involved, this "sedimentary-doped" magmatic degassing can be at the origin of environmental crises (e.g. Svensen et al. 2004, 2007, 2009, 2015; Reetallack & Jahren 2008; Ganino and Arndt 2009; Aarnes et al. 2010; Iacono-Marziano et al. 2012b; Ogden & Sleep 2012; Heimdal et al. 2018, 2019). The severity of the mass extinction associated to the emplacement of the major large igneous provinces (LIPs) indeed does not seem to be related to the volume of emplaced magma, but rather to the occurrence of volatile-rich sedimentary rocks in the basin beneath the flood basalts (Fig.1.1 from Ganino and Arndt 2008). The mechanisms of interaction and volatile release remain however largely hypothetical.

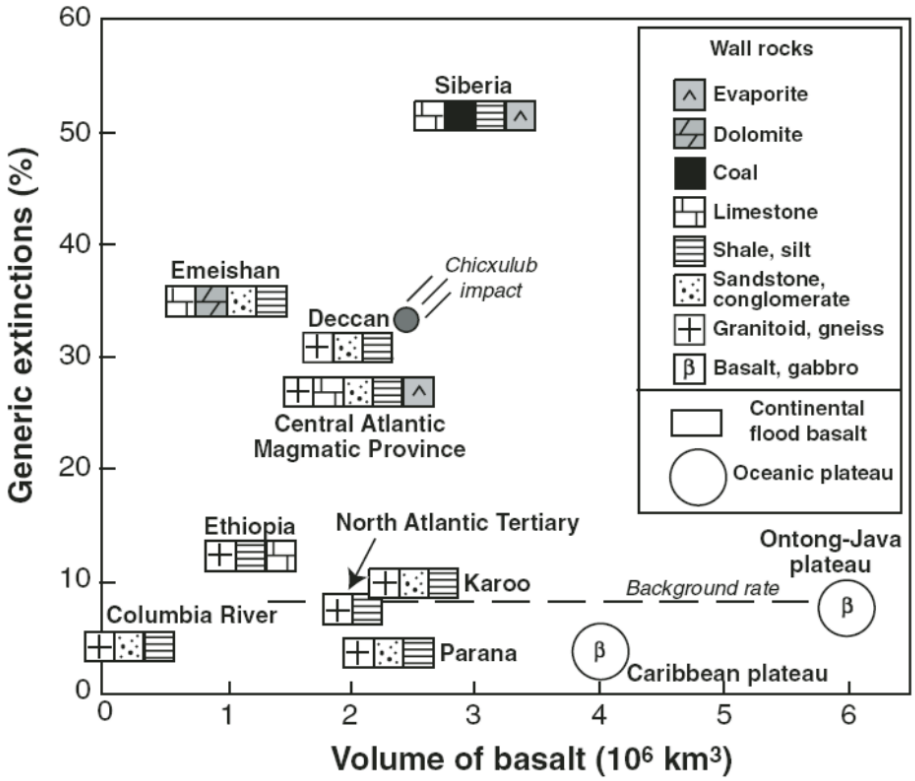

Fig.1.1 Percentage of generic extinctions versus volume of erupted basalt for major LIPs. There is no clear correlation between these two parameters: the volume of magma emplaced by the Emeishan Traps is for instance about half the one of the Karoo and Parana provinces, but its environmental effect is markedly higher. Moreover, oceanic plateaus produced largely higher volumes of magmas than any continental LIP, without marked environmental impact. The LIPs that are associated to the highest rates of extinction are those that intrude sedimentary rocks releasing abundant greenhouse and/or toxic gases. From Ganino and Arndt 2008.

Furthermore, volatiles produced by assimilation of sedimentary rocks may strongly affect the redox conditions of the magma, and therefore the ore forming processes associated with magmatism and magmatic-related hydrothermalism (e.g. Lehmann et al. 2007; Ganino et al. 2008; Iacono-Marziano et al. 2012, 2017, submitted; Li et al. 2015). These redox effects are often neglected, while most of the attention is focused on the chemical input of assimilation. Strong geochemical evidence for instance indicates that crustal sulfur is often required to form magmatic Ni-Cu sulfide deposits (e.g. Ripley and Li 2003, 2013; Barnes & Lightfoot 2005; Keays and Lightfoot 2010; Lesher 2017). The assimilation of sedimentary host rocks is proposed to be at the origin of the sulfide ores of several world-class deposits, e.g. the Duluth Complex in the USA (Mainwaring & Naldrett 1977; Ripley 1981; Thériault & Barnes 1998; Thériault et al. 2000; Queffurus & Barnes 2014; Samalens et al. 2017), the Noril'sk-Talnakh intrusions in Russia (Naldrett 2004; Arndt et al. 2005; Jugo and Lesher 2005; Li et al. 2009b;

Ripley et al. 2010; Iacono-Marziano 2014, 2017), and the Platreef of the Bushveld complex in South Africa (Maier et al. 2008; Pronost et al. 2008; Yudovskaya et al. 2018).

In addition to ore formation, the assimilation of volatile-rich sedimentary rocks can also affect the stability of major magmatic minerals and therefore magma composition. The effects are generally limited when assimilation rates are low, but some extreme cases of carbonate assimilation have been observed to produce highly silica-undersaturated, alkali-rich magma compositions (Iacono-Marziano et al. 2007, 2008; Freda et al. 2008). As chemical sediments are commonly depleted in incompatible trace elements, the trace element composition of the magma is only slightly modified by their assimilation. A common feature of the different types of assimilation is however that resulting magmas have heterogeneous compositions (often clearer in terms of trace elements and isotopic ratios), because assimilation is a local process and may occur to different extents within a same magma batch (e.g. Barnes et al. 2005; Iacono-Marziano et al. 2008, 2017).

Assimilation is proposed to take place by means of different mechanisms, the two more invoked on the basis of field evidence are (i) thermal breakdown of carbonates (e.g. Ganino et al. 2008), organic matter-rich rocks (e.g. Ganino & Arndt 2009) or sulfide minerals (e.g. Ripley 1981) and incorporation of the resulting fluids into the magma, and (ii) partial melting of xenoliths of (meta)sedimentary rocks (e.g. Thériault and Barnes 1998; Lesher & Burnham 2001; Ganino et al. 2013b; Schofield et al. 2014; Lesher 2017; Samalens et al. 2017). The Energy-Constrained, Recharge, Assimilation and Fractional Crystallization Model (Bohrson & Spera 2001, 2003; Spera & Bohrson 2001, 2002) and the Magma Chamber Simulator (Bohrson et al. 2014) only consider wall-rock partial melting. However, experimental studies show that different assimilation mechanisms are likely. This manuscript will review the assimilation mechanisms possible for each type of sedimentary rocks, the stoichiometry of the assimilation reactions, together with the possible consequences for magma differentiation, volatile emissions, and ore formation.

1. Carbonate rocks

1.1 Mechanisms of assimilation

The hypothesis that alkali-rich, desilicated magmas could be generated by the assimilation of sedimentary carbonates was first proposed by Daly (1910), on the basis of the frequent association between alkaline magmas and carbonate rocks (marble, limestone). The author suggests that the desilication of the magma, accompanied by pyroxene crystallization, is the main consequences of limestone dissolution in the magma. In the first half of the 20th century, other authors describe magma-limestone exchanges caused by basaltic intrusions in carbonate rocks, leading to silica depletion of the residual liquid (e.g. Rittmann 1933; Shand 1945). A crucial contribution to the understanding of the mechanisms of magma-carbonate interaction however comes from experimental studies employing natural magma compositions, mainly mafic (e.g. Iacono-Marziano et al. 2007, 2008; Freda et al. 2008; Conte et al. 2009; Mollo et al. 2010; Deegan et al. 2010; Jolis et al. 2013; Pichavant et al. 2014; Carter & Dasgupta 2015, 2016, 2018).

On the basis of these experiments calcite assimilation can be expressed by three extremely simplified reactions:

$$CaCO_3 \rightarrow CaO^{melt} + CO_2{}^{fluid} \quad (2.1)$$

in magmas that are MgO-poor or at near-liquidus conditions (high temperature and/or high H_2O content),

$$CaCO_3 + 2\ SiO_2{}^{melt} + MgO^{melt} \rightarrow CaMgSi_2O_6{}^{cpx} + CO_2{}^{fluid} \quad (2.2)$$

in MgO-rich magmas not at near liquidus conditions, or

$$2\ CaCO_3 + 3\ SiO_2{}^{melt} + Mg_2SiO_4{}^{olivine} \rightarrow 2\ CaMgSi_2O_6{}^{cpx} + 2\ CO_2{}^{fluid} \quad (2.3)$$

in olivine-bearing magmas.

Mollo et al. (2010) proposes a modified version of eq.2.2 accounting for all magmatic components involved in the crystallization of a diopside-hedenbergite-Ca-Tschermak clinopyroxene solid solution:

$$CaCO_3 + SiO_2{}^{melt} + MgO^{melt} + FeO^{melt} + Al_2O_3{}^{melt} \rightarrow (Di\text{-}Hd\text{-}CaTs)_{ss}{}^{cpx} + CO_2{}^{fluid} \quad (2.4)$$

Moreover, Carter & Dasgupta (2016) show that clinopyroxene can be replaced by wollastonite in intermediate to evolved compositions assimilating significant amounts of calcite (>25 wt%).

Several other reactions are suggested by Carter & Dasgupta (2016) to account for the entire range of interactions observed in their experiments at variable temperature, pressure and silicate melt

composition. However, equations 2.1 and 2.2 (or 2.4) alone summarise the most important effects of limestone assimilation that are: (i) CaO enrichment in the silicate melt (eq.2.1) or clinopyroxene crystallization (eq.2.2 or 2.4), (ii) desilification (eq. 2.2), and (iii) CO_2 production (eqs. 2.1 and 2.2).

The MgO content of the magma controls the mechanism and the effects of limestone assimilation (see next section), as also suggested by field observation (Barnes et al. 2005). Primitive magmas can experience higher degrees of limestone assimilation than evolved magmas, due to their higher heat capacity, but also to their higher MgO content that avoids extreme CaO enrichments in the silicate melt by means of clinopyroxene crystallization (eq.2.2 - 2.4). For this reason the first experiments simulating calcite assimilation by simple MgO-free synthetic compositions (hydrous albitic systems) show the existence of a thermal barrier that precludes the transition from ''granitic'' to ''feldspathoidal'' (i.e. silica-oversaturated to silica-undersaturated) melts by limestone assimilation (Watkinson and Wyllie 1969). In these systems massive plagioclase crystallization is triggered by calcite addition and the complete solidification of the system occurs for ~25 wt% of calcite added. For more than 30 years, these experimental results relegated carbonate assimilation to a very local process, merely restricted to the vicinity of the side-wall and unable to significantly affect the whole magma body (Watkinson and Wyllie 1969; Wyllie 1974). The more recent experiments performed using complex MgO-bearing compositions indicate that other assimilation mechanisms can operate, making limestone assimilation a viable process in both hydrous and anhydrous mafic magmas. These experiments also investigated dolostone assimilation, showing that more dolomite is assimilated than calcite (e.g. Iacono-Marziano et al. 2007; Mollo et al. 2010; Jolis et al. 2013; Carter & Dasgupta 2018). Dolomite assimilation can be expressed as:

$$CaMg(CO_3)_2 + 2\ SiO_2^{melt} \rightarrow CaMgSi_2O_6^{cpx} + CO_2^{fluid} \quad (2.5)$$

However, the magnesite end-member also produces MgO-rich olivine via:

$$2MgCO_3 + SiO_2^{melt} \rightarrow Mg_2SiO_4^{ol} + 2CO_2^{fluid} \quad (2.6)$$

If calcite is assimilated together with and at a higher amount of dolomite, no Mg-rich olivine is observed in the experimental products (Iacono-Marziano et al. 2007; Carter & Dasgupta 2018).

The MgO content of the bulk system (magma + host rocks) therefore seems to control (i) the amount of carbonate rocks that can be assimilated without extreme CaO enrichment of the residual melt, and (ii) the produced phase assemblage. Desilication occurs for all types of carbonate rocks, together with CO_2 release (eqs. 2.1-2.6).

Interaction mechanisms between anhydrous and hydrous mafic magmas and calcite or dolomite were explored by means of unpublished experiments juxtaposing anhydrous or hydrous trachybasaltic

glasses with calcite or dolomite cylinders at a pressure of ~200 MPa and temperatures between 920 and 1180°C for a duration of 6 hours (Fig.2.1). In some of these samples a CO_2-bearing bubble forms at the magma-carbonate interface (Fig.2.1 B,C), allowing a clear distinction between the originally magmatic and originally sedimentary parts, i.e. the endoskarn and the exoskarn.

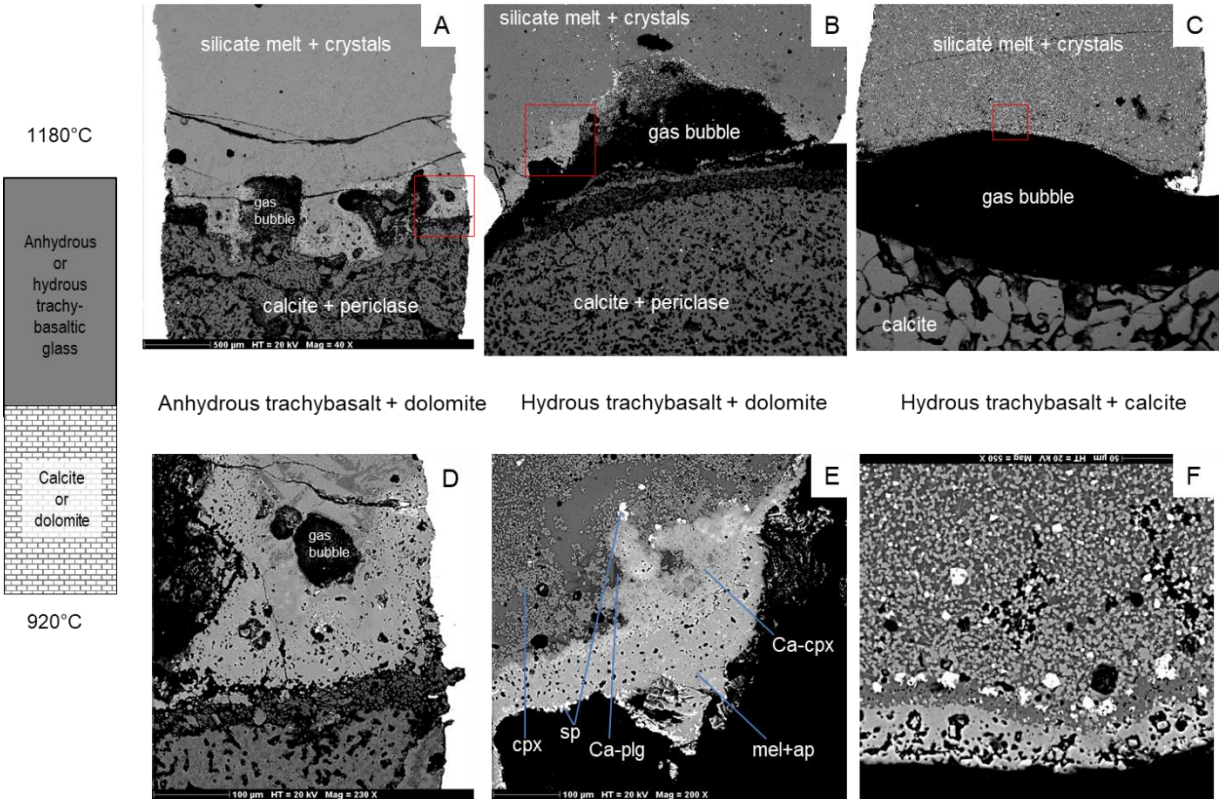

Fig.2.1 Magma-carbonate interaction experiments performed at ~200 MPa for a duration of 6 hours. A thermal gradient was imposed in the vessel to have a temperature of 1180°C at the top of the sample and 920°C at the bottom. (A), (B), (C) BSE images of the central part of the capsule where the interaction is maximum. (D), (E), (F) Zoomed-in BSE images of the red squares in (A), (B), and (C).

The endoskarn is significantly more developed in dolomite-bearing samples (Fig.2.1 D, E) than in calcite-bearing ones (Fig.2.1 F), suggesting that chemical diffusion from dolomite is more effective than from calcite. In dolomite-bearing samples the endoskarn consists in an outer rim of melilite, spinel and apatite, and an inner rim of calcium-rich plagioclase and calcium-rich clinopyroxene (Fig.2.2A), indicating CaO and MgO diffusion from the dolomite to the magma (Fig.2.2B). Differently, the exoskarn consists in magnesium-rich olivine and calcite, and suggests SiO_2 diffusion from the magma to the dolomite (Fig.2.2B). These exchanges occur at the magmatic stage, although they are probably fluid-assisted. Elemental diffusion being temperature-dependent, the interactions are facilitated at high temperatures.

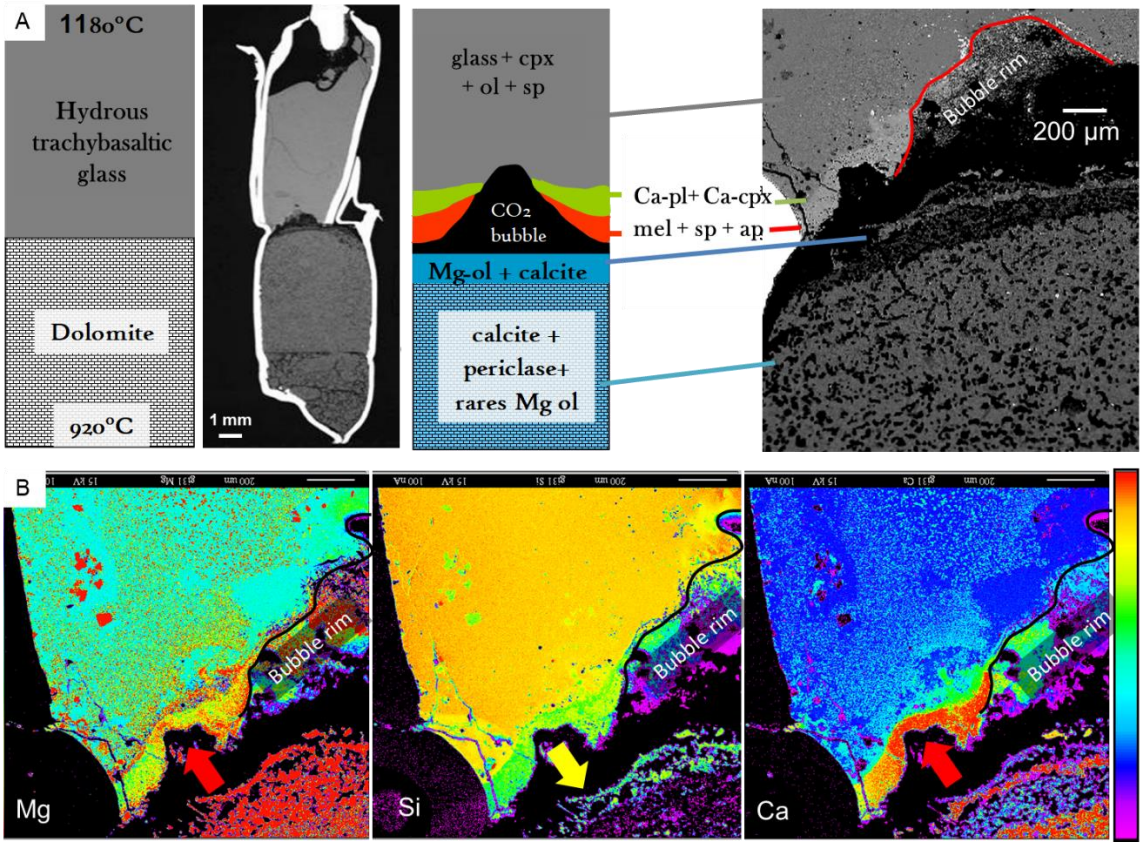

Fig.2.2 Interaction experiment between dolomite and hydrous trachybasaltic glass, performed at ~200 MPa and 920-1180°C, for a duration of 6 hours. (A) Schemes showing the sample geometry before and after the experiment, and BSE images of the whole sample and of the magma-dolomite interface. Ca-pl: calcium plagioclase, Ca-cpx: calcium-rich clinopyroxene, mel: melilite, sp: spinel, ap: apatite, ol: olivine, Mg-ol: forsteritic olivine. (B) Mg, Si, and Ca elemental maps of the magma-carbonate interface obtained by electron microprobe (colour scale on the right). The arrows stress SiO_2 diffusion from the magma to the dolomite, and CaO-MgO diffusion from the dolomite to the magma. The bubble rim is marked to identify the parts of the sample that are inside the bubble, below the polished surface. Unpublished results.

Carter & Dasgupta performed similar experiments at higher pressures (0.5-1 GPa) reacting hydrous/anhydrous basaltic/andesitic/dacitic melts with calcite/dolomite (Carter & Dasgupta 2015, 2016, 2018). Experimental durations were significantly longer (24-72 h) and the degree of interaction higher (assimilation up to 32 wt%) than those experienced by the experiments in Figures 2.1 and 2.2. The interaction fronts were therefore larger and more homogeneous and, in calcite-bearing experiments (Carter & Dasgupta 2015, 2016), mainly consisted of clinopyroxene with minor amounts of spinel, plagioclase, scapolite (decreasing with increasing silica content from basalt to dacite), and wollastonite (increasing with increasing silica content from basalt to dacite). In contrast, when the melts interacted with variable proportions of dolomite and calcite (Carter & Dasgupta 2018), the

interaction fronts consisted of clinopyroxene and spinel accompanied by Mg-rich olivine (decreasing with increasing silica content from basalt to dacite), and minor plagioclase. Apatite was only observed in one sample containing dacite melt and dolomite+calcite. These experiments show that: (i) the maximum amounts of calcite assimilation possible in basaltic and andesitic magmas are relatively similar (48% and 65%, respectively), whereas those in dacitic magmas are significantly lower (18%), and (ii) more dolomite can be assimilated than calcite (Carter & Dasgupta 2018). Assimilation therefore can still occur in evolved magmas, but is a less efficient and more localized process (Del Moro et al. 2001; Fulignati et al. 2004).

In the experiments, carbonates breakdown, CaO and MgO are incorporated in silicates (crystals + melt), while CO_2 is partitioned between the fluid phase, the silicate glass and the possible CO_2-bearing minerals (mainly scapolite), with a strong preference for the fluid. No newly formed carbonate phases, such as an immiscible carbonate melt, are observed, in both carbonate-undersaturated (i.e. all loaded carbonate is digested by the magma) and carbonate-saturated samples (i.e. containing residual carbonate). Carbonate melting is however an alternative mechanism of assimilation proposed in the literature. Experimental studies show that carbonates partially melt at relatively low temperatures in the presence of water: in the MgO-CaO-H_2O-CO_2 system the beginning of melting lies between 625°C and 660°C in the pressure range 1-400 MPa (Wyllie 1965). The high water contents required to ensure low temperature melting (> 10 wt% H_2O) are common in infiltrative magmatic-hydrothermal (pneumatolytic) skarn systems (Lentz 1999), but probably not in other magmas, and particularly not in mafic ones. In the absence of water, $CaCO_3$-$MgCO_3$ mixtures start melting at significantly higher temperatures, e.g. 1075°C at 1 GPa (Byrnes and Wyllie 1981), higher than those necessary for decarbonation to occur (e.g. Wyllie 1965; Wenzel et al. 2001; Carter & Dasgupta 2018).
Natural examples of carbonate melting are rare, possibly owing to occurrence of decarbonation reactions at lower temperature, or to the difficulty of establishing whether melting took place, i.e. crystallized carbonate melts can be indistinguishable from carbonate rocks (Ganino et al. 2013b). Ganino et al. 2013b observe patches of carbonate melts in the contact aureole of the **Panzhihua intrusion** (SW China), and propose that partial melting of dolostones results from a combination of heat from the main intrusion, emplacement of multiple mafic dykes into the contact aureole, and circulation of water flushing carbon dioxide from the rock and lowering melting temperature. Owing to their low density and viscosity, these carbonate melts would percolate upwards in the contact aureole during its deformation (Ganino et al. 2013b). The produced volume of these melts and whether they are assimilated by the main intrusion or the peripheral dikes are however difficult to estimate.

Carbonate partial melting, extraction of pure calcite melts from the host rock, and mixing with the surrounding mafic magma are proposed to occur at the **Ioko-Dovyren intrusion** in Russia (Wenzel et

al. 2001, 2002). These processes would account for CaO depletion of the periclase-rich xenoliths and Si depletion of the olivine cumulates. No direct evidence of the calcite melts is however observed.

1.2 **Effect on magma composition**

The experiments show that carbonate-melt reactivity is relatively rapid even at low melt fractions, i.e. few hours for calcite consumption (Deegan et al. 2010; Jolis et al. 2013), and less than 48 h for mineral equilibration in andesitic melts (Carter & Dasgupta 2016). The variable experimental conditions (mainly temperature and pressure), magma compositions (ultramafic to dacitic) and carbonate compositions (calcite and/or dolomite) illustrate that the effects of assimilation on magma composition can differ, and yet share some common points.

The assimilation of limestone by mafic magmas favours clinopyroxene (cpx hereafter) crystallization at the expenses of olivine (Iacono-Marziano et al. 2007, 2008; Freda et al. 2008; Mollo et al. 2010; Pichavant et al. 2014), or orthopyroxene (Carter & Dasgupta 2015, 2016), due to CaO-enrichment in the silicate melt. Accordingly, petrological studies that have documented the effects of carbonate assimilation by magmatic dikes intruding limestone or marble series (e.g. Tilley 1952; Joesten 1977; Baker and Black 1980; Barnes et al. 2005; Coulson et al. 2007) show that magma contamination is marked by the overgrowth of Ca-rich phases (mainly calcic clinopyroxene, but also Ca-amphibole, wollastonite, scapolite, etc.) on primary minerals. In particular, olivine destabilization in favour of cpx has been described with progressive carbonate assimilation (Barnes et al. 2005 and references therein). The composition of cpx from experiments is sensitive to the amount of limestone incorporated: the Ca-Tschermak/diopside and hedenbergite/diopside ratios of the diopside-hedenbergite-Ca-Tschermak cpx solid solution increase with increasing carbonate assimilation (Mollo et al. 2010).

The general broadening of the cpx stability field is responsible for the increase in both liquidus temperature and degree of crystallization in samples affected by carbonate assimilation (e.g. Iacono-Marziano et al. 2007, 2008; Carter & Dasgupta 2015, 2016). This effect is not caused by the heat transfer from the magma to the colder carbonates, because in most of the experimental setups magma and carbonates are kept at the same temperature.

Other phases such as plagioclase and amphibole can also be destabilized by the assimilation of pure limestone at high temperature (≥1050°C at 200MPa, Iacono-Marziano et al. 2008, or ≥1175°C at 1.0 GPa, Carter & Dasgupta 2015). Extremely Ca-rich plagioclase (up to An_{100}) is observed in many of the eruptive products of Merapi volcano and ascribed to carbonate assimilation (Chadwick et al. 2007; Borisova et al. 2013; Costa et al. 2013). Scapolite has been observed to crystallize at magma-limestone interface (Carter & Dasgupta 2015), whereas melilite, spinel, apatite and magnesian olivine occur at

magma-dolomite interface (interaction experiments in Fig.2.2; Carter & Dasgupta 2018). These phases are observed in volcanic ejecta proposed to have formed by high temperature reaction between magma and dolomitic rocks, e.g. at Mt. Vesuvius and Alban Hills (Federico et al. 1994; Fulignati et al. 2000, 2004; Jolis et al. 2015), but also in the contact aureoles of several plutons, e.g. the **Boulder batholith** (Rice 1977) and the **Christmas Mountains** (Joesten 1977) in the USA, the **Kiglapait Intrusion** in Canada (Owens 2000), the **Ioko-Dovyren intrusion** in Russia (Wenzel et al. 2001, 2002 and references therein), the **Hortavaer igneous complex** in Norway (Barnes et al. 2005), and the **Jinchuan intrusion** in China (Lehmann et al. 2007). In particular, MgO-rich olivine is observed in the "zebra-rocks" that constitute the magma-carbonate contact of doleritic dikes intruding contact aureoles of intrusions (Fig.2.3A, B, C), described in the **Panzhihua intrusion** (China; Ganino et al. 2008, 2013b) and at the **Isle of Skye** (Scotland; Holness 1997, 2000). They consist of alternating bands of olivine (Fo 94-99), rimmed by magnetite and calcite, at the margin of doleritic dikes (Fig.2.3D, E, F), and are attributed to a process of self-organization during grain growth as element from the dolerite migrate out into the marble (Holness 1997, 2000). These rocks are probably equivalent to the Mg-rich olivine+calcite layer observed at the contact with the magma in the interaction experiments described in the previous section (Fig.2.2). Moreover, the experimental studies show that Mg and Ca-rich olivine (Fo>92, CaO>0.8 wt%) can also crystallize as a magmatic phase, if dolostone assimilation occurs in the absence of limestone assimilation (eq. 2.6 in section 2.1; Iacono-Marziano et al. 2007; Mollo et al. 2010; Jolis et al. 2013; Carter & Dasgupta 2018). A significant increase in the forsterite content (from 79 to 91 mol%), accompanied by a decrease in the Ni content, is indeed observed in the olivine of a picritic dike intruding dolostones in the Panzhihua intrusion (Tang et al. 2017).

The chemical composition of the residual liquid is also greatly affected by limestone incorporation. When the MgO content of the magma is too low or the temperature and the H_2O content are high, cpx crystallization is limited and the CaO content of the melt increases (eq.2.1 in section 2.1; Iacono-Marziano et al. 2008; Deegan et al. 2010; Jolis et al. 2013; Carter & Dasgupta 2015, 2016). Carter & Dasgupta (2015) propose that these experimental ultracalcic melts are the equivalent of nepheline-normative ultracalcic melts identified in arc settings (e.g. Schiano et al. 2000; Kogiso and Hirschmann 2001).

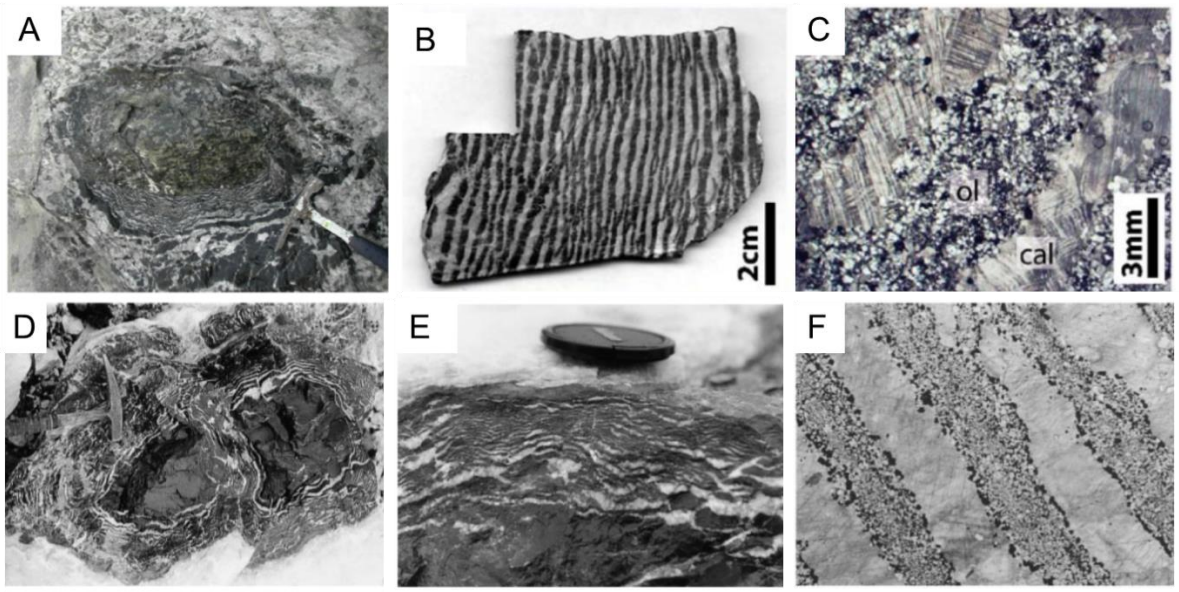

Fig.2.3 « Zebra rocks » of the Panzhihua intrusions, SW China (A-C; Ganino et al. 2008, 2013b) and the Isle of Skye, Scotland (D-F; from Holness 2000). (A) and (D) Zebra-rocks developed around a small dolerite boudin. (B) and (E) Hand samples of zebra rocks. (C) Plane-polarized microphotograph showing alternating bands of partially altered olivine with oxides and calcite. (F) Alternating bands of calcite and olivine, rimmed by magnetite; field of view 6 mm across.

In most of the cases (lower temperatures and H_2O contents and higher MgO contents), cpx crystallization generally accommodates CaO excess derived from limestone (eqs.2.2-2.5 in section 2.1): the higher the MgO content of the melt, the higher the amount of limestone that can be assimilated without increasing the CaO content of the melt (Iacono-Marziano et al. 2008). Dolomite assimilation produces residual melts that are richer in MgO and less enriched in CaO than those of magmas experiencing calcite assimilation (Iacono-Marziano et al. 2007; Carter & Dasgupta 2018).

The silica content of the melt is highly modified by limestone assimilation, due to (i) silica dilution by CaO addition (eq.2.1), and (ii) silica removal by cpx crystallization (eqs.2.2 - 2.4). As a consequence of massive cpx crystallization, the residual melt can be strongly silica-depleted and become nepheline and leucite-normative. Figure 2.4 shows that, for a given amount of calcite assimilation, MgO-richer magmas crystallize higher amount of cpx and their residual melt is more silica-undersaturated than for MgO-poorer magmas (Iacono-Marziano et al. 2008).

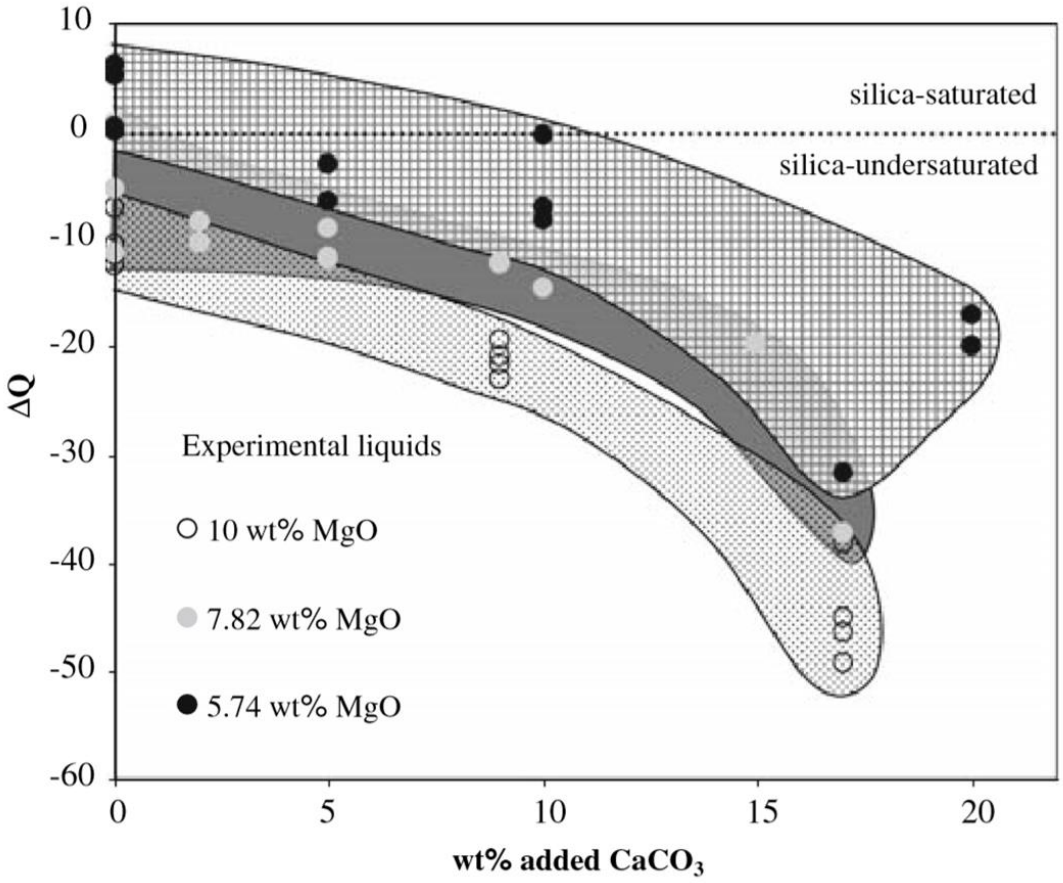

Fig. 2.4 Degree of silica saturation of experimental residual melts as a function of the amount of calcite assimilated. ΔQ = normative quartz – normative olivine – normative leucite – normative kalsilite– normative nepheline, calculated after Peccerillo (2005). The experiments were performed at 200 MPa and temperatures between and 1050 and 1150°C, with the three initial MgO contents indicated in the legend. From Iacono-Marziano et al. (2008).

The alkali content of the residual melt passively increases during carbonate assimilation: alkalis are indeed concentrated in the residual liquid by massive cpx crystallization, maintaining the initial K_2O/Na_2O ratio (Iacono-Marziano et al. 2008; Conte et al. 2009; Mollo et al. 2010). The alkali enrichment of the residual melt is limited by leucite crystallization at low temperatures or in H_2O-poor melts (Iacono-Marziano et al. 2007; Freda et al. 2007; Conte et al. 2009).

Figure 2.5 B shows the variations in SiO_2 and total alkali contents of experimental residual melts for different degrees of carbonate (calcite ± dolomite) assimilation observed by Iacono-Marziano et al. (2008). For this study, different initial compositions were used, basaltic and trachybasaltic, as well as variable temperatures (1050-1150°C) and pressures (1 atm-500 MPa). The coloured fields in figure 2.5B illustrate variations observed at 200 MPa, a typical depth of magma storage in the crust. The differentiation trends observed in the presence of carbonate assimilation lack the silica enrichment typical of carbonate-free compositions, whereas the alkali enrichment is more important.

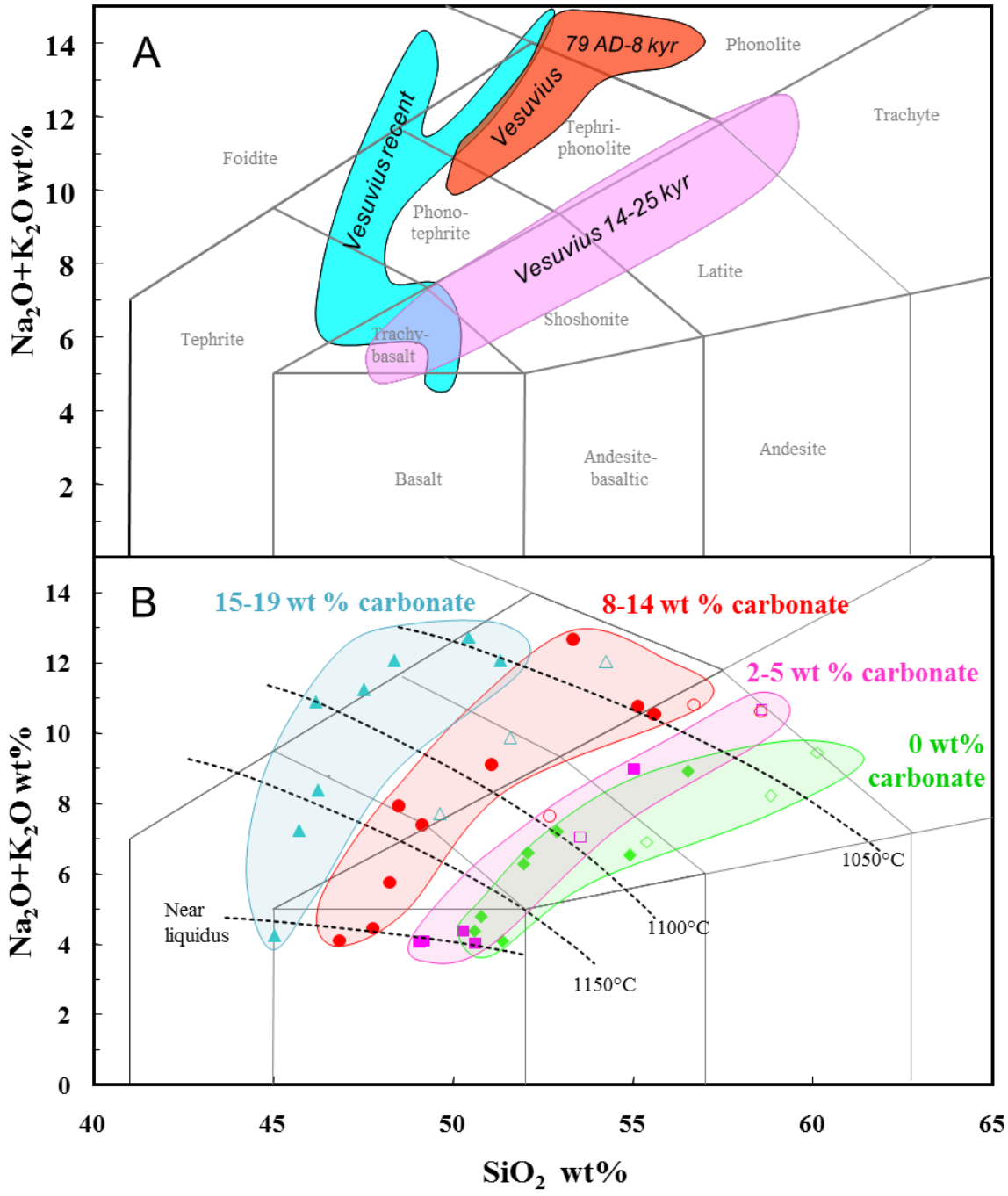

Fig.2.5 (A) TAS diagrams showing whole rock compositions of Mt. Vesuvius eruptive products of the last 25 ky. Three eruptive periods indicated by Ayuso et al. (1998) are distinguished: 25-14 ky, 8 ky-79 AD (Pompeii eruption), younger than Pompeii eruption. (B) TAS diagrams showing experimental residual melts obtained for different amounts of carbonate assimilation by basaltic and trachybasaltic compositions. Experiment were performed at different temperatures (indicated on the diagram), and different pressures: filled symbols represent experiments at ~200 MPa, while open symbols represent experiments at 1 atm or 500 MPa. Modified from Iacono-Marziano et al. 2008.

The progressive depletion in silica and enrichment in alkali are also observed in natural environments. Variations are mostly described at the meter scale, but they can affect plutonic bodies up to several kilometres wide, and degrees of assimilation of carbonate rocks in the range of 20 wt% or higher have been proposed. Barnes et al. (2005) studied the **Hortavær igneous complex**, a 466 Ma old magmatic intrusion in carbonate and silicate rocks in Norwegian Caledonides, where massive carbonate assimilation is revealed by the crystallization of Ca-rich cpx and the desilication of the magma. These features are described over a several kilometre wide zone, which shows extreme heterogeneities in terms of bulk rock composition, but similar mineral compositions and assemblages. In this magmatic complex dioritic rocks coexist with syenitic and monzonitic rocks in the form of sheets. Mutual intrusive relationships suggest that magma emplacement occurred as repeated injections of hundreds of sub horizontal sheet-like bodies experiencing different degrees of assimilation (Barnes et al. 2005).

Mt. Vesuvius in Italy is probably the site where the effect of carbonate assimilation on magma composition have been more extensively documented. Whole rock compositions of Vesuvius eruptive products are characterized by important temporal variations in the degree of silica-saturation (Fig.2.2A): three periods/eruptive cycles have been recognized in the last 25 ky, the younger the lavas, the more silica-undersaturated (Joron et al. 1987; Ayuso et al. 1998). The decrease in the silica content of the most primitive rocks (MgO> 6wt%) from Period I to Period III is accompanied by an increase in the CaO content, the other elements being generally unchanged (Iacono-Marziano et al. 2008). Both this compositional evolutions and the mineralogical characteristics of Vesuvius eruptive products suggest that carbonate assimilation increased during the last 25 ky of activity, probably as a consequence of increasing wall-rock temperatures (Table 2.1; modified from Iacono-Marziano et al. 2008). The compositions of MgO-rich (> 6 wt% MgO) melt inclusion entrapped in magmatic minerals of Period II and III and those of melt inclusions in high temperature skarns (MgO = 3–4.5 wt%; Fulignati et al. 2004) also clearly show desilification trend with decreasing MgO content, accompanied by alkali and Al_2O_3 increase (Fig.2.6). These trends have been modelled using experimental results to estimate that 10-11 wt% is the average amount of carbonate assimilation (mainly composed of dolomite) involved in the formation of the youngest Vesuvius eruptive products (1631-1944; Fig.2.6).

Table 2.1 Petrological and geochemical variations with time of Mt. Vesuvius eruptive products

	Whole rock major element composition	**MI major element composition ***	**Mineral paragenesis**	**Whole rock trace elements**
Period I 14 - 25 ky	Slightly SiO_2-undersaturated		Cpx, ol, pl	Sr compatible Strong Eu anomaly
Period II 79 AD - 8 ky	Mildly SiO_2-undersaturated Higher alkali content than Period I	Desilification from 52 to 49 wt% SiO_2	Cpx, ol, pl	Sr mildly compatible Weak Eu anomaly
Period III 1944 -79 AD	Highly SiO_2-undersaturated Higher alkali content than Period II Higher CaO content than Period I and II	Desilification from 52 to 46 wt% SiO_2	Ca-cpx, rare ol, rare pl	Sr incompatible No Eu anomaly
References	*Joron et al. 1987;* *Ayuso et al. 1998*	*Cioni et al. 1998; Cioni 2000; Fulignati et al. 2004; Marianelli et al. 1995, 2005*	*Joron et al. 1987; Piochi et al. 2006; Di Renzo et al 2007*	*Ayuso et al. 1998; Peccerillo 2005;* *Di Renzo et al. 2007*

** Melt inclusions with MgO content > 6 wt%*

More generally, carbonate assimilation is likely to occur in the plumbing system of most of Italian quaternary volcanoes, given (i) the widespread presence of limestone and dolostone in the sedimentary basements (5–20 km thick, e.g. Barberi et al. 1994; Peccerillo 1998, 2005; Mazzotti et al. 2000; Neri et al. 2005), (ii) the abundance of high temperature skarns in the eruptive products (e.g. Joron et al. 1987; Federico et al. 1994; Nappi et al. 1995; Michaud 1995; Peccerillo 1998; 2005; Gilg et al. 2001; Fulignati et al. 2000; Del Moro et al. 2001; Di Battistini et al. 2001; Jolis et al. 2015), and (iii) the massive CO_2 diffuse degassing of debated origin (Chiodini et al. 2001, 2004, see next section). Carbonate assimilation is likely to substantially contribute to the extreme variability of the chemical compositions of Italian eruptive products in terms of major elements, trace elements and isotopic composition (e.g. Peccerillo 2005). Carbonate assimilation probably controls the degree of silica undersaturation of these rocks, which compositions span from calco-alkaline to hyperalkaline, foiditic (Fig. 2.7A). Variations in silica saturation are generally decoupled from variations in K_2O/Na_2O (Fig.2.7B), which are ascribed to an increasing degree of mantle metasomatism from the South to the North, i.e. mantle contamination by upper crustal material during subduction processes (e.g. Dallai et al. 2004; Civetta et al 2004; Peccerillo 2005).

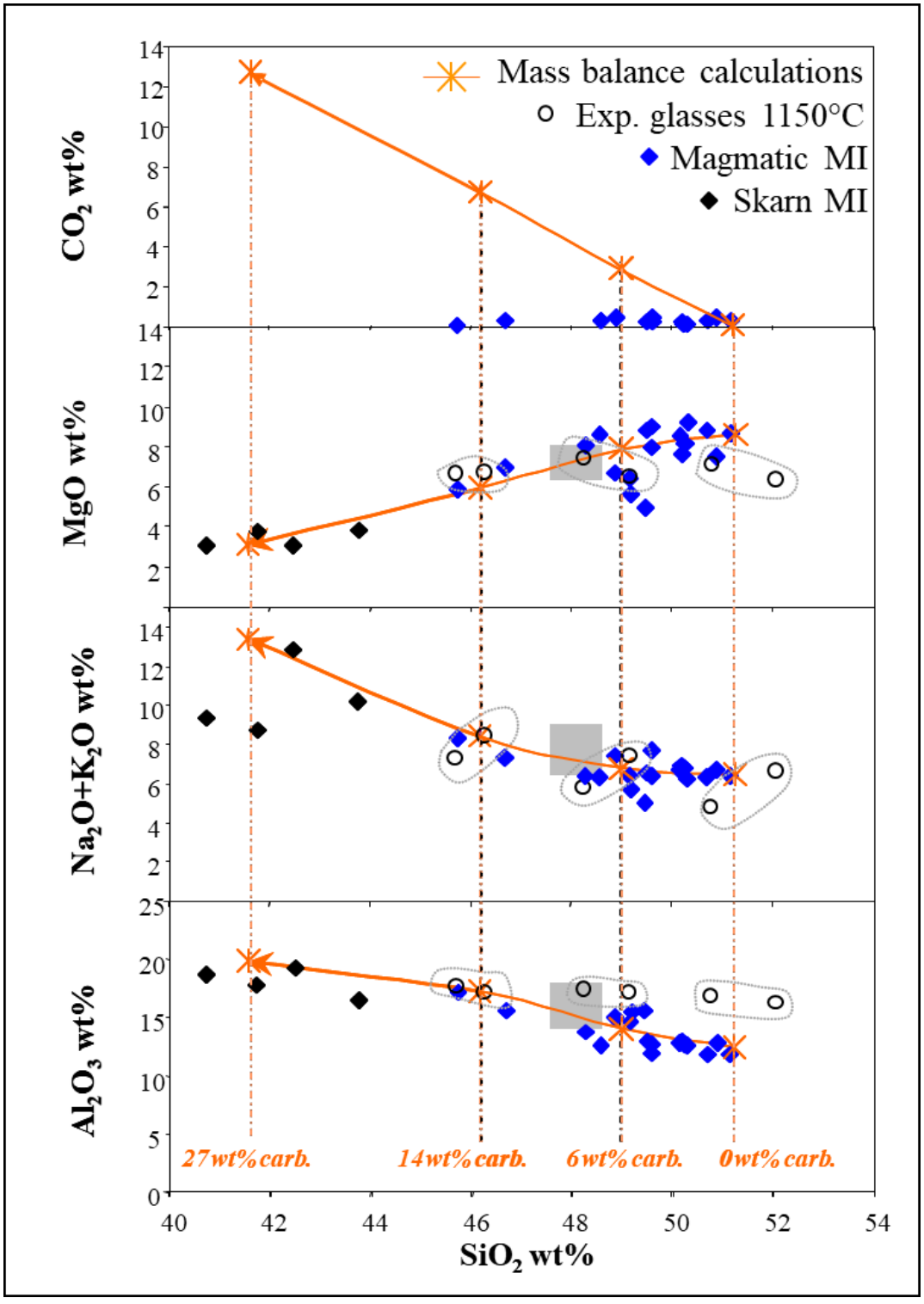

Fig. 2.6 Quantification of carbonate assimilation from chemical trends of Vesuvius melt inclusions (MI). Blue diamonds: primitive MI of A.D. 1794–1944 eruptive period (MgO > 6 wt%; Marianelli et al. 2005; Fulignati et al. 2004). Black diamonds: MI compositions in high-temperature skarn xenoliths from 1944 eruption (MgO > 3 wt%; Fulignati et al. 2004). Open circles: residual liquids of interaction experiments at 1150 °C and 200 MPa (Iacono-Marziano et al., 2008). Red lines: mass balance calculations simulating chemical changes in melt composition in response to carbonate assimilation plus crystallization. Red crosses: calculated melt compositions for 0, 6, 14 and 27 wt% carbonate assimilation. The grey field represents the average whole-rock composition of 1631-1944 lavas (Joron et al. 1987), which is reproduced by 9.8-11.2 wt% carbonate assimilation. Modified from Iacono-Marziano et al. (2009).

Changes in the degree of silica saturation do not correlate with any significant change in the isotopic composition (Ayuso et al. 1998; Peccerillo 2005; Di Renzo et al. 2007; Frezzotti et al. 2007), but are related to the geographic position of the volcanic centre and the thickness of the carbonate basement through which the magma ascents (Fig. 2.7C). An extreme case of carbonate assimilation is therefore likely represented by the **Intra-Apennine centres** (Fig.2.7), extremely small volumes of silica-undersaturated, alkali-rich rocks of kamafugitic composition, with $\delta^{18}O$ signatures >12‰ (Peccerillo 2005 and references therein).

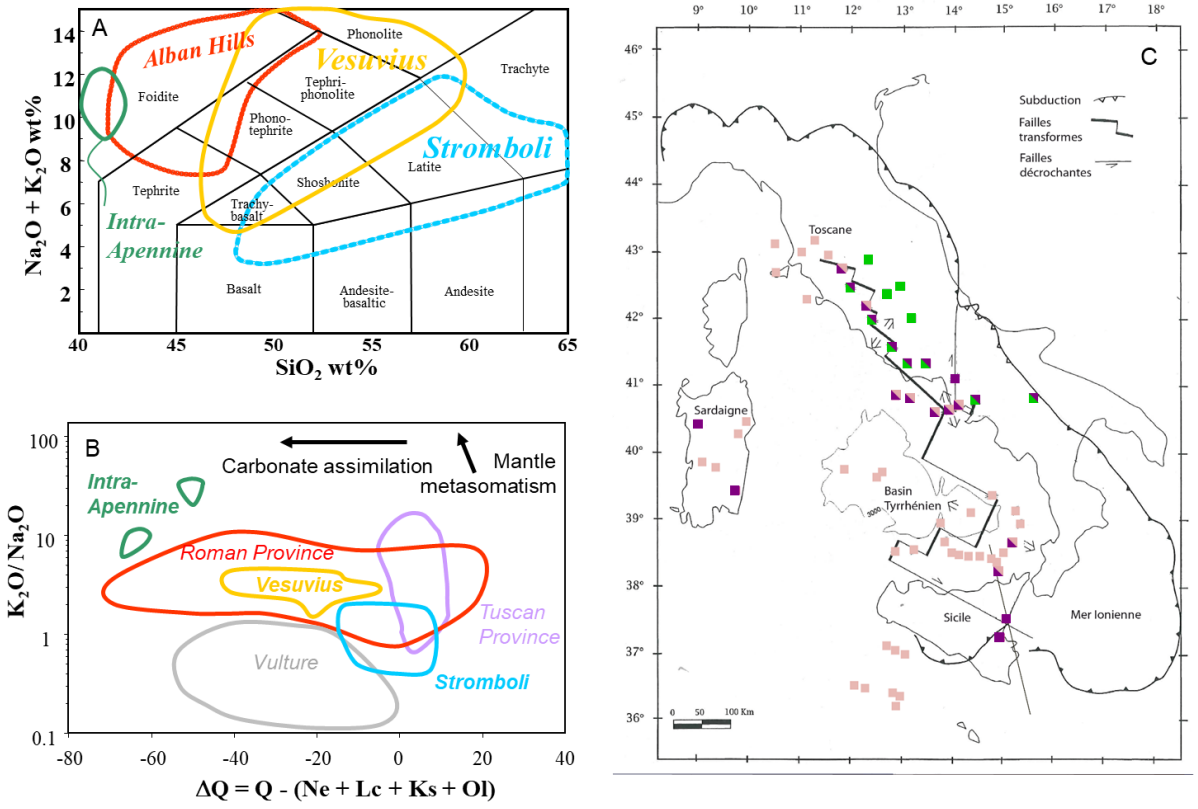

Fig.2.7 Whole rock compositions of Italian quaternary volcanoes. (A) TAS diagram showing the eruptive products of the Intra-Apennine Province and of several other volcanoes: Stromboli, Vesuvius and Alban Hills (in the Roman Province). (B) K_2O/Na_2O ratio versus silica saturation index of the eruptive products of several volcanoes or magmatic provinces. ΔQ = normative Quartz – normative Olivine norm – normative Leucite – normative Kalsilite– normative Nepheline. Only mafic rocks are represented. The black arrows indicate the effects of carbonate assimilation and mantle metasomatism on the composition of the magma. Modified after Peccerillo (2005) and Iacono-Marziano et al. (2008). (C) Distribution of Italian quaternary volcanoes, and degree of silica saturation of their eruptive products. The most silica-undersaturated rocks are observed in the inner parts of the Italian peninsula, within the Apennine Chain, where the thickness of the carbonate rocks in the basement of the volcanoes is higher.

Merapi volcano (Java, Indonesia) also present evidence of magma-carbonate interactions, although less extensive. Chadwick et al. (2007) investigate the petrology and Sr isotopic composition of both recent basaltic andesite lavas and skarn xenoliths from Merapi. The authors observe important variability in the anorthite content of plagioclase in the lavas, correlating with the $^{87}Sr/^{86}Sr$ ratio. Calc-silicate xenoliths contain extremely calcic plagioclase (up to An_{100}) and have the highest whole-rock $^{87}Sr/^{86}Sr$ ratio, suggesting significant magma-carbonate interactions at Merapi. Borisova et al. 2013 also observe high $^{87}Sr/^{86}Sr$ ratios in the bulk rocks of the highly explosive 2010 eruption, and highly calcic plagioclase cores (up to An_{97}) with low FeO contents and ^{18}O enrichment. Deegan et al. (2010) produce Ca-enriched, highly radiogenic strontium contaminant melts by means of decarbonation experiments at 1200°C, proposed to reproduce magma-carbonate interactions at Merapi. However, petrological constrains and bulk rock compositions do not seem to be indicative of large amounts of assimilation (Costa et al. 2013).

2.3 Effect on volatile emissions

As illustrated by equations 2.1-2.6, carbonate assimilation systematically liberates large quantities of CO_2. At crustal pressures, the amount of CO_2 produced cannot completely dissolve in the silicate melt because CO_2 solubility does not exceed 1 wt% in mafic melts (Iacono-Marziano et al. 2012c). If the magma is hydrous, CO_2 released by assimilation increases CO_2 fugacity and decreases H_2O fugacity, triggering water exsolution from the melt. In natural systems, CO_2 resulting from carbonate assimilation may therefore promote the formation of a free fluid phase at depth. Depending on the porosity of the wall rocks, this fluid phase may coexist with the magma or rapidly separate from it. If coexisting with the magma, its presence would undoubtedly affect the density and viscosity of the magma, and therefore its degassing behaviour (Iacono Marziano et al. 2007, 2008).

Highly explosive activity of **Merapi volcano** is for instance proposed to be due to the elevated partial pressures of CO_2 deriving from the assimilation of carbonate xenoliths (Borisova et al. 2013; Troll et al. 2013). Carr et al. (2018) tested this scenario using numerical modelling and conclude that both CO_2 release by assimilation/decarbonation and water exsolution from the magma, due to CO_2 introduction, may have participated to generate the overpressure required to account for the peak phase of the Merapi 2006 eruption. The experimental study of Blythe et al. (2015) explore CO_2 generation and bubble migration from carbonate into crystal-free magmas. Their experiments show how the viscosity of the melt controls bubble migration, with the less viscous melt facilitating bubble removal, and the more viscous ones favouring bubble concentration causing local over-pressure.

Whenever the CO_2-rich fluids deriving from magma-carbonate interactions are dissipated through the fault system of the surrounding rocks, CO_2 emissions in volcanic areas (plume degassing, soil diffuse degassing and CO_2 content in groundwaters) can be affected. CO_2 emissions in **Central-Southern Italy** are for instance particularly intense and centred on volcanic areas (Fig.2.8). Chiodini et al. (2004) estimate the amount of CO_2 dissolved in spring waters of the Tuscan, Roman and Campanian regions to reach 9 Mt/y. Additional contributions come from the CO_2 directly discharged by gas vents, volcano craters or soil degassing (e.g. Chiodini & Frondini 2001; Chiodini et al. 2001; Gambardella et al. 2002; Frondini et al. 2004).

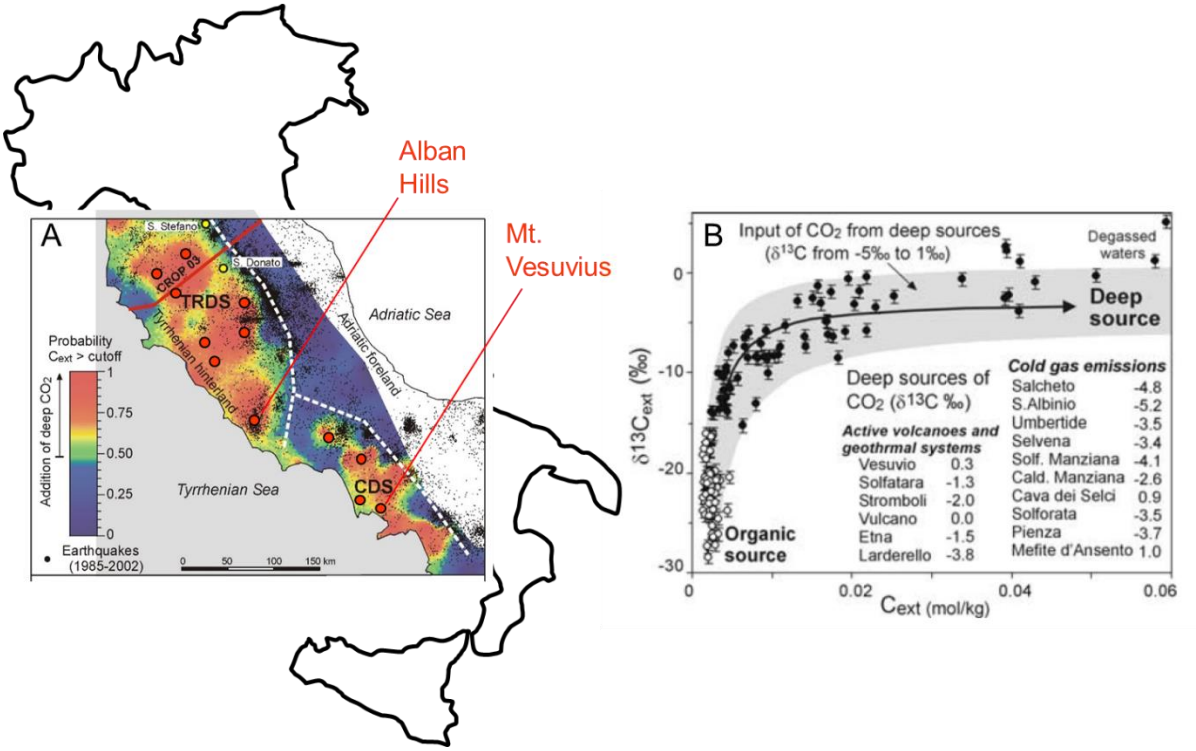

Fig.2.8 CO_2 emissions in Central-Sothern Italy. Modified from Chiodini et al. 2001. (A) Map of the probability that the carbon dissolved in spring waters at any location (C_{ext}) is higher than the cutoff value (maximum value expected for a biological carbon source: 0.004 mol/kg). To produce this map, chemical and isotopic data of 139 springs were integrated. Carbon directly derived from the dissolution of carbonate rocks hosting the aquifers is removed (C_{carb}=Ca+Mg-SO_4). The positions of the main volcanic complexes in the area are shown by the red dots. The total calculated CO_2 flux for both the Tuscan-Roman and Campanian areas is $2.1*10^{11}$ mol/y, i.e. ~9 Mt/y. The recent seismic activity recorded by the National Seismic Network of INGV is also shown (small black dots). (B) Diagram of $\delta^{13}C_{ext}$ versus C_{ext} of Apennine groundwater. Open circles are compatible with dissolution of biological CO_2 only, while dots are compatible with an input of deeply derived CO_2. The carbon isotopic composition of CO_2 released by Italian volcanoes, geothermal systems and cold gas emissions is reported for a comparison.

Mt. Vesuvius and **Alban Hills** volcanic areas are particularly well studied: they currently degas 301 and 580 t/day, respectively (Fig.2.9). These emissions occur from the crater area (at Vesuvius) or from

localized gas vents (at Alban Hills), and are partly dissolved in the groundwater of the volcano flanks (Chiodini & Frondini 2001; Frondini et al., 2004; Caliro et al., 2005). CO_2 amounts produced by carbonate assimilation at Mt. Vesuvius and Alban Hills during their last eruptive periods are estimated to reach 335-1566 and 98-784 t/day, respectively, on the basis of natural and experimental petrological constraints (Iacono-Marziano et al. 2007, 2009). Most of the produced CO_2 is not dissolved in the magma, as indicated by the CO_2 contents of melt inclusions not exceeding 0.3 wt% (Fig.2.6; Marianelli et al. 2005), and is therefore likely to reach the surface through the hydrothermal system.

The estimated CO_2 fluxes are very similar to those currently measured in the two volcanic areas (Fig. 2.9), which represent minimum estimations of the current CO_2 production rate at depth. This suggests that most of the CO_2 currently degassed at Mt. Vesuvius and Alban Hills is originated by the interaction between magmas and carbonate rocks (Iacono-Marziano et al. 2007, 2009). C and He isotopic compositions of the fumaroles of these two volcanic centres are distinctly different from typical mantle signatures, i.e. $\delta^{13}C$ between 0.06 and 0.34 ‰VPDB (Chiodini et al. 2001) and $^3He/^4He$ between 2.51 and 3.98 Ra (Tedesco et al. 1998) for Vesuvius, and $\delta^{13}C$ between-3.5 and 0.9 ‰VPDB and $^3He/^4He$ between 0.94 and 1.54 Ra, for Alban Hills (Chiodini & Frondini 2001). The two approaches proposed by Sano & Marty (1995) allow the proportions of mantle-derived and sedimentary-derived gases to be inferred from the isotopic compositions: they corroborate the significant contribution from sedimentary rocks (52-100%; Iacono-Marziano et al. 2009).

Like Mt. Vesuvius and Alban Hills, several other volcanic centres, either quiescent or active, that have been recognized to be emplaced over carbonate sedimentary successions and/or showing skarn xenoliths in their eruptive products, are characterized by elevated rates of CO_2 degassing (high ratios of emitted gas to emitted magma), like **Mt. Etna** in Italy (Michaud 1995; Chiodini et al. 2011), **Popocatépetl** in Mexico (Goff et al. 2001; Obenholzner et al. 2003), **Yellowstone** in the USA (Werner and Brantley 2003), **Merapi** in Indonesia (e.g. Chadwick et al. 2007; Troll et al. 2012), **La Soufriere St.Vincent** in the Lesser Antilles (Bouvier et al. 2010; Bezard et al. 2014). It is however difficult to distinguish between slab-derived and crustal sedimentary CO_2, as the two isotopic signatures overlap, precluding an accurate estimate of crustal contribution to emitted gases (Aiuppa et al. 2017).

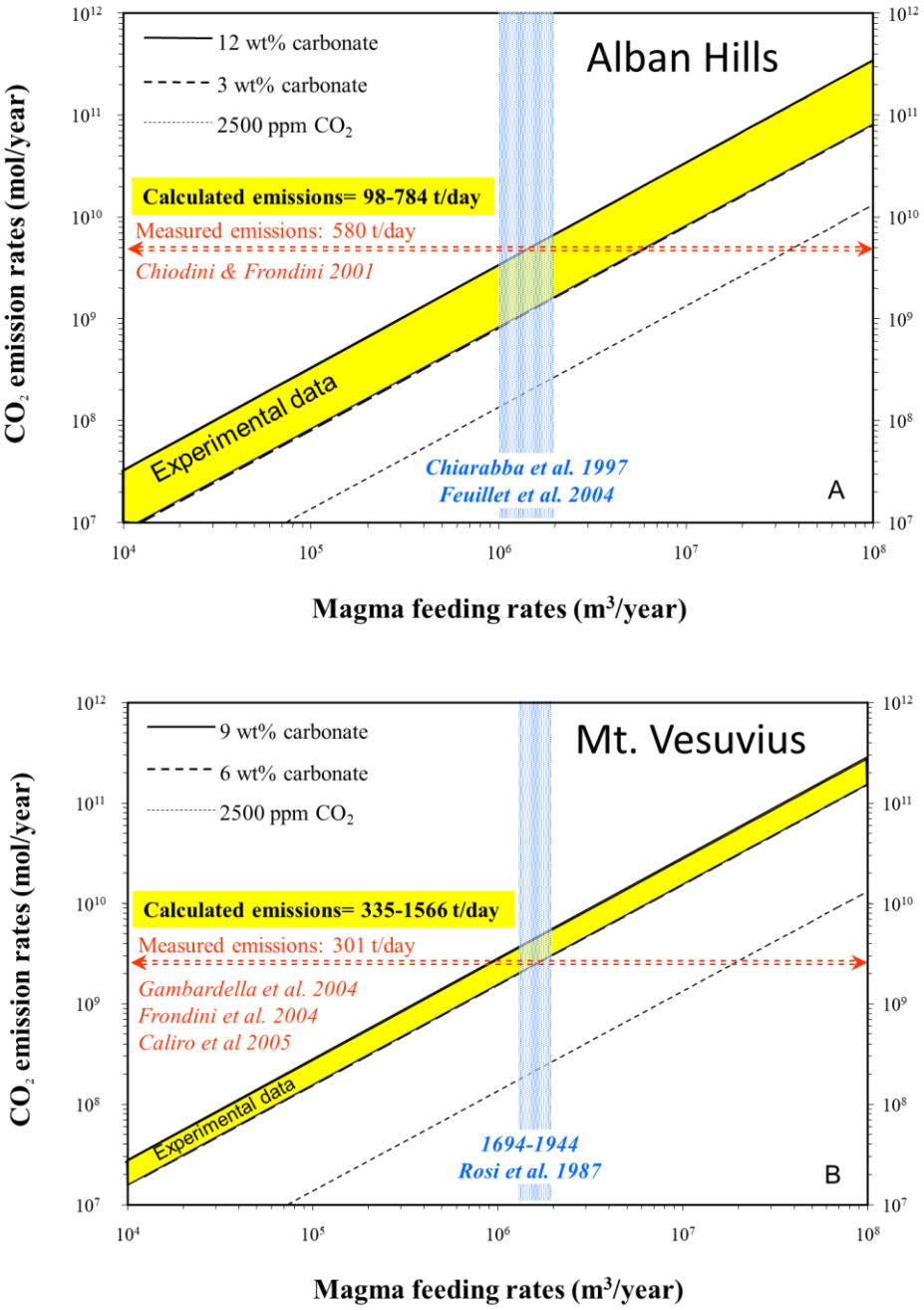

Fig.2.9 Calculated CO_2 emission rates as a function of magma emission rate for magmas containing 2500 ppm CO_2 (average solubility at 200 MPa), or assimilating variable amounts of carbonate rocks. Modified from Iacono-Marziano et al. (2007). (A) Calculations for Alban Hills (Italy): assimilation degrees of 3-12 wt% carbonate were estimated by experimental constraints. Magma feeding rates are from soil uplift between 1951 and 1994 (Chiarabba et al. 1997; Feuillet et al. 2004). Measured CO_2 emissions are from Chiodini & Frondini (2001). (B) Calculations for Vesuvius (Italy): assimilation degrees of 6-9 wt% were estimated by experimental constraints, while the magma feeding rate is the magma eruption rate for the last eruptive period (1694-1944) (Rosi et al. 1987). Measured CO_2 emissions are the sum of the contributions of crater and soil diffuse degassing and CO_2 dissolved in the groundwaters (Gambardella et al. 2004; Frondini et al. 2004; Caliro et al. 2005).

At the global scale Aiuppa et al. (2017) use the association between volcanic gas CO_2/S_{total} ratios and non-volatile trace elements in magmas to distinguish between slab-derived and crustal sedimentary-derived emissions (Fig.2.10). The authors estimate that the amount of CO_2 produced by volcanoes experiencing magma-carbonate interactions in the upper crust represent ~19-32% of the present-day global CO_2 budget vented by arc volcanism ($1.2\text{-}1.9*10^{12}$ mol/y). This significant fraction is produced by few volcanoes (mainly Etna and Popocatepetl, with minor contributions from Stromboli and Vulcano Island in Italy, Soufriere of St.Vincent in the Lesser Antilles, Bromo and Merapi in Indonesia). This work is based on 56 volcanoes and clearly shows that a few volcanoes can make a difference in changing current estimations, since the CO_2 budget of some magmatic areas experiencing interactions with carbonate rocks can be significantly higher than those of other volcanoes.

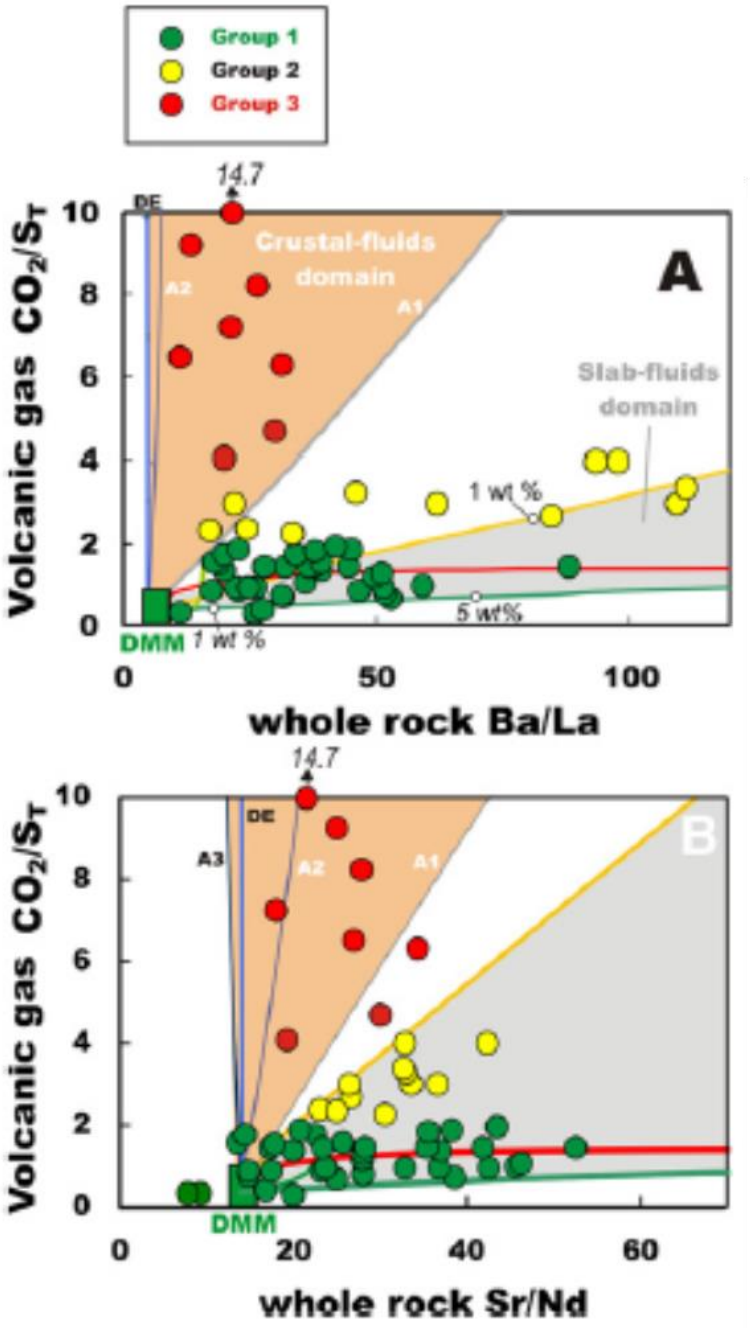

Fig.2.10

Mean CO_2/S_T molar ratios for arc volcanoes with available high-T (> 450°C) gas information versus: (A) Ba/La, and (B) Sr/Nd ratios in their respective magmas.

For each volcano, the mean Ba/La, and Sr/Nd ratios in magmas with <56 wt% SiO_2 were calculated averaging available whole-rock results.

Volcanoes are divided into 3 Groups based on their CO_2/S_T ratios:

Group 1= $CO_2/S_T \leq 2$, Group 2= $2< CO_2/S_T <4$, Group 3= $CO_2/S_T \geq 4$.

The respective domains of slab-fluids and crustal-fluids are illustrated in grey and orange, respectively.

From Aiuppa et al. 2017.

Mason et al. (2017) use a global dataset for carbon and helium isotopes from volcanic arcs to evaluate the contribution of crustal carbonate assimilation to the global arc volcanic carbon flux (Fig.2.11A). The authors conclude that assimilation and outgassing of crustal carbon may dominate global volcanic CO_2 fluxes, and is a key parameter controlling both the magnitude of the CO_2 flux and its carbon isotope composition. Volcanic arcs with the highest CO_2 fluxes have indeed higher $\delta^{13}C$ (Fig.2.11B).

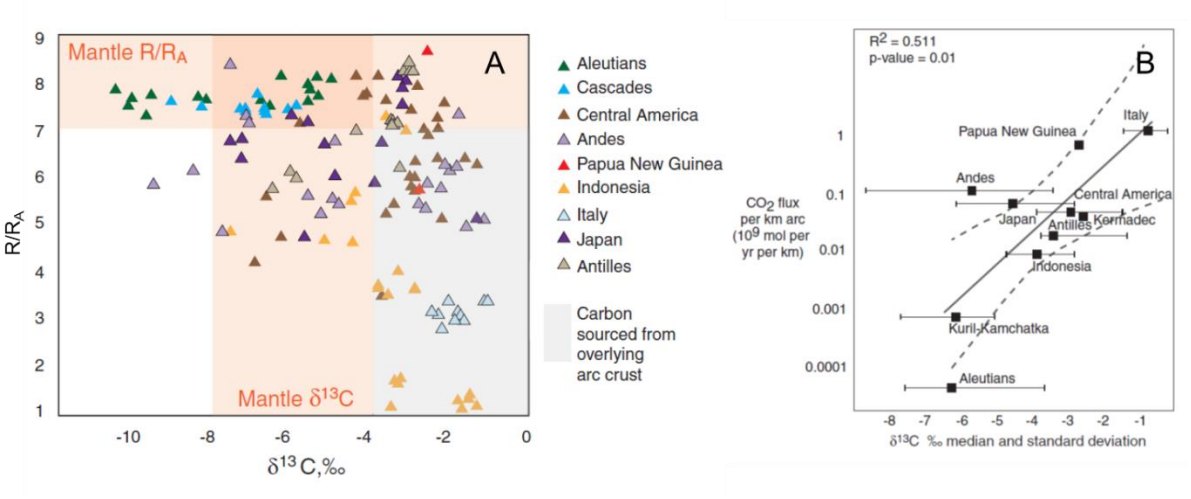

Fig.2.11 (A) Plot of helium isotope composition ($^3He/^4He$ normalized with the same ratio for air) against carbon isotopic composition of volcanic gases from arc volcanoes. The data points are each from an individual volcano and are coloured by volcanic arc. Mantle ranges are shown in orange. Assimilation of crustal carbonates would push values to the grey area, which is characterized by an enrichment in isotopically heavy carbon and radiogenic He from U and Th. (B) Plot of CO_2 flux per kilometre of arc length against median carbon isotope composition for each arc. The horizontal bars are standard deviations around a median value. The solid line is a linear regression, and the dashed lines are the 95% confidence limits. From Mason et al. 2017.

These emissions are fed by CO_2-rich gases produced by both assimilation at the magma-carbonate interface and thermal breakdown processes in the aureole of the magma chamber (possibly without direct contact with the magma). The greatest challenge is to distinguish between these two contributions and/or to determine which one is dominant. Carter & Dasgupta (2018) explore both assimilation and thermal breakdown of calcite-dolomite mixed carbonates: they show that the composition of the carbonate rocks is crucial in controlling the amount of CO_2 released by both assimilation and thermal breakdown. Dolomite-rich carbonates breakdown at lower temperatures, and therefore produce more CO_2 than calcite-rich carbonates at a given temperature. Dolomite-rich carbonates are also assimilated more extensively than calcite-rich ones, therefore releasing higher amounts of CO_2. Assimilation of calcium-rich carbonates produces significantly higher amounts of CO_2 in basaltic magmas than in dacitic ones, while assimilation of dolomite-rich carbonates releases similar

amounts in the two magma compositions. At similar temperatures, the assimilation of calcite-rich carbonates by both basaltic and dacitic magmas produces slightly more CO_2 than thermal decomposition, while the assimilation of dolomite-rich carbonates releases less than thermal breakdown. Carter & Dasgupta (2018) therefore conclude that thermal breakdown is more likely to be the prevalent process releasing CO_2 when the host carbonates are magnesian, particularly with felsic plutonic intrusions likely to sit in the crust and crystallise for a duration.

I would like to stress that magma intrusion style is another factor that could potentially affect the relative importance of assimilation and thermal breakdown. Pichavant et al. (2014) propose that magma supply rate, together with magma composition, aspect ratio and volume of the reservoir control the extent of carbonate assimilation. Mafic magma batches intruding the base of the carbonate sequence as an array of dykes would develop magma-carbonate interfaces promoting assimilation. Interaction would be maximized by multiple intrusions of small volume with high aspect ratios. Conversely, in a large-volume, low aspect ratio reservoir, less frequently recharged and hence colder, magma-carbonate interaction would be more limited. This behaviour is observed at Mt. Vesuvius, when the compositions and the volumes of the products of different eruptions are considered (Pichavant et al. 2014).

The two current highest CO_2 emitters, Mt. Etna and Popocatepetl volcano, have relatively high magma intrusion/extrusion rates (10^{13}-10^{14} g/y according to Harris et al. 2011 and Roberge et al. 2009). High magma intrusion rates are indeed likely to favour carbonate decomposition, but probably not assimilation, if the reservoir has a low aspect ratio. This could explain why Popocatepetl eruptive products do not show clear evidence of carbonate assimilation, e.g. desilication and alkali enrichment, and Mt. Etna products only limited evidence (Salem et al. 2019).

2.4 Effect on redox conditions and ore processes

Magma-carbonate interactions may generate skarn deposits via the production of metal enriched fluids. Meinert et al. (2005) distinguish seven major skarn types, depending on the enriched element: Fe, Au, Cu, Zn, W, Mo and Sn, with a general increase in evolution of the associated pluton from the Fe to the Sn type. The topic is too broad to enter the details, but the common feature of these deposits is that the elements are thought to precipitate from high-temperature metasomatic fluids that are more or less enriched in magmatic components. Deposits derived from direct magmatic crystallization are not included in this classification; these magmatic deposits are significantly more difficult to recognize and their magmatic origin is generally controversial.

Some iron-oxide deposits are proposed to be produced by fluid-assisted magmatic crystallization, as a result of the interaction with carbonate rocks. These Fe-Ti oxide deposits are found inside magmatic intrusions and/or at the magma-carbonate interface, and are associated with mafic-ultramafic magmas or more evolved ones. In the **Panxi region** in China, for instance, titanomagnetite ores are hosted in layered intrusions belonging to the Emeishan large igneous province, which intrude Paleoproterozoic and Neoproterozoic sedimentary rocks including dolomitic limestone, dolostones and marlstones. Titanomagnetite saturation occurs relatively early in these magmatic systems as compared with other layered intrusions; in the **Panzhihua intrusion**, in particular, the massive magnetite layers are at the base of the intrusion. Carbonate assimilation is proposed to produce anomalously Mg-rich olivine (Fo up to 91 mol %) frequently associated to magnetite (Tang et al. 2017), while the release of CO_2-rich fluids in the contact aureole of the intrusion is suggested to have increased the oxygen fugacity of the magma, resulting in an early crystallization of magnetite (Ganino et al. 2008). Figure 2.12A shows how the stability field of titanomagnetite in ferrobasaltic magma is strongly affected by redox conditions (Toplis & Carroll 1995).

Similarly, Mathieu (2019) suggest that the interaction with a carbonate-facies iron formation could have played a role in the genesis of the titanomagnetite deposit hosted in the **Lac Doré** tholeiitic layered intrusion. The assimilation of Ca-Mg-carbonates may favour magma desilication and crystallization of Mg-rich olivine, and CO_2 degassing promote magnetite crystallization.

Yazd and Sirjan iron-oxide deposits in central Iran, associated with more evolved rocks, are also likely to be linked to the interaction with carbonate rocks. These deposits have mineral assemblages characteristic of Kiruna-type ores and are hosted within and close to felsic igneous rocks intruded in limestone and evaporites. Peters et al. (2019) propose magmatic assimilation of carbonate rocks as possible genetic mechanism, on the basis of oxygen isotope ratios ($^{17}O/^{16}O$ and $^{18}O/^{16}O$), suggesting that magnetite forms from magmatic fluids interacting at high temperature with carbonate rocks (Sirjan deposit) and evaporites (Yazd deposit).

All these occurrences and the frequent presence of Fe-Ti oxides associated with worldwide magma-carbonate interactions (e.g. Rice 1977; Joesten 1977; Holness 2000; Owens 2000; Wenzel et al. 2001, 2002) suggest a causal link between interactions and oxide crystallization. Ganino et al. (2008) proposed that CO_2-rich fluids released during decarbonation of sedimentary host rocks can increase the oxygen fugacity of the magma. The oxidation effect of CO_2 can be simplified as:

$$CO_2 + 2\,FeO \rightarrow CO + Fe_2O_3 \qquad (2.7)$$

The efficiency of the reaction is relatively limited: the addition of 10 wt% CO_2 to the basaltic magma increases oxygen fugacity of a log unit (Fig.2.12B; Ganino et al. 2008). CO_2 fluxing through the magma would induce higher oxidation, due to H_2O extraction from the silicate melt (Fig.2.12B; Ganino et al. 2008). The presence of external H_2O fluxing through the magma would additionally increase magma oxidation state, but it is not clearly documented in any natural context.

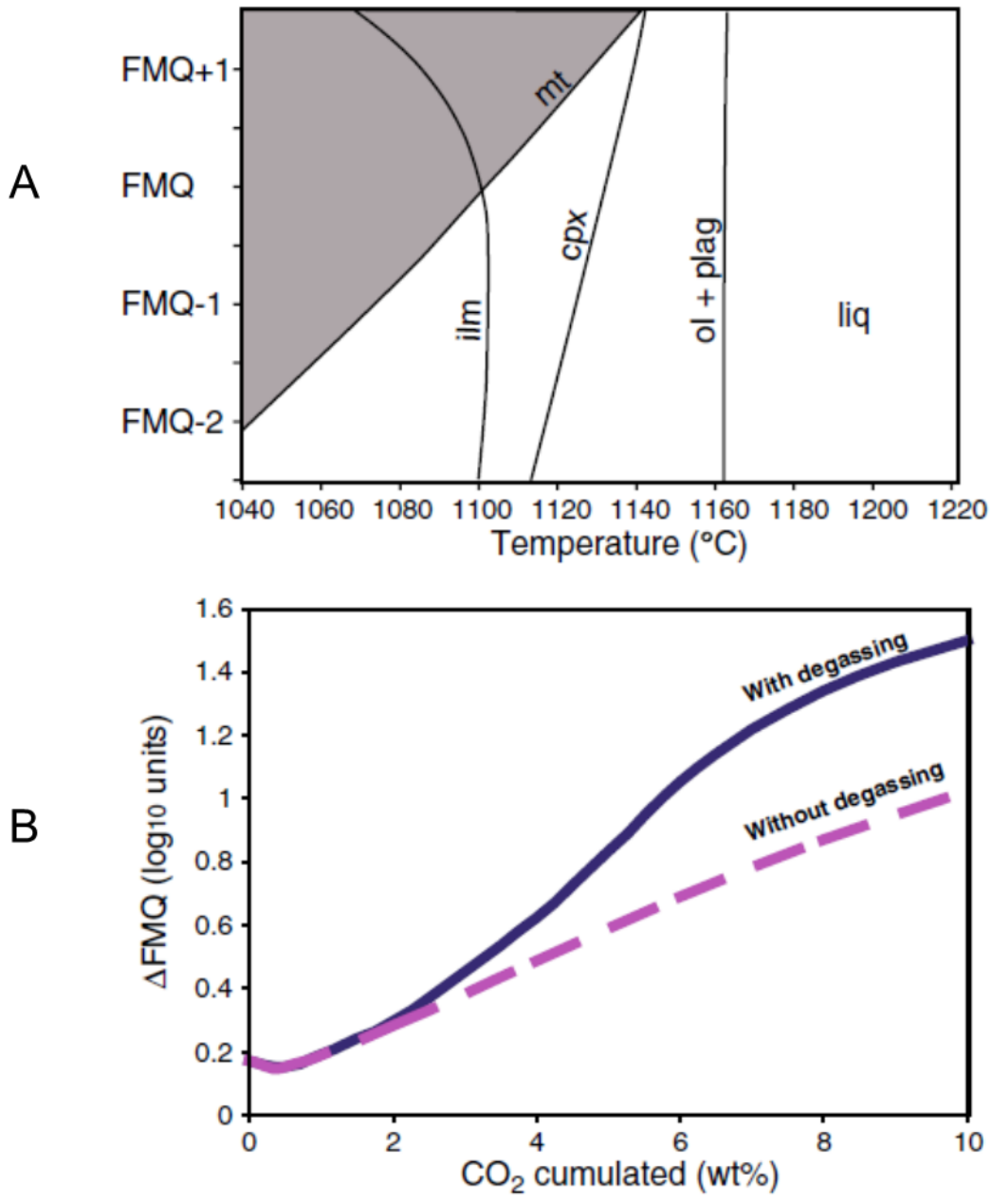

Fig.2.12 (A) Phase equilibria of a ferrobasalt as a function of oxygen fugacity (expressed as logarithmic units relative to the Fayalite-Magnetite-Quartz buffer), experimentally determined by Toplis & Carroll 1995. mt= magnetite, ilm=ilmenite, cpx=clinopyroxene, ol=olivine, plag=plagioclase, liq=liquid (B) Diagram illustrating the effect of interaction between a CO_2-rich fluid and a basaltic magma on the oxygen fugacity of the system. The curve named «without degassing» only accounts for CO_2 addition to the magma, while the one named «with degassing» also accounts for H_2O degassing from the magma to the fluid phase. From Ganino et al. 2008.

Two world-class sulfide deposits have also been linked to the assimilation of carbonate rocks, the Jinchuan (China) and the Platreef (South Africa) Ni-Cu-PGE deposits. Lehmann et al. (2007) attribute ore formation at **Jinchuan** to the assimilation of carbonate rocks by a magma that is close to sulfide saturation as a result of earlier assimilation of granitic crust. The segregation of the sulfide melt would be caused by an increase in the oxygen fugacity due to decarbonation of the host marble and CO_2 penetration into the intrusion. A similar hypothesis is raised for the **Platreef deposits** at the Bushveld Complex, due to the numerous pieces of evidence corroborating the assimilation of footwall dolomites (Pronost et al. 2008; Maier et al. 2008). In both cases, however, the exact link between carbonate assimilation and sulfide melt segregation remains unclear. Increasing oxygen fugacity has indeed been observed to significantly increase the sulfur content of the silicate melt at sulfide saturation (e.g. Jugo et al. 2005; Jugo 2009), therefore implying a decrease in the amount of sulfide melt segregated. Carbonate assimilation is therefore unlikely to represent a trigger for sulfide saturation.

2.5 Assimilation marker and tracers

The frequent occurrence of high temperature skarns in the eruptive products of a volcano is the clearest marker of carbonate assimilation occurring in its plumbing system. These skarns include magmatic minerals that need high CaO and/or MgO concentrations to crystallize, such as melilite, apatite, wollastonite, forsteritic olivine (Fig.2.2). Lower temperature skarns also indicate the occurrence of magma-carbonate interactions, but assimilation is significantly less effective in this case, its efficiency decreasing with decreasing temperature and increasing silica content of the magma (e.g. Carter & Dasgupta 2016).

Sedimentary carbonates are strongly depleted in trace elements and therefore leave light fingerprints in magmas assimilating them. Sr isotopic ratios are classically used to quantify assimilation, because Sr is one of the more enriched elements in carbonates, whereas other elements like Nd can be more than one order of magnitude less concentrated than in magmas (e.g. Tang et al. 2017). Experiments show how assimilation of carbonate rock increases both the Sr content and the $^{87}Sr/^{86}Sr$ ratio of the magma (Deegan et al. 2010; Jolis et al. 2013).

Sr isotopic ratios are employed to investigate carbonate assimilation at **Mt. Vesuvius** (e.g. Del Moro et al. 2001; Civetta et al. 2004; Piochi et al. 2006; Di Renzo et al. 2007), although Vesuvius magmas have high strontium contents and isotopic ratios, relatively similar to those of crustal carbonates. The

differences between less contaminated shoshonitic rocks and highly contaminated phonotephritic rocks can be modelled in terms of assimilation plus fractional crystallization. Di Renzo et al. (2007) used Sr-Nd contents and isotopes to calculate that 14 % limestone assimilation accompanied by 38% crystallization would account for these variations. Similarly, $^{87}Sr/^{86}Sr$ ratios versus Sr contents can also be used (Piochi et al. 2006; Iacono-Marziano et al. 2008). Figure 2.13 however shows that these estimations need accurate values of Sr concentration and isotopic composition of the carbonate contaminant, which are often challenging, because the contaminant is usually not a single lithology. The high variability of Sr isotopic ratio of Mt. Vesuvius eruptive products belonging to a single eruptive period (e.g. Di Renzo et al. 2007) can therefore be produced by different contaminants and/or different degrees of assimilation in the magmatic reservoir.

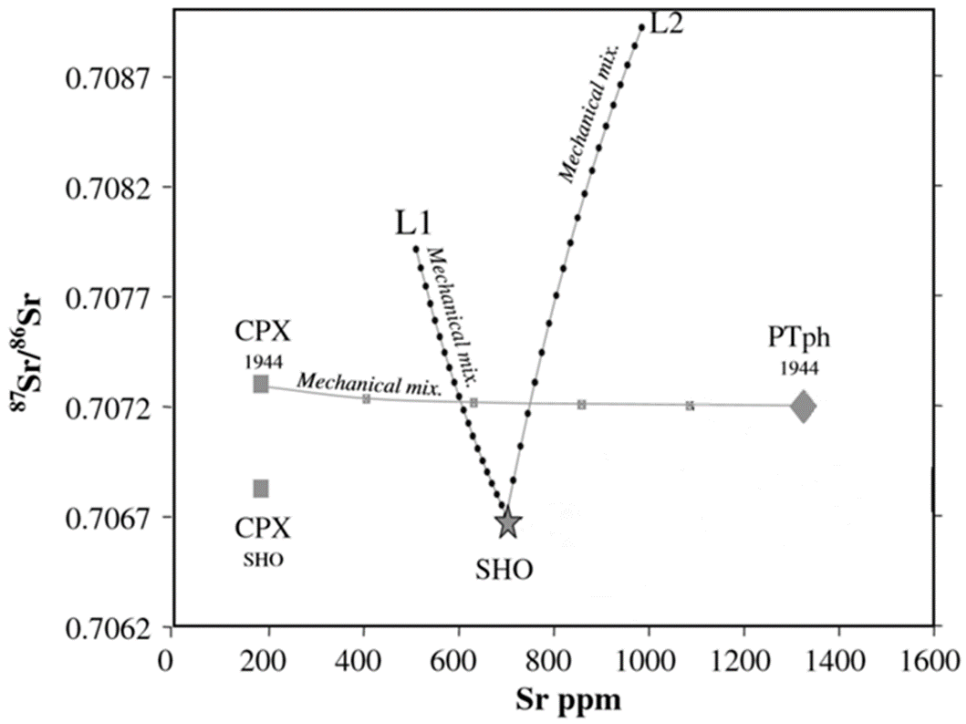

Fig.2.13 Geochemical modelling of Sr isotopic ratio versus Sr content of Vesuvius rocks. The star indicates recent shoshonite that are considered as one of the least differentiated compositions of Mt. Vesuvius (Di Renzo et al. 2007): they are here considered as the least contaminated rocks. The grey diamond indicate 1944 phonotephrites, representative of contaminated rocks. CPX SHO and CPX 1944 represent the cognate cumulates of clinopyroxenite associated to the shoshonite and the phonotephrite, respectively. Two possible contaminants have been chosen, L1 and L2, bracketing the Sr contents and isotopic ratios of Campanian carbonates (Piochi et al. 2006; Di Renzo et al. 2007). Mixing lines simulate carbonate assimilation (a dot every 5 w%), or clinopyroxene crystallization (a square every 20 %). The contaminated phonotephrite can therefore be produced by 45-50 % assimilation of L1 and ~60 % of cpx crystallization, or, more realistically, by 15-20 % of assimilation of L2 and 50 % of cpx crystallization. Modified from Iacono-Marziano et al. (2008).

Geochemical signatures of carbonate assimilation also come from oxygen isotopic studies, owing to the strong enrichment in ^{18}O of carbonate rocks ($\delta^{18}O$ generally higher than 20‰). Constraints from separate minerals are generally preferred to those from whole rocks, which are more susceptible to post-emplacement alteration. $\delta^{18}O$ values of magmatic clinopyroxenes from the Alban Hills and Mt. Vesuvius reach 8.33 and 7.30‰ respectively (Dallai et al. 2004, 2007), therefore substantially higher than mantle values ($\delta^{18}O_{cpx}$: 5.6± 0.3‰; Eiler 2001). These values approach the ones measured in cpx from thermometamorphic ejecta of the Alban Hills area (8.4 ± 0.20 ‰), corroborating magma contamination by sedimentary carbonates as genetic process (Dallai et al. 2004, 2007). Extremely anomalous oxygen isotope values are measured in the **Intra-Apennine ultrapotassic volcanic** rocks (kamafugites) and in the associated carbonate-rich rocks (Stoppa and Woolley 1997; Peccerillo 1998). $\delta^{18}O$ values in the kamafugites are in the range 11.9–14.4‰ (Holm and Munskgaard 1982; Taylor et al. 1984), while in the carbonate-rich rocks are 21.1– 25.4‰, very similar to the one of limestone (Stoppa and Woolley 1997), and very different from the one of mantle-derived carbonatites (Hoefs 1987). The strong silica-undersaturated nature of the kamafugites (Fig. 2.7) is in agreement with the estimation that these rocks experienced ~ 20 wt% carbonate assimilation (Peccerillo 1998).

A combination of O and C isotopes can be used to model the compositions of carbonate-bearing xenoliths, as Jolis et al (2015) did for marble and skarn xenoliths of Mt. Vesuvius: both types of xenoliths cannot be explained by pure decarbonation and need a magmatic contribution up to 55% for marbles and up to 75-80% for skarns.

Elemental ratios and isotopic signatures employed to trace carbonate assimilation in volcanic gases are already discussed in section 2.3.

3. Evaporitic rocks

In contrast to carbonate rocks, the information available on the assimilation of salts, both sulfates and chlorides, is generally limited. Still these rocks are extremely common in sedimentary basins worldwide, particularly in rifted margins (Schofield et al. 2014). Magma-salt interactions and subsequent salt mobilization could therefore occur more often than currently recognized. Moreover, the involvement of evaporitic rocks in the generation of high temperature hydrothermal fluids is highly debated (e.g. Barton 2014; Li et al. 2015). Although hydrothermal processes are not the main focus of this manuscript, the possible production of hydrothermal fluids by magma-evaporite interactions will be briefly discussed in the next paragraphs, together with the petrologic and environmental consequences of evaporite assimilation.

3.1 Sulfate rocks

3.1.1 Mechanisms of assimilation

The interaction with sulfate rocks is suggested to take place through the erosion and disintegration of footwall rocks by dynamic pulses of hot magma, followed by the assimilation of the produced xenoliths (Yudovskaya et al. 2018). Several mechanisms of assimilation are discussed by Yudovskaya et al. (2018), in a detailed petrological study of anhydrite-bearing magmatic rocks of the **Bushveld Complex** (South Africa): (i) thermal decomposition, (ii) chemical dissolution, and (iii) melting of anhydrite or anhydrite-bearing rocks of the Duitschland Formation, which in some localities of the Bushveld northern limb constitutes the footwall rocks of the intrusion. These shallow-marine sediments have a total thickness of 1 km and consist of carbonaceous shales, carbonate rocks, anhydrite and quartzite. Yudovskaya et al. (2018) conclude that the three mechanisms are viable and may occur to different extents at the northern limb of the Bushveld Complex. Round anhydrite inclusions in orthopyroxene could derive either from an immiscible sulfate melt at high temperature, or from dissolution of anhydrite in the mafic melt. The occurrence of anhydrite-bearing granitic veins could suggest the partial melting of anhydrite-bearing pelites.

The melting temperature of pure anhydrite is ~1400°C (Naumov et al. 1974), however Jugo et al. (2005) observe round quenched sulfate blebs in their experimental samples obtained at 1315°C and 1.1 GPa, which are consistent with the presence of an immiscible sulfate liquid at run conditions. Moreover, van der Sluis (2010) observe partial melting of anhydrite-dolomite mixtures at significantly lower temperatures (down to 900°C). The decomposition temperature of pure anhydrite is similar to the melting temperature: ~1400°C at 0.1 MPa, but in the presence of impurities, such as alumina, silica or kaolin, it can be lowered to 1150°C (Yudovskaya et al. 2018, and references therein).

Chemical dissolution of anhydrite is the assimilation mechanism that is more thoroughly characterized by means of interaction experiments coupling mafic magmas and anhydrite at 1200°C and ~70 MPa (Iacono-Marziano et al. 2017, submitted). At these conditions, anhydrite dissolves into the silicate melt without any evidence of melting, and enriches it in Ca and S (Fig.3.1 b,c):

$$CaSO_4^{anhydrite} \rightarrow CaO^{silicate\ melt} + SO_3^{silicate\ melt} \quad (3.1)$$

Sulfur enrichment is markedly more important due to the substantial difference in concentration between the anhydrite and the silicate melt (Fig.3.1 c); calcium enrichment is less striking, i.e. a few wt% (Fig.3.1 b).

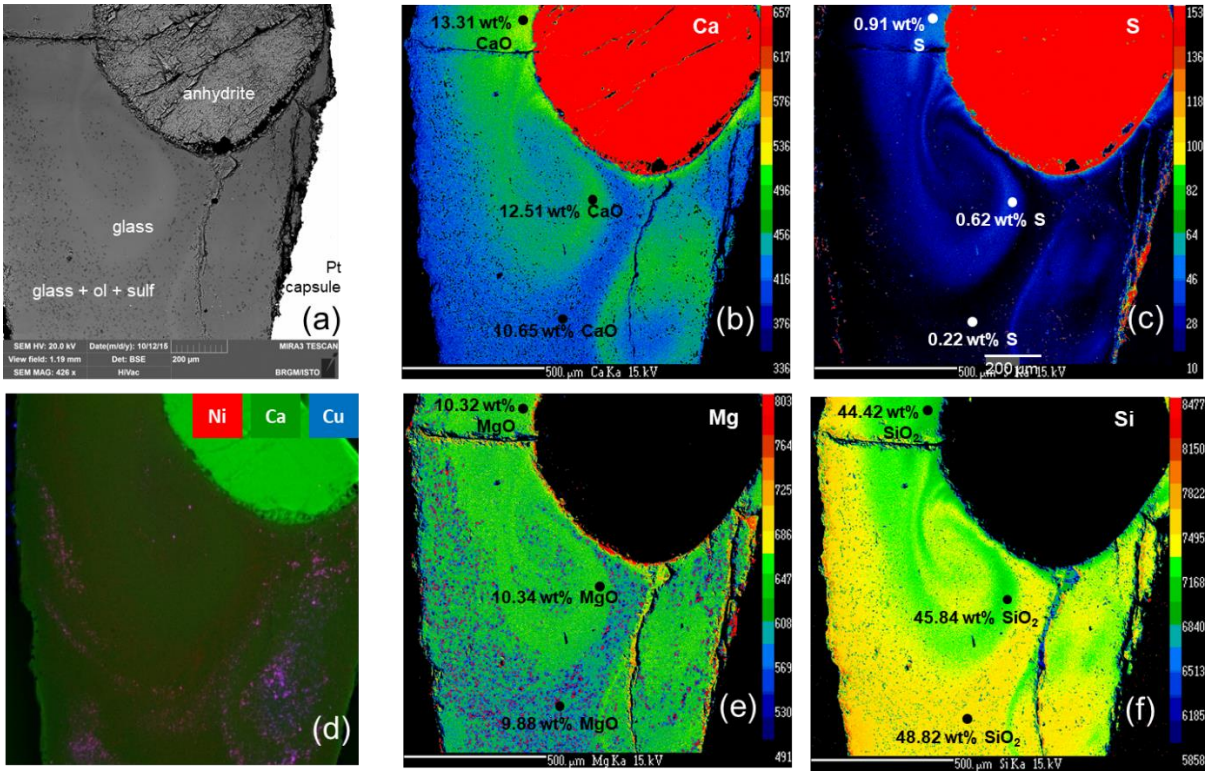

Fig.3.1. Experimental sample illustrating the assimilation of an anhydrite chip by a mafic magma. Experimental temperature, pressure and duration are 1200°C, 80 MPa and 10 minutes, respectively. (a) BSE image showing the glass-richer zones (clear areas). X-ray images obtained by electron microprobe showing the distribution of CaO (b), S (c), MgO (e), and SiO_2 (f). (g) Three element XFM map (red=Ni, green=Ca, blue=Cu). The purple spots (Ni+Cu) represent sulfide globules that are imaged over the whole sample thickness (~100 µm). Modified from Iacono-Marziano et al. 2017.

Dissolution produces sharp margins in the anhydrite xenoliths and Ca-S-enriched boundary layers around them. This boundary layer probably has a different density to the rest of the silicate melt that makes it unstable and causes composition-driven convection (Fig. 3.1). The composition-driven

convection breaks away the boundary layer, and increases the rate of dissolution, which otherwise would be limited by diffusion across the boundary layer (Kerr 1994; Barnes and Robertson 2019a).

Whereas all CaO derived from anhydrite is dissolved in the silicate melt, part of the sulfur can be degassed to the fluid phase (Iacono-Marziano et al. submitted). Although the absolute amounts of degassed S are limited, never attaining more than 1 wt% of the magma, they can however represent an important proportion of the sulfur deriving from anhydrite. The amount of degassed sulfur most likely depends on the initial redox conditions of the magma, the lower the oxygen fugacity, the lower the amount of S that can be dissolved in the melt and therefore the higher the proportion of S in the fluid phase. Thermodynamic calculations in Iacono-Marziano et al. (2017) also clearly show that the amount of degassed sulfur depends on the amount of fluid phase coexisting with the magma. To account for the effects of both redox conditions and fluid phase proportion, anhydrite dissolution can be better expressed as:

$$CaSO_4^{anhydrite} + a\ FeO^{silicate\ melt} \rightarrow CaO^{silicate\ melt} + b\ SO_3^{silicate\ melt} + c\ Fe_2O_3^{silicate\ melt} + d\ FeS^{silicate\ melt} + e\ SO_2^{fluid} \quad (3.2)$$

where $SO_3^{silicate\ melt}$ and $FeS^{silicate\ melt}$ indicate the oxidized (S^{6+}) and reduced sulphur (S^{2-}) dissolved in the silicate melt as SO_3 and FeS. Note that $FeS^{silicate\ melt}$ does not represent a sulphide melt.

In equation (3.2), coefficients a, b, c, d and e can be expressed as a function of two variables x and y, which depend on the proportion of fluid phase and the initial oxygen fugacity of the magma:

$a = 2\ x\ (1-y) + 9y$

$b = (1-x)(1-y)$

$c = x\ (1-y) + 4y$

$d = y$

$e = x\ (1-y)$

y varies between 0 and 1 with decreasing oxygen fugacity. When y=1 all the sulphur derived from anhydrite assimilation dissolves in the silicate melt in the reduced form (FeS), giving:

$$CaSO_4^{anhydrite} + 9\ FeO^{silicate\ melt} \rightarrow CaO^{silicate\ melt} + 4\ Fe_2O_3^{silicate\ melt} + FeS^{silicate\ melt} \quad (3.3)$$

When y=0 (if the initial oxygen fugacity of the magma before anhydrite assimilation is already oxidizing) sulphur is dissolved in the silicate melt as SO_3 or degassed as SO_2, giving:

$$CaSO_4^{anhydrite} + 2x\ FeO^{silicate\ melt} \rightarrow CaO^{silicate\ melt} + (1-x)\ SO_3^{silicate\ melt} + x\ Fe_2O_3^{silicate\ melt} + x\ SO_2^{fluid} \quad (3.4)$$

When x=0 there is no fluid phase coexisting with the magma and all the sulfur derived from anhydrite assimilation dissolves in the silicate melt in the oxidized form, without sulfur degassing and Fe oxidation:

$$CaSO_4^{anhydrite} \rightarrow CaO^{silicate\ melt} + SO_3^{silicate\ melt} \quad (3.5)$$

In the extreme case x=1 all the assimilated sulfur is degassed into the fluid phase, involving Fe oxidation:

$$CaSO_4^{anhydrite} + 2\ FeO^{silicate\ melt} \rightarrow CaO^{silicate\ melt} + Fe_2O_3^{silicate\ melt} + SO_2^{fluid} \quad (3.6)$$

Reactions (3.3) and (3.6) imply that both sulfur dissolution in the silicate melt as FeS and sulfur degassing as SO_2 involve Fe oxidation. In particular sulfur dissolution in the silicate melt as FeS is relatively limited, but its oxidizing effect particularly important, explaining why the most important oxidation of the magma is observed for the first tenths of wt% of anhydrite assimilated by a relatively reduced magma (Fig.3.2a, b, c).

Although partially limited by degassing, the S content of the silicate melt significantly increases during anhydrite assimilation, up to a factor of 10 (from ~1000 ppm to 1 wt% S, Figs. 3.1c and 3.2d, e,f). The important oxidation experienced by the magma allows the S content of the silicate melt to considerably increase without reaching sulfide saturation (Jugo, 2007; Iacono-Marziano et al. 2014, 2017). The inhibition of sulfide saturation is due to the modification of the redox conditions and therefore the variation of S speciation in the silicate melt (Fig.3.2). Sulfide saturation can be maintained for few tenths of wt% of assimilated anhydrite; for higher amounts of assimilation the proportion of the S^{2-} species rapidly decreases in the melt (Fig.3.2g,h,i), preventing sulfide saturation, while that of S^{6+} species increases (Fig.3.2j,k,l; Iacono-Marziano et al. 2017). The assimilation of about 3 wt% anhydrite is calculated to lead a fluid phase-free magma to sulfate saturation at 1200°C and 100 MPa (Fig.3.2j), while more than 6 wt% $CaSO_4$ are necessary if the magma is hotter (1350°C) and volatile-rich (2 wt% fluid phase; Fig.3.2l).

The increases in oxygen fugacity and in the S content of the melt due to anhydrite assimilation are predicted to mainly depend on temperature (Fig.3.2a,d) and the amount of fluid phase (Fig.3.2c,f), while pressure has a negligible effect (Fig.3.2b,e). The lower the temperature and the initial gas content of the magma, the higher the S content of the melt and the oxygen fugacity induced by the assimilation of a given amount of anhydrite (Iacono-Marziano et al. 2017).

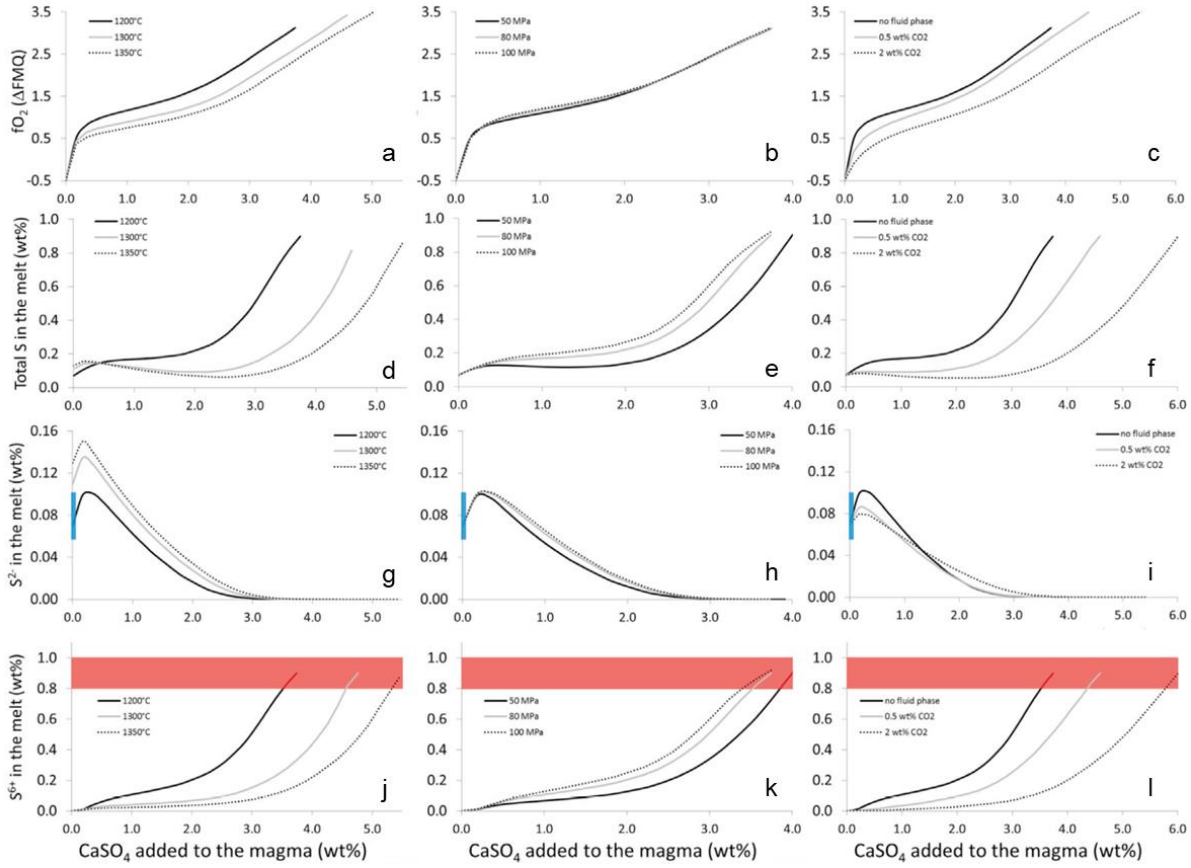

Fig.3.2. Results of thermodynamic calculations simulating anhydrite assimilation up to 5.5 wt% in a mafic magma containing 10.8 wt% total FeO. Evolution of the oxygen fugacity (fO_2), expressed as log units relatively to the Fayalite-Magnetite-Quartz buffer at 80 MPa and variable temperatures (a); at 1200°C and variable pressures (b); at 1200°C and 80 MPa and variable initial proportions of fluid phase (c). Evolution of the total sulfur content of the melt at 80 MPa and different temperatures (d); at 1200°C and variable pressures (e); at 1200°C and 80 MPa and variable initial proportions of fluid phase (f). Evolution of the reduced sulfur (S^{2-}) content of the melt at 80 MPa and different temperatures (g); at 1200°C and variable pressures (h); at 1200°C and 80 MPa and variable initial proportions of fluid phase (i). Evolution of the oxidized sulfur (S^{6+}) content of the melt at 80 MPa and different temperatures (j); at 1200°C and variable pressures (k); at 1200°C and 80 MPa and variable initial proportions of fluid phase (l). The blue boxes indicate the field of sulfide saturation obtained by the experiments at 1200°C, 80 MPa and fO_2 < FMQ-1, while the pink boxes indicate the field of sulfate saturation obtained by the experiments at 1200°C, 80MPa and fO_2 of FMQ + 3.5. From Iacono-Marziano et al. 2017.

In addition to chemical dissolution, the high temperature interaction of hydrous sulfates, such as gypsum, with a magma could imply the fluidization of the sulfate rock. As the hydrous salts lose their structural water, they are likely to behave as viscous fluids when interacting with magmas (Schofield et al. 2014). This behaviour has been observed in carnallite layers intruded by doleritic magma (see section 3.2.1), and is proposed to have the potential to mobilize salts at the scale of a sedimentary basin (Schofield et al. 2014).

3.1.2 **Effects on magma composition**

The main consequence of sulfate assimilation for the composition of the magma is the significant increase in the sulfur content of the silicate melt. By enhancing the oxygen fugacity of the magma, anhydrite assimilation may increase the S content of the silicate melt of a factor of 10 (Fig.3.1c; Iacono-Marziano et al. 2017, submitted). Sulfide-saturated mafic magmas at oxygen fugacities close to the Fayalite-Magnetite-Quartz (FMQ) buffer contain about 1000 ppm S dissolved in the silicate melt, while sulfate-saturated magmas at oxygen fugacities higher than FMQ+3 contain about 1 wt% S (e.g. Jugo et al. 2005; Jugo 2009; Iacono-Marziano et al. 2017). When the magma is sulfide saturated, anhydrite assimilatation therefore favours the dissolution of the sulfide melt (Fig.3.1d).

The CaO content of the silicate melt is also increased by anhydrite assimilation (Fig.3.1 b), and this probably limits olivine crystallization (Fig.3.1 e; Iacono-Marziano et al. 2017, submitted). At temperatures lower than 1200°C, this Ca-enrichment would probably favour clinopyroxene crystallization, as observed for limestone assimilation. In anhydrite-contaminated igneous rocks of the northern limb of the **Bushveld Complex**, olivine seems to be destabilized by the contamination, in favour of orthopyroxene. Olivine appears to be the liquidus phase together with Cr-spinel, rapidly replaced by orthopyroxene that is the dominant phase (Yudovskaya et al. 2018). Corroded olivine grains of amoeboid or round shapes are also observed in orthopyroxene-dominated rocks. A clear interpretation is however prevented by the heterogeneous nature of the anhydrite-bearing contaminants, which are variably enriched in aluminosilicates and carbonaceous material.

When the contaminant is constituted by relatively pure anhydrite, CaO addition, coupled with the inhibition of olivine crystallization and sulfide segregation, may also slightly decrease the SiO_2 content of the silicate melt (Fig.3.1 f). The high oxygen fugacity and the absence of sulfide melt in the sulfate-saturated magmas produced by extreme anhydrite assimilation favour the crystallization of Ni-rich olivine and Cr-bearing spinel (Iacono-Marziano et al. 2017, submitted).

Extreme assimilations (>3 wt% $CaSO_4$) may trigger anhydrite saturation in the silicate melt (Iacono-Marziano et al. 2017). Magmatic anhydrite has been observed in intrusive rocks that are produced by the crystallization of relatively reduced magmas, like those of the Bushveld Complex or of the Noril'sk-Talnakh intrusion**s** that belong to the Siberian Traps (Li et al. 2009a, b; Ripley et al. 2010; Yudovskaya et al. 2018). In the picritic gabbro of the **Kharaelakh intrusion** of the Noril'sk region, magmatic anhydrite is associated with disseminated sulfide ores (Fig.3.3a-c; Li et al. 2009a,b). Anhydrite is also observed in several rocks of the northern limb of the Bushveld Complex, in the form of interstitial crystals (Fig.3.3f) and as inclusions of round or irregular morphology in orthopyroxene (Fig.3.3d,e;

Yudovskaya et al. 2018). In both Noril'sk-Talnakh and Bushveld cases, anhydrite occurrence is ascribed to the assimilation of the evaporite-bearing country rocks (Li et al. 2009a, b; Ripley et al. 2010; Yudovskaya et al. 2018).

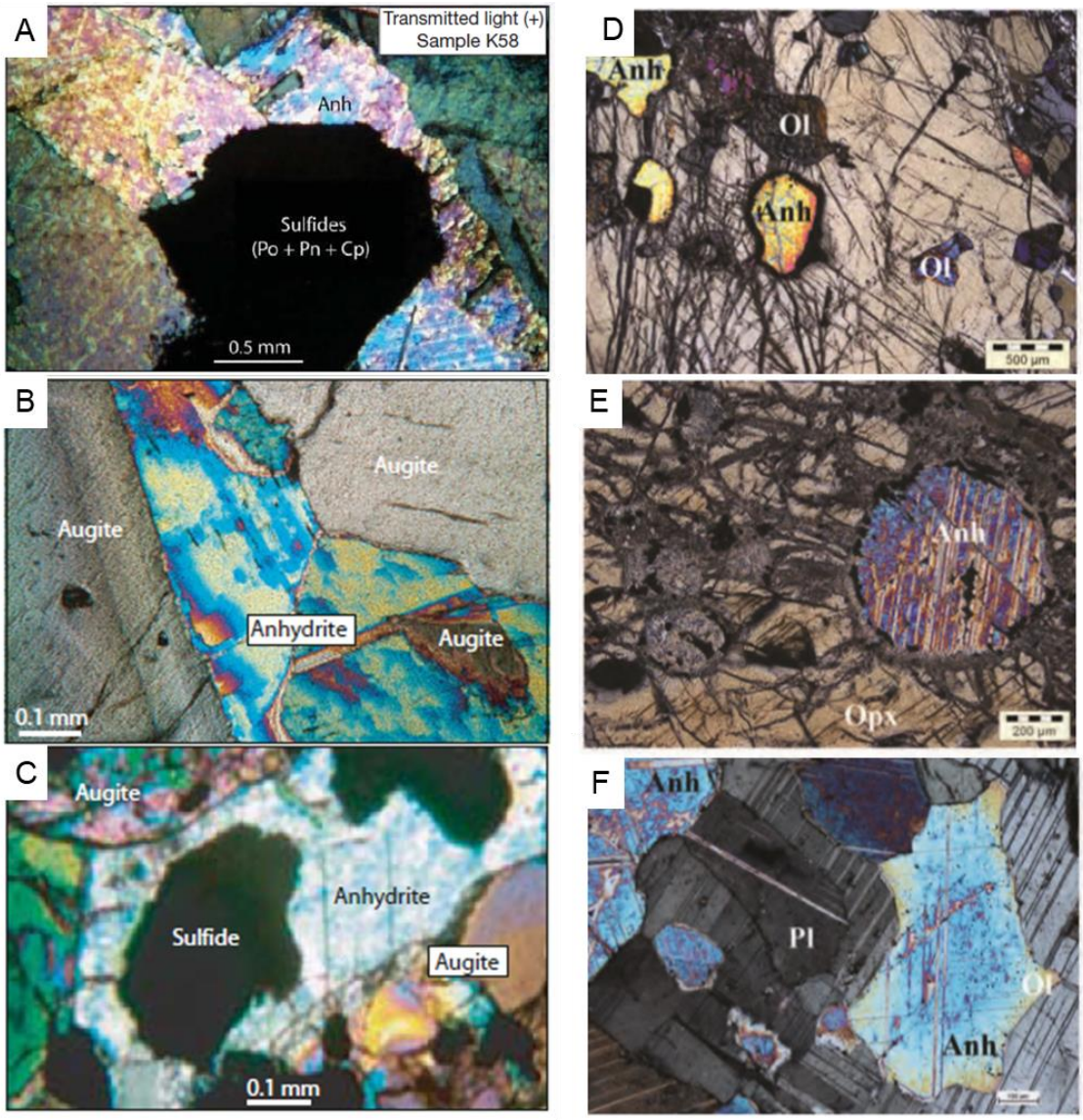

Fig. 3.3 (a), (b), (c) Photomicrographs of magmatic anhydrite-sulfide assemblages in the olivine-bearing (picritic) gabbros of the Kharaelakh intrusion. From Li et al (2009 a, b). (d), (e), (f) Anhydrite grains in Platreef contaminated mafic to ultramafic rocks. From Yudovskaia et al. (2018). Ol=olivine, Anh= anhydrite, Opx=orthopyroxene, Pl= plagioclase.

When the anhydrite-bearing host rocks contain other components, the petrology of the contaminated rocks can vary accordingly. Anhydrite-bearing host rocks at the northern limb of the Bushveld Complex present for instance variable proportions of aluminosilicate and carbonaceous material (Yudovskaya et al. 2018). The contaminated rock have therefore variable compositions, and the assimilation mechanisms are also likely to vary (see section 4.1). Granitic veins and quartz-bearing norites could

derive from the partial melting of SiO_2-rich portions of the host rocks. Anorthite-rich plagioclase and Al-rich orthopyroxene are likely to be the products of the reaction between anhydrite-bearing high-Al shales and ultramafic melts (Yudovskaya et al. 2018). Finally, magmatic sulfides can be produced by the assimilation of anhydrite-bearing sedimentary rocks, in the presence of a reducing agent that is generally represented by carbonaceous material (see sections 3.1.4 and 4.4): the higher the reduction experienced by the magma, the higher the amount of sulfide melt that can be segregated.

3.1.3 **Effects on volatile emissions**

The interaction of mafic magmas with evaporitic rocks produces SO_2-rich gases, their amount being controlled by the nature and the degree of interaction. Thermal decomposition of anhydrite would supply the highest amount of sulfur, but requires high temperatures that are not consistent with the thermal regime inferred for the contact aureoles (Yudovskaya et al. 2018 and references therein). If occurring, anhydrite thermal decomposition is therefore probably confined to the magma-whole rock contact. The amount of fluid phase produced by anhydrite assimilation is not particularly high, due to sulfur dissolution into the silicate melt. However, a significant portion of the assimilated sulfur can be degassed depending on the redox conditions of the magma: the lower the oxygen fugacity of the magma before anhydrite assimilation, the higher the amount of sulfur that can be degassed (Iacono-Marziano et al. submitted). In this case, as in that of partial melting, the amount of produced SO_2 mainly depends on the volume of magma interacting with sulfate rocks. Large igneous provinces represent the most voluminous magma productions over limited timescales (< 1 Ma; e.g. Courtillot and Renne 2003) and the best candidates for widespread interaction with crustal rocks (e.g. Svensen et al. 2015). A large-scale sill emplacement in the Amazonas and Solimöes basins, associated with the Central Atlantic Magmatic Province, is suggested to have extensively interacted with evaporitic rocks, in addition to carbonate and carbonaceous rocks (Heimdal et al. 2018). The end-Triassic environmental crisis is contemporaneous with the sill emplacement and implied major carbon cycle perturbations, global warming and mass extinction (Heimdal et al. 2019). Among the numerous processes proposed to have concurred to the mass extinction, high SO_2 concentration in the atmosphere are suggested to have caused ecosystem instability, the evidence being physiognomic changes and damage structures in fossil leaves (Bacon et al. 2013; Elliott-Kingston et al. 2014).

Sedimentary sulfates are highly enriched in $\delta^{34}S$, their assimilation is therefore likely to profoundly influence the sulfur isotopic composition of volcanic gasses, in addition to boosting their sulfur content. The assimilation of gypsum-rich sedimentary rocks is proposed to contribute to the intense sulfur degassing of Popocatépetl volcano, particularly during the 1993-1994 period, which saw an

increase in both seismic and fumarolic activity. During this period, Goff et al. (1998) measured heavy sulfur isotopic compositions of fumarolic gasses (up to 6.5‰ $\delta^{34}S$), and calculated that a minor assimilation of the Cretaceous gypsum (≤1 wt%) may account for them. These kind of estimations are however particularly complex, due to the fact that the fractionation factor between sulfur dissolved in the melt and exsolved in the fluid phase depends on the speciation of sulfur in both phases, which in turn depends on oxygen fugacity, temperature and water fugacity of the magma. Sulfur can indeed experience wide isotopic fractionation during volcanic degassing due to the differential partitioning of its isotopes among reduced and oxidized sulfur species in the gas and in the melt (e.g. Métrich and Mandeville 2010; Liotta et al. 2012).

The implication of sulfur-rich fluids in the genesis of hydrothermal deposits is discussed in the next section.

3.1.4 **Effects on redox conditions and ore processes**

As already discussed in section 3.1.1, sulfate assimilation oxidizes the magma by introducing oxygen. Thermodynamic calculations indicate that the oxydation is particularly important for low amounts of assimilation: in fluid phase-poor magmas the ingestion of few tenths of a percent of $CaSO_4$ generally increases oxygen fugacity of one log unit (Fig.3.2; Iacono-Marziano et al. 2017). The oxidation is more important at low than at high temperature (Fig.3.2a), and in the absence of a fluid phase coexisting with the magma (Fig.3.2c). Anhydrite assimilation therefore represents an effective way to strongly enrich the magma in sulfur and ensure its transport possibly over long distances (far from the source zone), provided that the magma remains oxidized. Extremely oxidized magmas resulting from the assimilation of anhydrite may indeed transport up to 1 wt% S dissolved in the silicate melt. The assimilation of gypsum is expected to further promote magma mobility, by introducing H_2O into the magma.

One of the consequences of sulfate assimilation is the destabilization of the sulfide melt (Fig.3.1 d). Sulfide segregation is suppressed when more than a few percent of anhydrite is assimilated (Iacono-Marziano et al. 2017). Evaporite assimilation alone is therefore likely not to be a genetic process for magmatic sulfide deposits, unless a reduction can occur by an independent process.

In the northern limb of the Bushveld Complex sulfide mineralization is commonly observed in the anhydrite-contaminated **Platreef** rocks (Yudovskaya et al. 2018). These contact-style mineralizations have generally lower tenors than those observed in the uncontaminated rocks of the eastern and western limb (Maier et al. 2008; Yudovskaya et al. 2018). This is due to the higher proportion of sulfides, which are commonly confined to the contacts between anhydrite and igneous of hybrid

lithologies. Anhydrite marbles and hornfels are generally barren, whereas low sulfide mineralizations found in anhydrite-rich rocks can locally present higher tenors (Yudovskaya et al. 2018). This suggests an important role of the carbonaceous component of the host rocks in controlling the amount of produced sulfide melt. The anhydrite-bearing rocks constituting the Platreef footwall are indeed shallow-marine sediments consisting of carbonaceous shales, carbonate rocks, anhydrite and quartzite (Duitschland Formation); the involvement of organic matter is indicated by abundant veinlet-disseminated graphite (see sections 4.2 and 4.4) in the Platreef magmatic rocks (Yudovskaya et al. 2018).

Similarly, anhydrite assimilation is also involved in the formation of Noril'sk-Talnakh ore deposits, coupled with an intense interaction with carbonaceous rocks. See next section for the isotopic evidence of anhydrite assimilation, and section 4.4 for the description of the ore deposits.

The assimilation of Triassic evaporites is proposed to be at the origin of brines and fluids forming the magnetite-apatite deposits along the **Middle and Lower Yangtze River** in China. Li et al. (2015) dismiss the orthomagmatic origin of these deposits, proposing that they were formed by fluids exsolving from magmas that assimilated substantial amounts of anhydrite and halite-bearing evaporites.

The involvement of evaporite-derived fluids is invoked for several iron oxide-copper-gold (IOGC) deposits (Chiaradia et al. 2006; Monteiro et al. 2008; Li et al. 2015 and references therein). These systems are extremely oxidized and the scarcity of sulfides in the mineralization does not straightforwardly reflect the low sulfur content of the fluids: the mineralizing fluids could simply be too oxidized for precipitating sulfides (Li et al. 2015).

3.1.5 Assimilation marker and tracers

Anhydrite assimilation can be difficult to recognize in the field, because it can occur distantly from where the magma finally crystallizes. Oxidized and sulfur-rich magmas produced by anhydrite assimilation can probably travel over long distances from the assimilation site because they do not experience massive crystallization and sulfide segregation. Ca enrichment due to assimilation is limited (0.4 wt% CaO for 1 wt% assimilated $CaSO_4$), but could be used as a tracer. The occurrence of magmatic anhydrite can also be an indicator of sulfate assimilation (Fig.3.3; Li et al 2009 a, b; Yudovskaya et al. 2018).

The clearest marker of sulfate assimilation by magmas is probably their sulfur isotopic composition. As most Proterozoic and Phanerozoic marine evaporite sulfates have heavy S signatures (10 ‰< $\delta^{34}S$ <35 ‰, Claypool et al. 1980), while mantle-derived magmas have significantly lighter signatures (the $\delta^{34}S$

of MORBs is 0.1 ± 0.5 ‰ or -0.91 ± 0.50 ‰, depending on the extraction method; Sakai et al. 1984; Labidi et al. 2012), relatively small amounts of assimilation (e.g. <1 wt.%) may significantly affect the sulfur isotopic composition of the assimilating magma.

In the **Noril'sk-Talnakh region** of the Siberian Traps (Russia), ascending magmas passed through thick sedimentary sequences (e.g. Likhachev 1994), and assimilated anhydrite-bearing rocks to different extents (e.g. Grinenko 1985; Naldrett et al. 1992, 1996; Arndt et al. 2003, 2005; Li et al. 2003, 2009 a, b; Ripley et al. 2010). The sulfur isotopic composition of sulfide mineralizations varies between -0.7 and 15‰ $\delta^{34}S$, the highest values being generally observed in the ore-bearing intrusions, and the lower ones in barren intrusions. Some uneconomic and subeconomic intrusions can however present relatively high values of $\delta^{34}S$ (Fig.3.4; Grinenko 1985; Li et al. 2003, 2009; Ripley et al. 2003, 2010; Malitch et al. 2014). Section 4.4 will clarify how the interaction with organic matter has been essential to trigger the segregation of sulfide melts in these intrusions.

It the northern limb of the Bushveld Complex, **Platreef** contact-style mineralization presents extremely wide variations of the $\delta^{34}S$ values (from -10 to 15‰). These variations are interpreted to be due to the highly heterogeneous isotopic composition of the different host-rock lithologies ($\delta^{34}S$ from -30 to 28‰), varying from anhydrite-bearing carbonaceous shales to almost pure anhydrite (Yudovskaya et al. 2018 and references therein). In contrast, reef-type mineralizations of the Platreef, which are considered to be formed by uncontaminated magmas, have generally homogeneous isotopic compositions ($\delta^{34}S$: 0 ± 2‰; Yudovskaya et al. 2018).

Also in the magnetite-apatite deposits along the **Middle and Lower Yangtze River** the main tracer of anhydrite assimilation is the sulfur isotopic signature of the anhydrite (+15.2‰<$\delta^{34}S$<+16.9‰) and pyrite (+4.6‰<$\delta^{34}S$<+12.1‰) associated to the mineralization (Li et al. 2015). The extrapolation of the anhydrite-pyrite pair data to zero anhydrite-pyrite fractionation suggests a total sulfur isotopic composition of the fluids of about + 16‰ (Li et al. 2015).

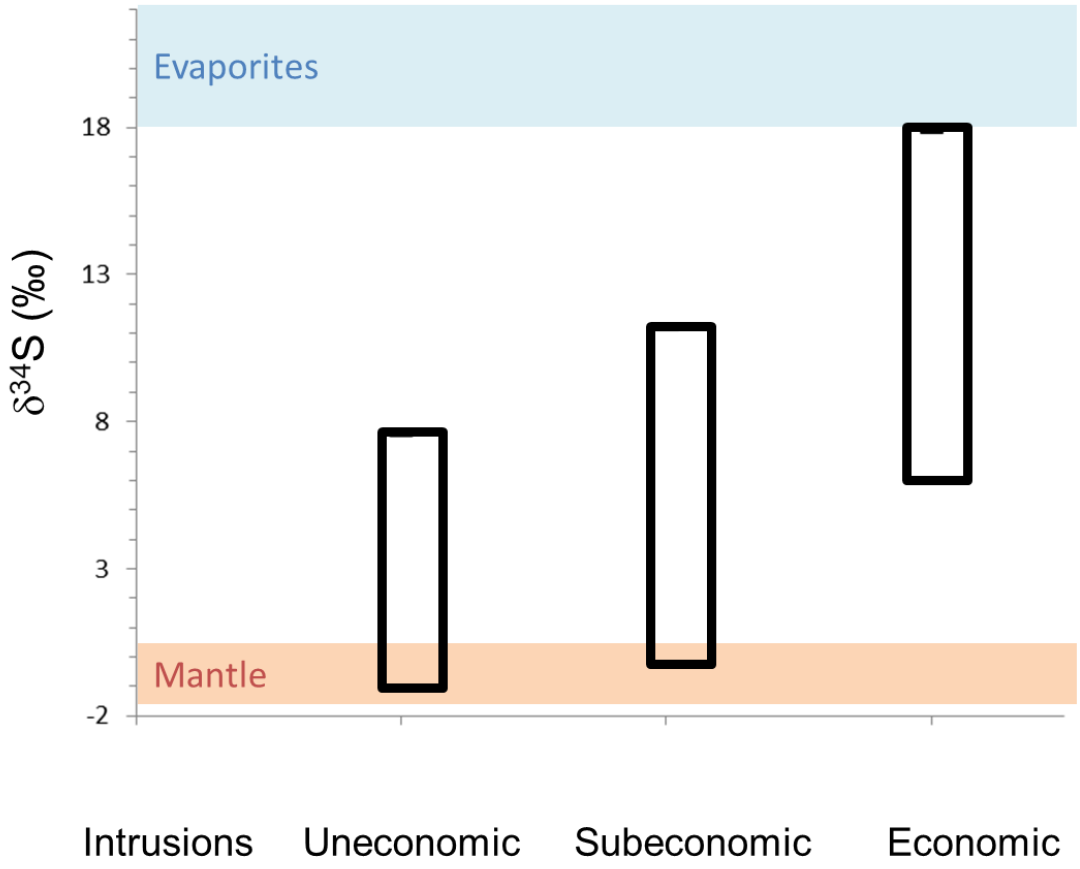

Fig.3.4.Sulfur isotopic composition of uneconomic, subeconomic and economic intrusions of the Noril'sk-Talnakh region. Data from Grinenko 1985; Li et al. 2009; Ripley et al. 2003, 2010; Malitch et al. 2014.

The Sr isotopic composition and content of the magma could also reveal the assimilation of sedimentary sulfates, which are generally enriched in Sr (Arndt et al. 2003). However, a contribution from detrital sediments, which have higher $^{87}Sr/^{86}Sr$ ratios, could mask the existing trends (Pang et al. 2013). Strontium isotopic composition ($^{87}Sr/^{86}Sr$) is indeed used to track anhydrite assimilation both at the Bushveld Complex (Yudovskaya et al. 2018) and in the Noril'sk-Talnakh intrusions (Arndt et al. 2003; Pang et al. 2013), but the high variability of the $^{87}Sr/^{86}Sr$ ratio of the contaminant makes the interpretation difficult.

3.2 Chloride-bearing rocks

3.2.1 Mechanisms of assimilation

No experimental work has been performed to simulate magma-chloride interactions; the available information on assimilation mechanisms concerns the larger field scale. Salt composition appears to control where ascending magmas can intrude as sills in a sedimentary sequence. Schofield et al. (2014) show that doleritic magmas preferentially intrude hydrous salts, e.g. carnallite, than anhydrous ones, e.g. halite (Fig.3.5). This could be due to (i) the loss of structural water at low temperatures (<200°C), resulting in the viscous behaviour of the salt, which can therefore act like a fluid and favour lateral magma intrusion (Schofield et al. 2014), and/or (ii) the melting of the hydrous salts. Salts have indeed relatively low melting temperatures, both sylvite and halite melt at ~800°C in anhydrous conditions (Mitchell and Kjarsgaard 2008), while halite can melt at temperatures lower than 200°C in the presence of water (Driesner and Heinrich 2007). Melting is therefore the most likely mechanism for hydrous salt assimilation.

At the basin scale, salt melting and/or dehydration can potentially lead to salt mobilization (halokinesis) contemporaneous to magma emplacement (Schofield et al. 2014).

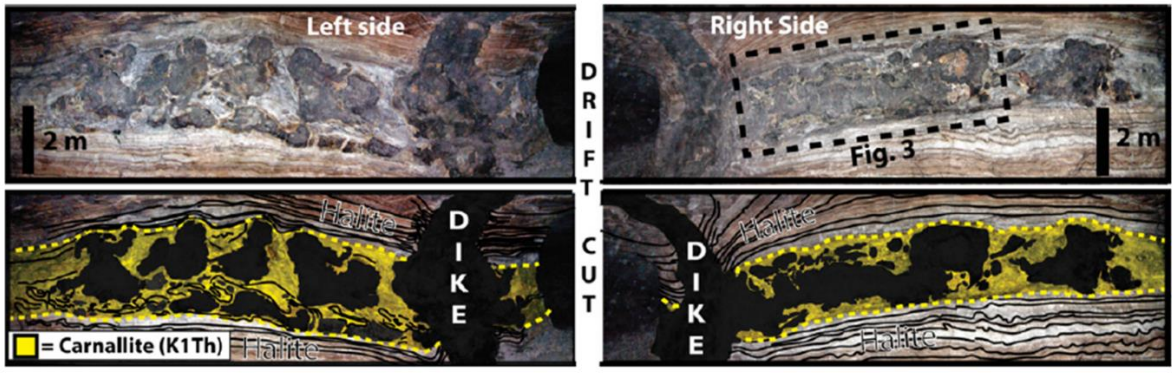

Fig.3.5.Doleritic magmas preferentially intruding hydrous salts (carnallite) than anhydrous ones (halite). From Schofield et al. 2014.

Magmatic intrusions into Permian hydrous salts is considered responsible for the formation of the hydrothermal vent complexes in the southern North Sea, as a result of salt dissolution, fluid pressure propagating upward and extrusion of remobilized sediments (Blažić and Moreau 2016). The interactions between magmas and saliferous rocks are also suggested to be at the origin of the pipe structures and the associated magnetite ores in the Southern Siberian Platform (Mazurov et al. 2007; Svensen et al. 2009). These complex ore-bearing volcano-tectonic structures are proposed to form at the top of mafic sills or shallow-seated magma chambers via the disintegration of the magma into

fragments and the mingling with melted saliferous rocks (Mazurov et al. 2007). The resulting salt solution-melt is considered to be the metasomatic agent altering the country rocks and producing the magnetite ores (Mazurov et al. 2007; see also section 3.2.4).

3.2.2 Effects on magma composition

Heimdal et al. (2019) recognize a significant enrichment in the biotite Cl content of doleritic sills contaminated with halite-rich evaporitic rocks. The doleritic sill were emplaced in the **Salimöes and Amazonas Basins**, in Brazil, and belong to the Central Atlantic Magmatic Province (CAMP). Samples presenting the highest Cl contents in biotite are generally the most evolved ones, i.e. alkali- and silica-richest and MgO- and CaO-poorest; they also have the highest Sr, Rb, and Ba contents. However, no particular evidence of an effect of halite assimilation on phase equilibria is observed, as the phase assemblage is the same in both Cl-rich and Cl-poor samples (Heimdal et al. 2019).

The main effect of the assimilation of halite-rich evaporitic rocks is therefore likely to be the increase in the halogen and alkali content of the magma. Evidence of this process are observed in intrusive rocks of the **Siberian Traps**, where two types of evaporitic rocks are present in the sedimentary basin: (1) salt-rich, anhydrite poor Cambrian evaporites that are thicker in the southern part and probably absent in the northern part, and (2) salt-poor, anhydrite-rich Devonian evaporites that occur only in the northern part, although their extent is not precisely known (Fig.3.6). Sobolev et al. (2009) describe Cl, K and B enrichment in olivine-hosted melt inclusions from the most primitive rocks of the Noril'sk region and attribute them to the contamination by evaporitic rocks. Markedly higher Cl (and F contents) are however observed in melt inclusions in olivine, plagioclase and clinopyroxene crystals from doleritic sills of the southernmost parts of the Siberian Traps (Fig.3.7; Black et al. 2013), where the Cambrian salts present the highest thickness. In contrast, melt inclusions from lava flows and mafic tuffs of the Maymecha-Kotuy region (in the northern part of the Traps, Fig.3.6a) show much lower Cl and F contents, but higher S contents (Fig.3.7; Black et al. 2013). Whereas olivine-hosted melt inclusions in Sobolev et al. (2009) have primitive compositions, these S-richer inclusions present more evolved compositions, suggesting that they experienced higher degrees of interaction with the anhydrite-rich, halite-poor Devonian evaporites.

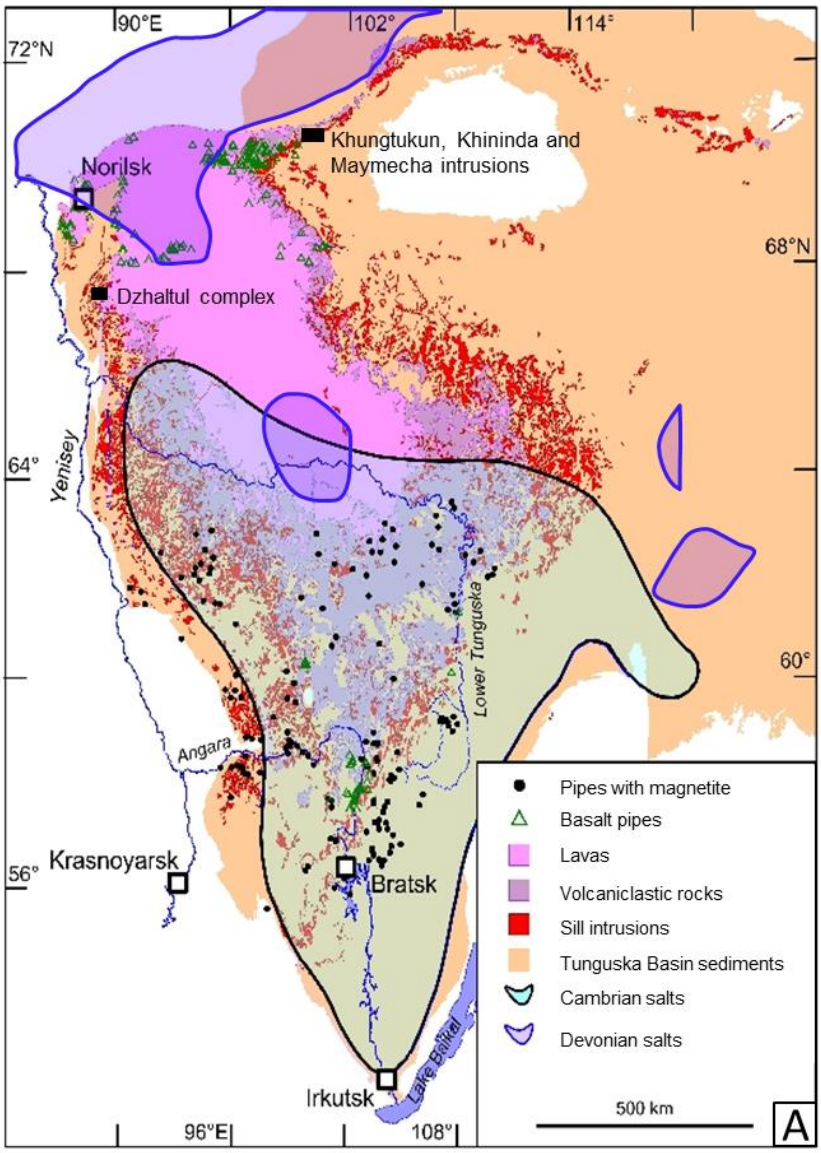

Fig.3.6. (a)

Geological map of the Tunguska Basin, showing the distribution of effusive and intrusive rocks, and sediments of the Tungusskaya series. The dark and light blue areas show the approximate extent of the Devonian and Cambrian evaporite-bearing sediments at depth. The black spots identify the phreato-magmatic pipes with magnetite. Modified from Malich et al. (1974), Zharkov (1984), Petrychenko et al. (2005) and Svensen et al. (2009).

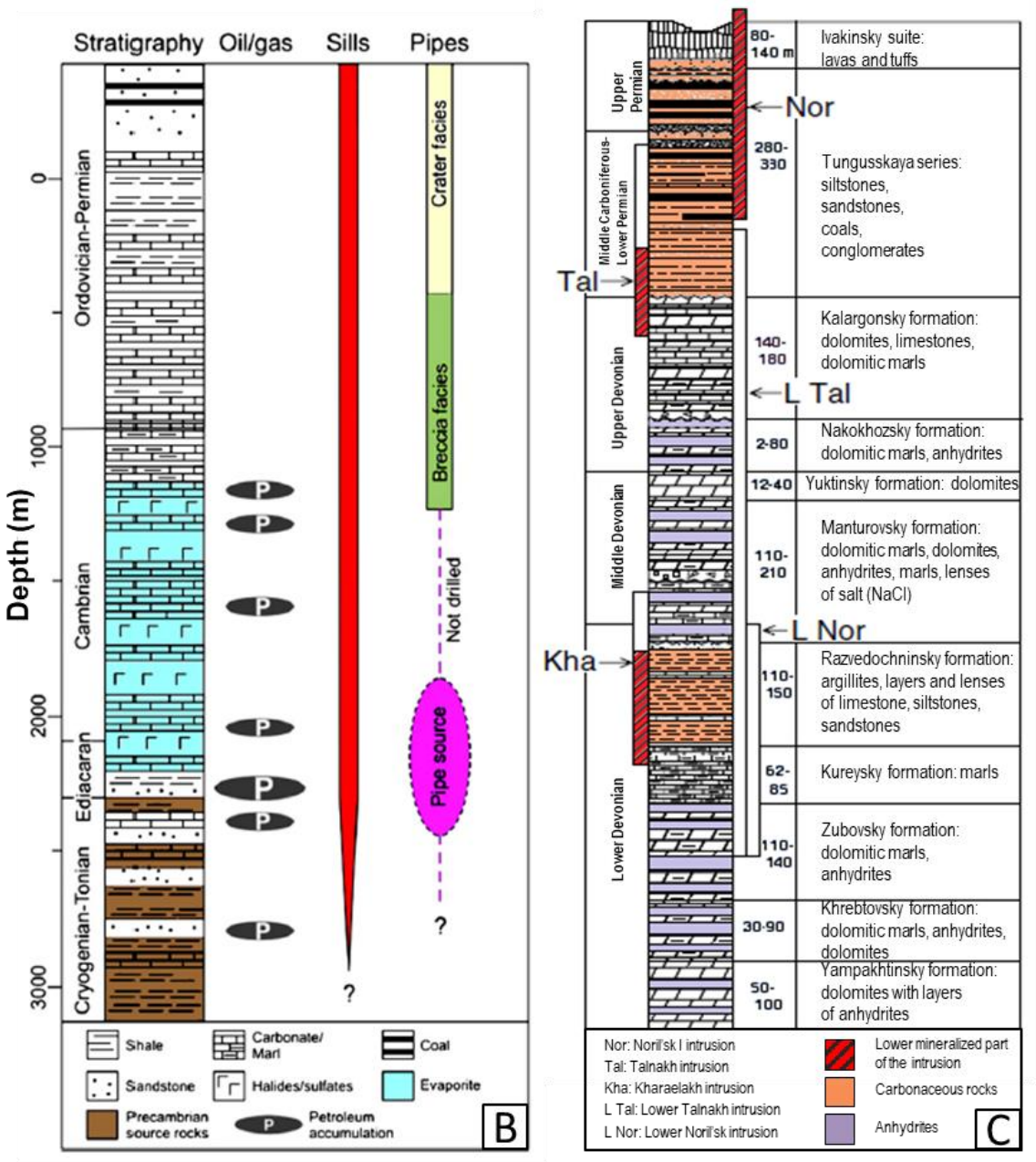

Fig.3.6. (b) Schematic stratigraphy considered representative of the basin segment with the pipes. The pipes are rooted in the Cambrian evaporite or possibly deeper. The thickness of the Precambrian strata vary considerably (1-10 km) but has not been drilled in the central parts of the basin. From Svensen et al. 2009.

(c) Generalized stratigraphic column of the Noril'sk-Talnakh region modified from Zen'ko and Czamanske 1994.The average thickness, the name and the rock types of the Silurian to Permian formations are shown. In purple the anhydrite-rich rocks and in orange the terrigenous rocks. The stratigraphic position of the intrusions is also shown (Nor: Noril'sk 1, Tal: Talnakh, L Tal: Lower Talnakh, L Nor: Lower Noril'sk, Kha: Kharealakh); the bars in red represent the lower, ore-bearing part of the intrusions.

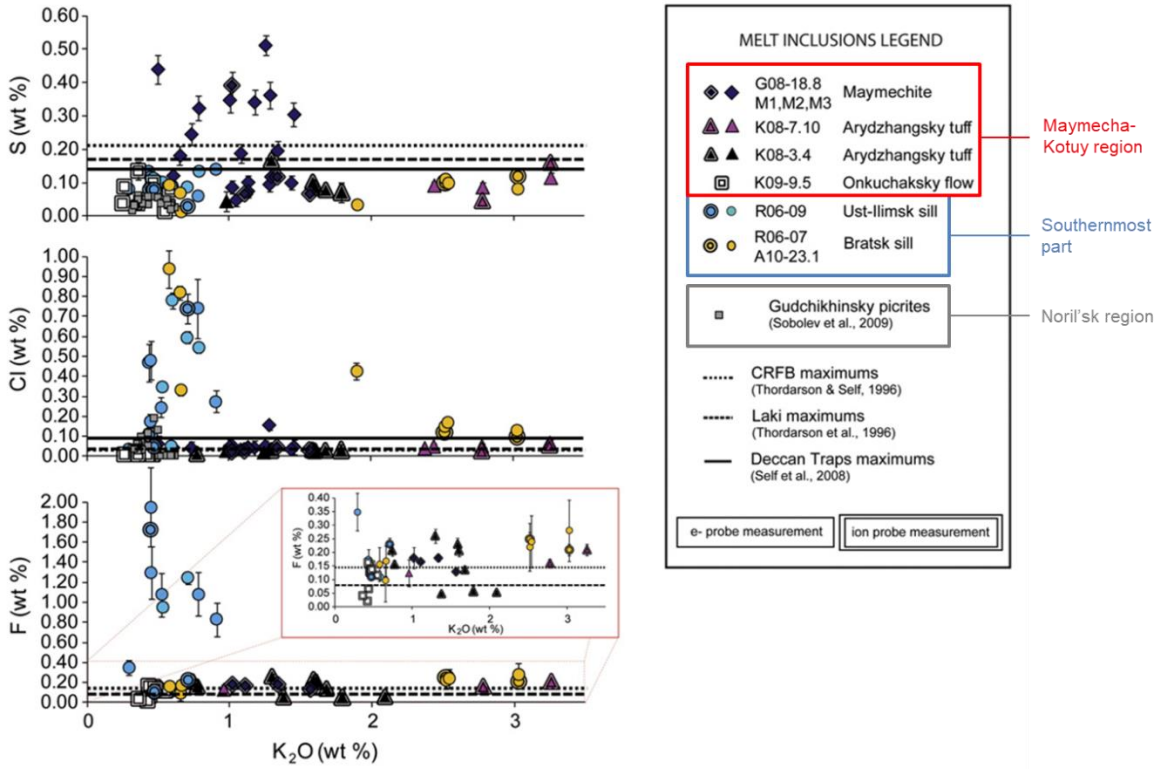

Fig.3.7. S, Cl, and F contents of olivine, plagioclase and clinopyroxene-hosted melt inclusions from the Noril'sk, the Maymecha-Kotuy and the Bratsk regions, respectively in the northwestern, norteastern and southern part of Siberian Platform. The maximum concentrations measured in Deccan Traps, Columbia River flood basalts (CRFB), and Laki melt inclusions are also shown. From Black et al. 2013.

3.2.3 Effect on volatile emissions

In the southern part of the **Siberian Platform**, where the sedimentary sequence includes Cambrian evaporites (Fig.3.6 a,b), volcanoclastic rocks are more abundant than lavas and magnetite-rich phreatomagmatic pipes are frequent (Fig.3.6 a; Svensen et al. 2009). This suggests that the interaction with the Cambrian salts produces abundant volatiles that ascend together with the magma, causing explosive activity. It is unclear whether the nature of the evaporitic rocks (halite-dominated Cambrian evaporites versus anhydrite-dominated Devonian evaporites), or the depth of interaction may play a major role in controlling magma explosivity.

Rock salts are often associated to oil and gas accumulations. Svensen et al. 2009 present both gas extraction and heating experiments on petroleum-bearing salt samples from a borehole in Nepa (Siberia). In gas extraction experiments fluid inclusions in salt samples from the contact aureole of a dolerite sill are crushed and the composition of the liberated gases is analysed. Released gases are mainly butane and benzene and sulfur-bearing gases. In contrast, in heating experiments of several salt samples to 275°C produce sulfur dioxide and halocarbons like methyl chloride and methyl bromide.

These two gases are attributed to reaction between petroleum-bearing fluid inclusions and the host salt and may have important environmental consequences due to their involvement in stratospheric ozone depletion (Svensen et al. 2009 and references therein). No studies have explored gas release due to higher temperature interactions between magmas and salts.

3.2.4 Effect on redox conditions and ore processes

There are no clear indicators of the effect of chloride assimilation on the redox state of the magma, in part because chlorides are generally accompanied by sulfates in evaporitic rocks, making difficult to distinguish between their effects.

Different types of magnetite ore deposits are associated with the interaction between mafic magmas and evaporitic rocks, and the subsequent production of abundant high-salinity brines that are able to extract iron from the magma and concentrate it in ore bodies. This is the case of magnetite-apatite deposits of the **Middle and Lower Yangtze** metallogenic belt, which are linked to the assimilation of anhydrite and halite-bearing evaporites (Li et al. 2015; already discussed in section 3.1.5). Also the magnetite ore deposits of the **Tunguska Basin** pipes are proposed to originated with iron leaching from the magma by hypersaline brines, and precipitation in the pipe breccia (Mazurov et al. 2007; Svensen et al. 2009; Neumann et al. 2017). This sort of contact metasomatism is proposed to begin at the magmatic stage and complete at the low-temperature hydrothermal stage (Mazurov et al. 2007). Magnetite is interpreted to co-precipitate with apatite during fluid flow through the pipe breccias (Neumann et al. 2017). Moreover, iron oxide-copper-gold (IOGC) deposits are also commonly associated with evaporite-derived fluids, although the exact nature of the fluid is often debated (Barton and Johnson 1996; Chiaradia et al. 2006; Xavier et al. 2008; Barton 2014).

Dissociating the effect of sulfates from that of chlorides is quite difficult in these natural cases, because the two salts are often associated. However a main role of chlorides, and particularly hydrous chlorides (see section 3.2.1) can be anticipated, because the salinity of a fluid controls its capacity of transporting iron, as iron is preferentially transported in the form of chloride complexes (Li et al. 2015 and references therein). Similarly, most metals such as Cu, Au and Pd are shown to be effectively transported by Cl-bearing, sulfur-free, oxidizing fluids (e.g. Candela & Holland 1984; Williams et al. 1995; Frank et al. 2002; Simon et al. 2005; Bazarkina et al. 2014).

3.2.5 Assimilation markers and tracers

Strong halogen enrichments in magmatic fluid or melt inclusions and/or halogen-bearing minerals are probably the strongest indicators of the assimilation of chloride salts. Chlorine and fluorine enrichment in melt inclusions can reach 1 wt% Cl and 2 wt% F, when halite-rich sedimentary rocks are assimilated (Fig.3.7; Black et al. 2012)

High chlorine and fluorine contents of biotite are observed in doleritic sills emplaced in halite-rich sedimentary rocks (Heimdal et al. 2019). Cl enrichments reaches 4.7 wt% and have never been observed before in magmatic biotites, but only in biotites found in skarns (up to 7.15 wt%; Tracy 1991). The average Cl content of the biotite in each dolerite sample is positively correlated with the whole rock $^{87}Sr/^{86}Sr$ ratio, suggesting that magmatic contamination with halite-rich sedimentary rocks also affect strontium isotopic composition (Heimdal et al. 2019).

4. Organic matter-rich rocks

4.1 Mechanisms of assimilation

The mechanisms of assimilation of coal-bearing rocks are characterized by means of interaction experiments performed at 1200°C and ~70 MPa (Iacono-Marziano et al. 2017; submitted). The experiments show that the assimilation of coal releases an abundant fluid phase (i.e. the gas bubbles in Fig.4.1), due the production of C-H species by coal destabilization. These reduced species decrease water activity and dehydrate the silicate melt, enhancing the formation of the fluid phase. On the basis of thermodynamic calculations constraining C-H-O equilibria (Iacono-Marziano et al. 2012a), coal incorporation into the magma can be simplified as:

$$CH^{coal} + y\ H_2O^{silicate\ melt} \rightarrow (y+1/2)\ H_2^{fluid} + y\ CO^{fluid} + (1-y)\ C^{graphite} \quad (4.1)$$

where y varies between 0 and 1 mainly depending on pressure. When y=0, coal converts into graphite and H_2, without any production of carbon monoxide and any dehydration of the silicate melt (high pressure). On the contrary, when y=1, degassing and silicate melt dehydration are maximum, and coal is completely devolatilized into CO and H_2 (low pressure). The clearest consequence of the silicate melt dehydration is the crystallization of silicate minerals, i.e. olivine, plagioclase and clinopyroxene (Fig. 4.1).

In Fe and S-rich magmas, the assimilation of coal triggers the segregation of a sulfide melt (Iacono-Marziano et al. 2017, submitted). Sulfide segregation is due to the reduction of the magma that causes the decrease of the sulfur content of the silicate melt at sulfide saturation (SCSS) and therefore the accumulation of the excess sulfur into the sulfide melt. In the experimental samples, the sulfide melt commonly concentrates at the silicate melt-coal interface (Fig.4.1e,f). The presence of Ca-Mg-Fe carbonates in the coal seems to favour the accumulation of the sulfide melt within the coal xenoliths: this is possibly due to the higher porosity of these areas, owing to decarbonation of the Ca-Mg-Fe carbonates (Iacono-Marziano et al. submitted).

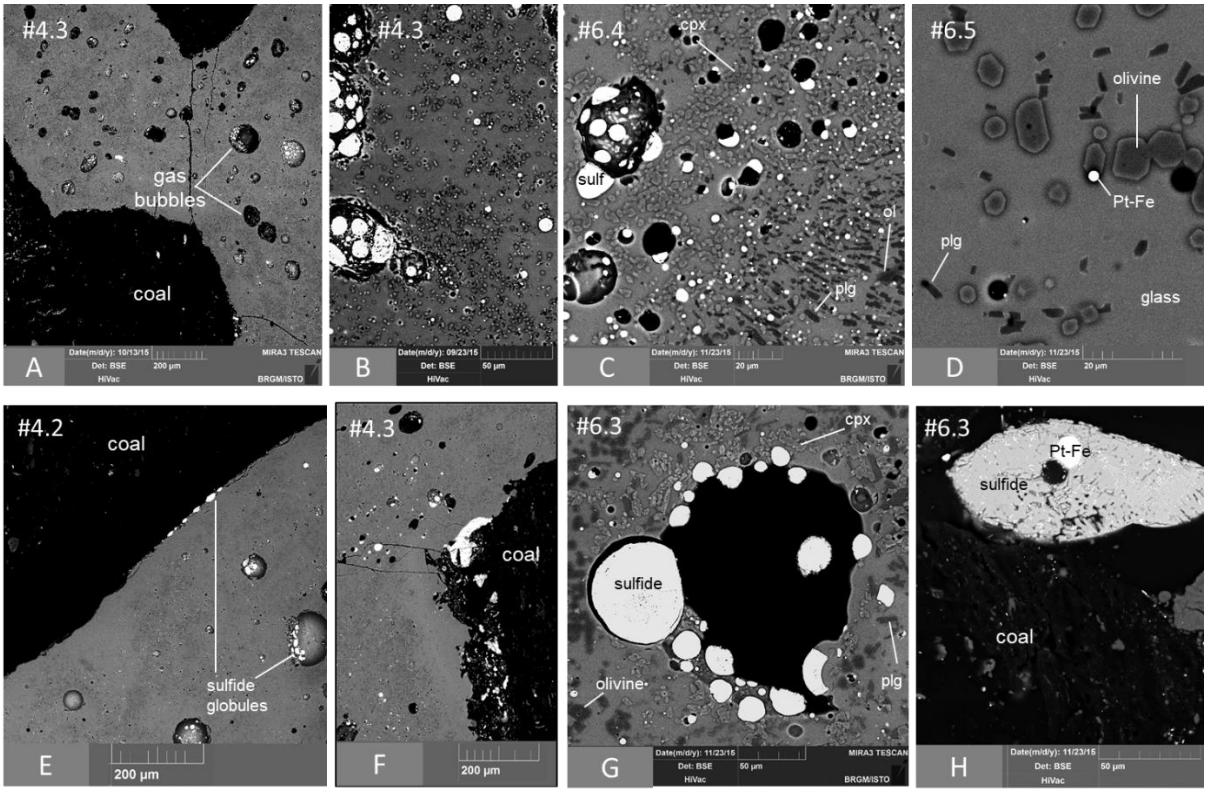

Fig.4.1. BSE images of experimental samples with coal addition. Experimental temperature and pressure are 1200°C and 75±7 MPa. The experimental duration is 10 minutes for (a), (b), (e) and (f), and 145 minutes for (c), (d), (g) and (h). Sulf: sulfide globule; cpx: clinopyroxene; plg: plagioclase; ol: olivine; coal: coal residues; Pt-Fe: Pt-Fe alloys. From Iacono-Marziano et al. submitted.

If the carbonaceous rocks contain abundant SiO_2-Al_2O_3-rich fractions, as in argillites and shales, these fractions are likely to undergo partial melting. This process is particularly evident in the Partridge intrusion of the **Duluth complex** (USA), where norite rocks are observed in proximity of country-rock xenoliths or at the base of the intrusion and are interpreted to represent a hybrid magma. This hybrid magma would be produced through mixing between the parental basic magma and an anatectic melt deriving from the partial or total melting of the Virginia Formation shales, which are one of the host rocks of the intrusion (Thériault and Barnes 1998; Thériault et al. 2000; Queffurus & Barnes 2014). Samalens et al. (2017) studied assimilation mechanisms of these sulfide-rich black shales, and more particularly of the Bedded Pyrrhotite Unit, a stratigraphic unit within the Virginia Formation (Fig.4.2). Textural observations and geochemical analyses show that (i) shale xenoliths undergo partial melting producing an anatectic silicate melt coexisting with a sulfide melt, (ii) the anatectic melt is expelled from the xenoliths carrying droplets of sulfide melt, and transferring them to the mafic magma, (iii) diffusion of Ni, Cu and PGE occur from the mafic magma to the sulfide melt, while diffusion of As and Sb from the xenoliths to the mafic magma (Fig.4.2).

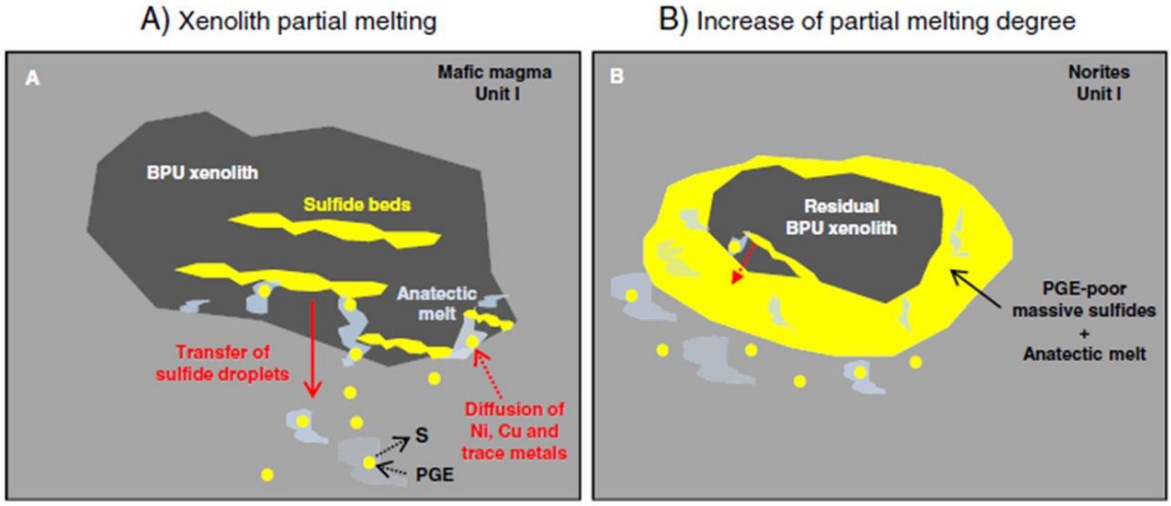

Fig.4.2 Schema illustrating magma contamination by the Bedded Pyrrhotite Unit (BPU) at the Partridge River Intrusion, Duluth Complex (USA). (a) Partial melting of carbonaceous S-bearing xenoliths. Sulfides are transferred to the mafic magma via anatectic silicate melt, leading to S and semimetal (As, Sb) contamination of the mafic magma. Diffusive transfer of Ni, Cu and PGE from the mafic magma to the sulfide droplets. (b) Massive sulfide accumulation after increase of partial melting degree. Massive sulfides are PGE-poor due to the lack of interaction with the magma. From Samalens et al. 2017.

Localized partial melting is also observed within a few centimetres of the contact between a dolerite sill associated with the Tertiary continental rifting and the hosting Cullaidh Shales on the **Isle of Skye** in Scotland (Yallup et al. 2013). In this context, the sulfur and carbon content of the shale increases with distance away from the sill contact, suggestive of sulfur and carbon degassing during interaction. Differently, the S content of the dolerite is substantially higher at the contact than in the rest of the sill (up to 0.39 wt% instead of 0.001-0.1 wt%), implying that at least part of the sulfur provided by the country rock is incorporated into the magma.

An alternative mechanism is proposed to transfer S from argillitic country rocks to the magma: break-down of sulfide minerals and incorporation of S-rich fluids into the magma (e.g. Ripley 1981). However, Robertson et al. (2015a) show that physical incorporation, melting and/or dissolution of country rock xenoliths are significantly faster than thermal decomposition of wall-rock minerals and diffusive or advective transport of the produced fluids into the magma. Xenolith incorporation by melting or dissolution is therefore likely to represents a more efficient mechanism to incorporate sulfur in a mafic magma from argillite-shale xenoliths.

4.2 **Effects on magma composition**

Coal assimilation by a hydrous mafic magma triggers plagioclase and clinopyroxene crystallization, due to the decrease in the H_2O content of the silicate melt (Iacono-Marziano et al. 2017, submitted). This also markedly boosts olivine crystallization, accelerating magma differentiation and producing SiO_2-richer and MgO-poorer magmas.

Moreover, the assimilation of organic matter by magmas reduces iron and the elements with variable valences in the silicate melt. In S-rich magmas the segregation of a sulfide melt is favoured (section 4.4). In experiments at relatively S-poor conditions a basaltic melt in graphite-lined Pt capsules was observed to form intergrowth of sullfide melt with Pt_3Fe alloy (Baker et al. 2001). In S-free experimental samples (Iacono-Marziano et al. submitted) coal assimilation produces Pt-Fe alloys, due to the availability of platinum from the Pt capsule (Fig.4.1d). In natural basaltic magmas the same process generates magmatic native iron enriched in siderophile elements (Fig.4.3), as observed at **Disko Island** in Greenland, **Bühl** in Germany and in several trap intrusions in the North and North-west of the **Siberian Platform** (Iacono-Marziano et al. 2012a and references therein; Pernet-Fisher et al. 2017).

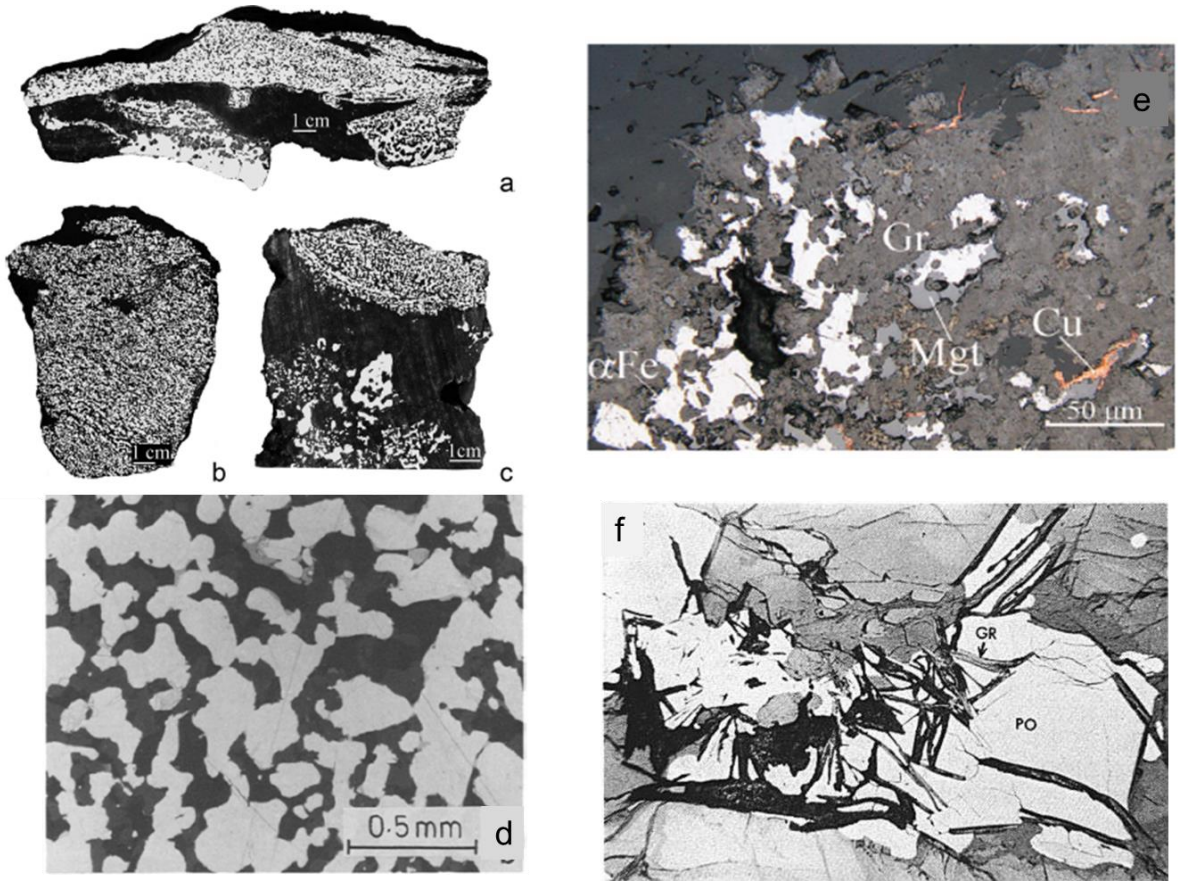

Fig. 4.3 (a), (b), (c) native iron blebs from the Dzhaltul and Khungtukun complexes in Russia (from Ryabov and Lapkovsky 2010). (d) sponge-like intergrowth of iron, silicates and troilite from Bühl, West

Germany (from Medenbach and El Goresy 1982). (e) ilmenite, native iron and native copper in graphite from Russian intrusions (from Ryabov and Lapkovsky 2010). (f) graphite filaments associated with pyrrhotite, olivine and biotite from the Water Hen intrusion of the Duluth Complex, USA (from Mainwaring and Naldrett 1977).

The typical silicate mineral assemblage of the rocks containing native iron consists of olivine, plagioclase, and less often clinopyroxene (Medenbach and El Goresi 1982; Pedersen and Larsen 2006; Pernet-Fisher et al. 2017). Native iron is often associated with minor graphite, wüstite, armalcolite, carbides, sulfides, ulvöspinel and several other reduced phases including native copper and native lead (Fig.4.3a-f; Ulff-Møller 1985; Ryabov and Lapkovsky 2010). Native iron is inferred to precipitate at temperatures higher than 988°C before the crystallization of ulvöspinel, due to the occurrence of iron-troilite eutectic inclusions in ulvöspinel (Medenbach and El Goresi 1982).

The occurrence of native iron and/or graphite in the contaminated rocks depends on the equilibration pressure and the degree of contamination, owing to the strong pressure-dependence of the carbon-oxygen equilibria (eq. 4.1), and the redox-dependence of the iron-oxygen equilibria. Pedersen and Larsen (2006) discuss the petrographic variability of the magmatic rocks of the southern part of the **Nuussuaq Basin**, in central West Greenland, where Palaeocene picritic magmas extensively interact with Mesozoic to Palaeocene carbonaceous clastic sediments (Fig.4.4a). The crustally contaminated rocks occur as dykes, necks, craters, lava flows and tuffs and they are all erupted from shallow-level magma chambers in contact with carbonaceous sediments. The andesitic tuffs (from Nuussuaq) are rich in graphite (up to several wt% of disseminated graphite) and poor in or free of native iron, while the andesitic lavas (from Disko) have much less graphite and more native iron. All rocks more evolved than basalt in Disko and Nuussuaq are considered to have been formed by repeated episodes of assimilation of crustal material, and include native-iron-bearing andesites, dacites and rhyolites (Larsen and Pedersen 2009). The native iron of Disko lavas is estimated to equilibrate at atmospheric pressure, while the graphitic tuffs are suggested to be quenched at pressures of 10-50 MPa (Pedersen and Larsen 2006).

Native iron segregation occurs at oxygen fugacity lower than FMQ-6 and low pressure by graphite volatilization (Iacono-Marziano et al. 2012a):

$$C^{graphite} + FeO^{magma} \rightarrow CO^{fluid} + Fe^{native} \quad (4.2)$$

Native iron formation therefore consumes graphite and produces CO. Iacono-Marziano et al. (2012a) calculated a maximum pressure of 10-12 MPa for native iron saturation in basaltic magmas with 8-13 wt% total FeO at 1200°C. At higher pressures graphite is stabler and no FeO is reduced to native Fe, i.e. equilibrium (4.2) is shifted to the left.

The occurrence of graphite, in the form of filaments, flakes, masses or inclusions is also observed in association with magmatic sulfide ores, as for instance in the Water Hen and the Partridge River intrusions of the **Duluth Complex** (Fig.4.3g; Mainwaring and Naldrett 1977; Samalens et al. 2017).

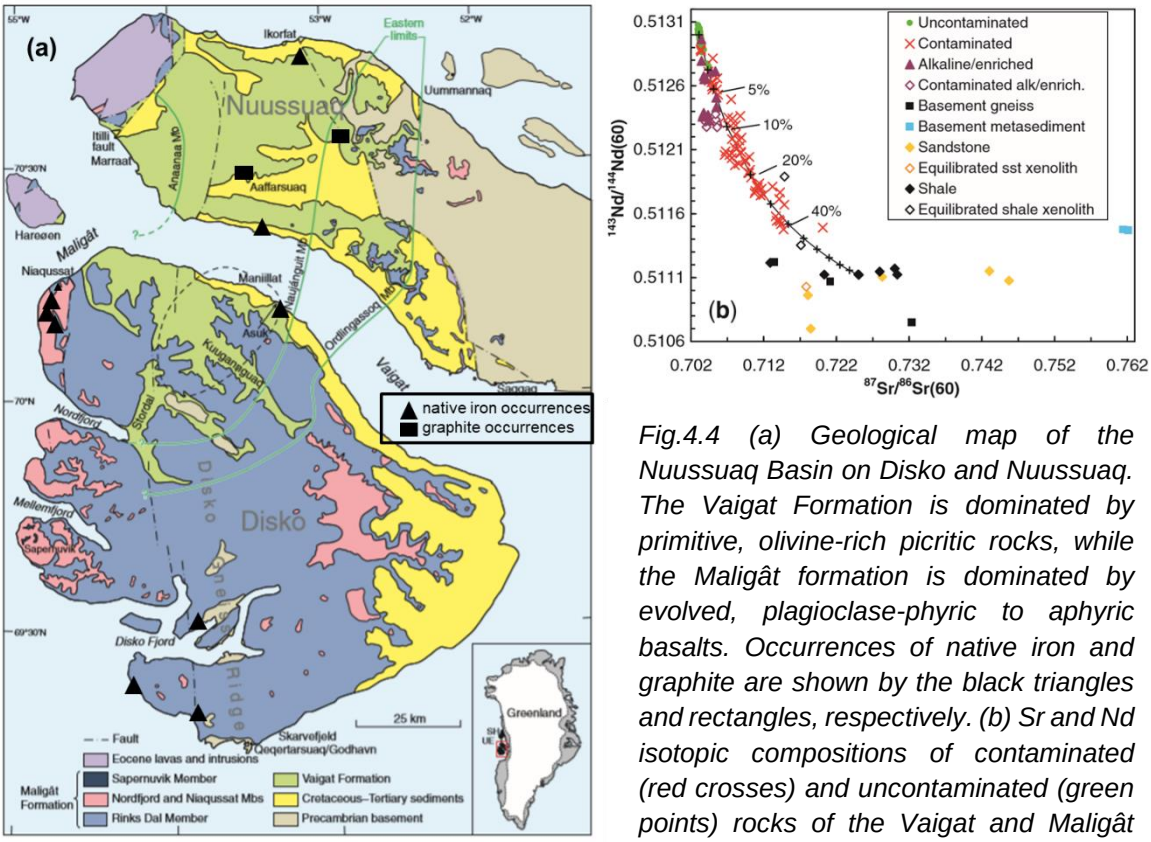

Fig.4.4 (a) Geological map of the Nuussuaq Basin on Disko and Nuussuaq. The Vaigat Formation is dominated by primitive, olivine-rich picritic rocks, while the Maligât formation is dominated by evolved, plagioclase-phyric to aphyric basalts. Occurrences of native iron and graphite are shown by the black triangles and rectangles, respectively. (b) Sr and Nd isotopic compositions of contaminated (red crosses) and uncontaminated (green points) rocks of the Vaigat and Maligât Formations.

The Cretaceous shales and sandstones of the Nuussuaq Basin (black and yellow diamonds) are used as contaminant to draw the mixing curve: Sr=230 ppm, Nd=39 ppm, $^{87}Sr/^{86}Sr(60)=0.7250$, $^{143}Nd/^{144}Nd(60)=0.5111$. Uncontaminated picrite end-member: Sr=120 ppm, Nd=7 ppm, $^{87}Sr/^{86}Sr(60)=0.7031$, $^{143}Nd/^{144}Nd(60)=0.5130$. From Larsen and Pedersen 2009.

4.3 **Effects on volatile emissions**

The assimilation of organic compounds increases the amount of fluid phase coexisting with the magma and radically modify its composition (Iacono-Marziano et al. 2012 a, 2017). Solovova et al. (2002) characterized melt and fluid inclusions in olivine crystals and in the glass of two native-iron bearing rocks from Disko Island. The high temperature composition of the fluids cannot be directly inferred from the solid phases observed in the fluid inclusions at room temperature. The authors evaluate the composition of the high temperature (1450°C) fluids in equilibrium with native iron, iron carbide and sulfide melt using thermodynamic calculations: estimated fluids are CO-H_2-dominated at pressures lower than 200 bar, and H_2-CH_4-dominated at higher pressures. Given that native iron is likely to have

equilibrated at atmospheric pressure (Pedersen and Larsen 2006, see section 4.2), these estimations are in good agreement with those of Iacono-Marziano et al. (2012a), who computed gas compositions at 1 bar (Fig.4.5c). According to this study dealing with sulfur-poor magmas, the composition of the fluid phase is dominated by CO and H_2 at high temperature and by H_2O, CO_2 and CH_4 at low temperature (Fig.4.5c). At 1200°C, the assimilation of 0.2-0.25 wt% CH is sufficient to shift gas composition from H_2O- CO_2-dominated to CO-H_2-dominated (Fig.4.5a,b). The amount of fluid phase liberated is generally proportional to the amount of organic material assimilated (expressed as C-H species), until graphite saturation is attained. For instance the assimilation of 0.5 wt% CH at 1200°C and 1 atm produces ~0.5 wt% fluid phase; for 1 wt% CH assimilated, graphite saturation is attained in the magma and the amount of fluid phase produced does not exceed 0.6-0.7 wt%.

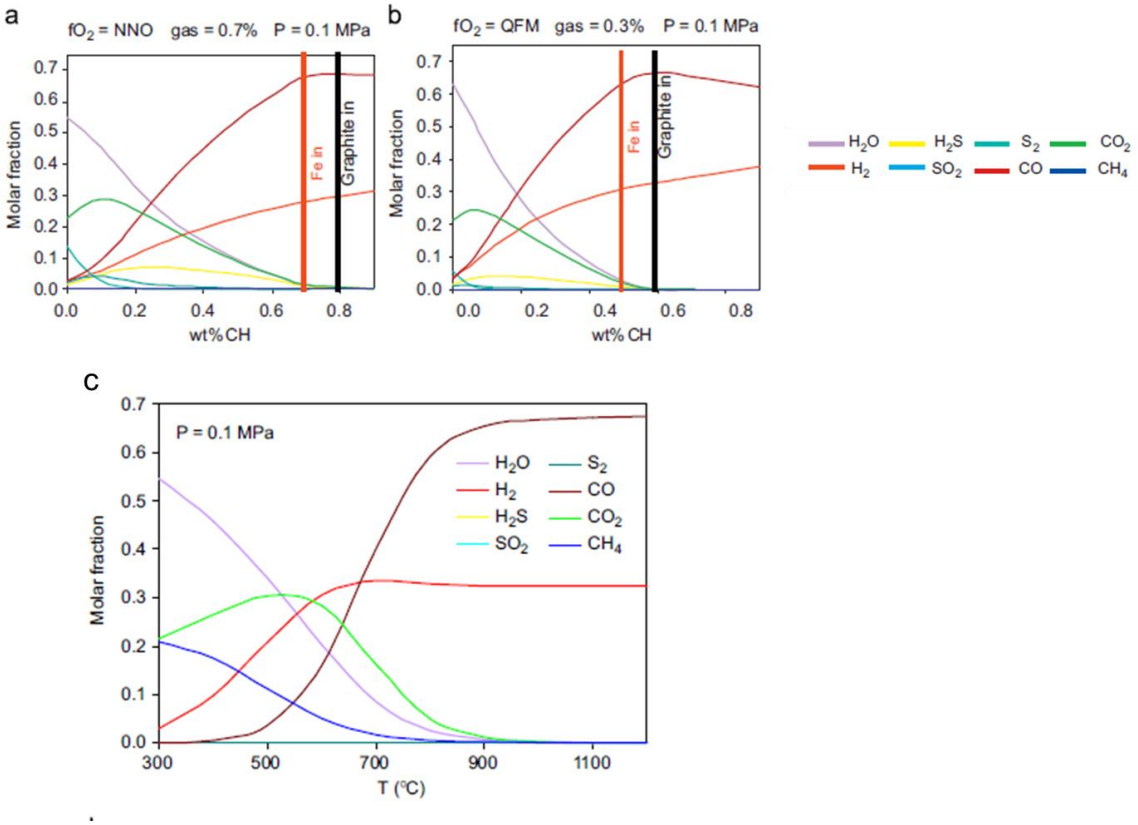

Fig.4.5 (a) and (b) gas compositions at 1200°C and 0.1 MPa expressed in mole fractions as a function of the amount of organic matter assimilated (in the form of CH). (a) The oxygen fugacity and gas proportion of the magma before interaction with organic matter are NNO and 0.7%, respectively. (b) The oxygen fugacity and gas proportion of the magma before interaction with organic matter are FMQ and 0.3%, respectively. Black and red lines indicate the amount of organic matter necessary to reach graphite and native iron saturation, respectively. (c) Gas compositions at 0.1 MPa expressed in mole fractions as a function of temperature. The amount of organic matter assimilated is 0.6 wt% CH and the magma is graphite and native iron saturated. From Iacono-Marziano et al. (2012a).

More oxidizing conditions (i.e. magmas with higher oxygen fugacity prior to interaction with organic matter) favour the survival of oxidized species (e.g. H_2O, CO_2) and S species in general (H_2S, S_2, SO_2) for a given amount of organic matter added to the system (Fig.4.5a,b). Higher gas contents in the magma also promote oxidized species relative to reduced ones (Fig. 4.5a,b).

When carbonaceous rocks are assimilated by sulfur-bearing magmas, S preferentially partitions in the fluid phase. The formation of H_2S is favoured over that of SO_2 (Iacono-Marziano et al. 2012 a, 2017).

Volatiles produced by assimilation are accompanied by more abundant volatiles produced by contact metamorphism. When C-rich sediments are heated to temperatures up to 600°C in anoxic conditions, the cracking of organic matter and the dehydration of hydrous mineral produce volatiles such as methane, water and carbon dioxide (e.g. Aarnes et al. 2010, 2011a, b). These volatiles promote volcanic degassing at surface that, in case of high magma production rate, can engender severe environmental consequences. Thousands of gigatons of greenhouse gases are estimated to be generated during the emplacement of Large Igneous Provinces in sedimentary basins (e.g. Aarnes et al. 2010).

The end-Guadalupian and end-Permian mass extinctions, for instance, coincide with the emplacement of the Emeishan and Siberian Traps, respectively. They are also accompanied by global carbon isotope excursions in both marine and non-marine strata (Retallack and Jahren 2008 and references therein; Svensen et al. 2009). The intensities of the excursions imply extremely large masses of isotopically light carbon, the lower the $\delta^{13}C$ value, the lower the mass required for isotopic mass balance. Accordingly, Retallack and Jahren (2008) propose that methane outbursts ($\delta^{13}C$ of about -60‰), generated by the intrusion of coal seams by feeder dikes to flood basalts, could have produced the observed carbon isotope excursions.

Svensen et al. (2004) propose that during the northeast Atlantic continental break-up (~55 My) the intrusion of voluminous mantle-derived melts into carbon-rich sedimentary strata may have generated a release of methane to the ocean and/or the atmosphere, which caused, or contributed to, the initial Eocene thermal maximum (IETM, an increase of 6-8°C) and the associated negative excursion in carbon isotopes. The Toarcian environmental crisis, characterized by global warming (~6°C), anoxic conditions in the oceans, extinction of marine species and a major perturbation of the global cycle, has also been related to the intrusion of mafic sills of the Karoo large igneous province into the organic-rich sedimentary rocks of the Karoo Basin, in South Africa (McElwain et al. 2005; Svensen et al. 2007).

Methane has currently a lifetime in the atmosphere of 5 y before oxidation to CO_2 (Wang et al. 2001). Iacono-Marziano et al. (2012b) calculate that this lifetime could be notably enhanced by the CO-H_2-

CH_4 emissions resulting from the intrusion of Siberian magmas into coaliferous sediments. After only 30 days of gas emissions, CH_4 lifetime could have increased to 20-100 y at a continental scale, due to the reduction of the radical OH concentration that represent the oxidizing potential of the atmosphere. CO emissions have more limited impact, but contribute to reduce atmosphere OH concentration. Repeated intrusions can potentially have a global effect, increasing the residence time of methane in the atmosphere and therefore enhancing the global warming potential of the end Permian- early Triassic (Iacono-Marziano et al. 2012b).

Large-scale combustion of coal is proposed by Ogden and Sleep (2012) to represent an additional mechanism for rapid release of carbon during the emplacement of the Siberian Traps. The authors suggest that the mafic magma preferentially intruded, heated and mixed with the thick coal seams of the Tunguska Basin: the basalt-coal mixture ascended due to its low density and ignited on contact with air, causing pyroclastic sulfate-rich fly ash to ascend into the atmosphere. These explosive combustion of coal is corroborated by the observation in northern Canada of fly ash in sediments contemporaneous to the flood basalts (Grasby et al. 2011).

4.4 **Effects on redox conditions and ore processes**

The assimilation of organic compounds is shown to have a dramatic effect on the redox state of the magma: even small amounts of organic matter can significantly decrease the oxygen fugacity of the magma. Figure 4.6 shows that the assimilation of 0.5 wt% CH by a magma containing 8 wt% FeO at 1200°C and 10 MPa, can decrease magma oxygen fugacity of 5 logarithmic units (Iacono-Marziano et al. 2012a). This is due to the introduction of reduced C and H species in the magma that subtract free oxygen to the silicate melt to form C-H-O volatile species.

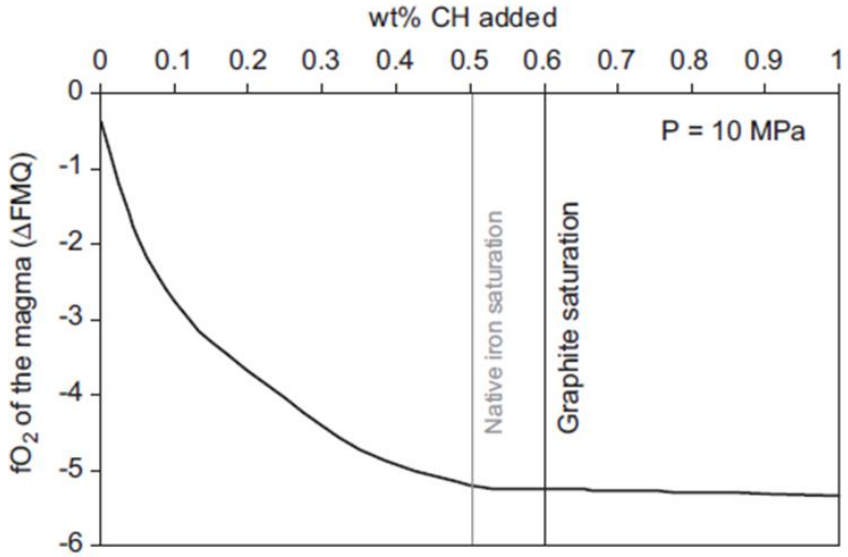

Fig.4.6 Variation of the oxygen fugacity of the magma (expressed as logarithmic units relative to the FMQ buffer) as a function of the amount of organic matter (CH) assimilated. Calculations where performed at 1200°C and 10 MPa for a magma containing 8 wt% FeO. The initial oxygen fugacity and gas fraction of the magma prior to assimilation were FMQ and 0.3%, respectively. From Iacono-Marziano et al. (2012a).

As already discussed in section 4.2, the introduction of carbon, coupled with the strong reduction of the magma, triggers Pt-Fe alloy segregation and graphite crystallization in sulfur-poor magmas (Fig.4.1d). The occurrence of native iron enriched in siderophile elements is observed in several mafic extrusive or intrusive rocks emplaced through or within carbonaceous sediments (mainly coal), i.e. at the island of **Disko**, in central West Greenland (Nordenskjöld 1872; Steenstrup 1884; Pedersen 1979a,b; Ulff-Møller 1985), at **Bühl** near Kassel, in West Germany (Medenbach and ElGoresy 1982), and in the **Maimecha, Khininda, Khungtukun, Ozernaya Mountain intrusions** and at the **Dzhaltul complex** in Russia (Ryabov and Lapkovsky 2010). A clear role of organic matter in the genesis of these unusual deposits is recognized in all contexts (Medenbach and El Goresy 1982; Pedersen and Larsen 2006; Ryabov and Lapkovsky 2010; Iacono-Marziano et al. 2012a; Pernet-Fisher et al. 2017). High Cu, Ni, Co, Pt, Pd, and Rh contents, similar to those of sulfide ores in Noril'sk-Talnakh intrusions and occasionally higher, are observed in the native iron nodules of the Siberian and Greenlandic intrusions, making them a possible new type of ore (Ryabov and Lapkovsky 2010, and references therein; Pernet-Fisher et al. 2017).

Graphite ore deposits can also be associated with the assimilation of carbonaceous metapelitic rocks. Two deposits are known worldwide, the **Borrowdale deposit** (Cumbria, UK), and the **Huelma deposit** (Southern Spain). Graphite is proposed to precipitate from carbon-bearing fluids deriving from the assimilation of carbonaceous metapelites by andesitic and basaltic magmas (Barrenechea et al. 1997, 2009; Luque et al. 1998, 2012; Ortega et al. 2009, 2010). In the Borrowdale deposit graphite occurs as nodules, up to 15 cm in diameter, mainly within andesite and diorite rocks in pipe-like bodies. Graphite is associated with epidote, chlorite, polycrystalline quartz and minor pyrite and chalcopyrite (Luque et al. 2012). Both deposits are hosted by magmatic rocks but graphite is interpreted to be of hydrothermal origin. The main evidence of this hydrothermal origin is the intense alteration of the magmatic rocks to an assemblage containing quartz, chlorite and albite (Luque et al. 2012; Ortega et al. 2009, 2010).

Ballhaus and Stumpfl (1985) also invoke an origin from magmatic C-O-H-S fluids for graphite mineralization associated with pothole depressions at the **Bushveld Complex** (South Africa). Potholes are circular to elongated depressions, tens to hundreds of meters in diameter, within which the platiniferous Merensky Reef is displaced by several meters into its anorthositic footwall. Inside the potholes, normal fine-grain pyroxenites grade into graphitic pegmatites with up to 80 vol% graphite,

associated with amphibole, biotite, chlorite, sulfides and platinum-group minerals. Both potholes and pegmatites are clearly formed at the magmatic stage, but their occurrence is related to locally higher volatile concentrations in Bushveld magmas than in the other parts of the complex. In this case, as in the precedent ones, we can probably say that graphite mineralization formed at the magmatic-hydrothermal transition. The source of fluids is not fully investigated at Bushveld, but carbon isotopic signature of graphite suggests a pronounced influence of sedimentary carbon (Ballhaus and Stumpfl 1985 and references therein). The sedimentary carbon source could be the dolomitic shales of the Duitschland Formation, which are present as the footwall rocks in some parts of the intrusion (total thickness up to 1 km; Yudovskaya et al. 2018).

The most valuable type of ore deposits produced by the assimilation of carbonaceous rocks are magmatic sulfides. Several magmatic sulfide ore deposits are suggested to be produced by the interaction of mafic magmas with carbonaceous rocks. The assimilation of argillaceous, organic matter and sulfide-bearing Precambrian rocks of the Virginia Formation is for instance recognized by several authors to be at the origin of the sulfide ores occurring in the Partridge River, South Kawishiwi, and Water Hen intrusions of the **Duluth Complex**, USA (e.g. Mainwaring & Naldrett 1977; Ripley 1981; Thériault & Barnes 1998; Thériault et al. 2000; Queffurus & Barnes 2014; Samalens et al. 2017). The addition of sulfur from the argillaceous rocks favours sulfide segregation. The sulfide melt is therefore proposed to form from the crustal xenoliths and to react with the magma: the higher the interaction between the sulfide melt and the magma, the lower the sedimentary signature and the higher the metal content of the sulfide melt. Indeed, Thériault & Barnes (1998) describe a general increase in the degree of contamination toward the base of the Dunka Road deposit of the Partridge River intrusion, associated with a decrease in metal concentration of the sulfides. Moreover, Thériault et al. 2000 identify three types of sulfide mineralization within the Dunka Road, Babbitt, Wetlegs and Wyman Creek deposits of the Partridge River intrusion: 1) semimassive to massive sulfides, 2) PGE-poor disseminated sulfides, and 3) PGE-rich disseminated sulfides. Type 1) sulfides are observed near the basal contact of the intrusions with the shales or within the shales. They show evidence of significant contamination (high sulfur isotope values and S/Se ratios), resulting in low metal concentrations. PGE-poor disseminated sulfides occur within the lower 250 m of the intrusion, where shale xenoliths are abundant. They show lower sedimentary signatures than type 1) sulfides. They present higher PGE contents than type 1). PGE-rich disseminated sulfides occur between 100 and 600 m above the basal contact and show little signs of contamination.

Similarly to Duluth, the magmatic sulfide ores of **Eagle** deposits (USA) are also interpreted to have formed by the interaction of mafic/ultramafic magmas with carbonaceous and sulfide-bearing country rocks. Ding et al. (2012) identify the rocks of the Michigamme Formation (considered to be laterally

equivalent to the Virginia Formation) as the possible source of Re and Os for the sulfide mineralization, while S isotopic compositions point to the Archean country rocks as the most likely source of sulfur.

Several other magmatic sulfide deposits are hosted by carbonaceous rocks, and contamination is suggested to play a role to different extents in their formation: at **Voisey's Bay**, in Canada, where graphite is present in several igneous rocks of the intrusion (Ripley et al. 2002); at **Huangshandong** and the other sulfide deposits of the southern Central Asian Orogenic Belt (Gao et al. 2013; Mao et al. 2017); at the **Duke Island Complex**, in Alaska, where graphite is observed in the sulfide-bearing olivine clinopyroxenite (Thakurta et al. 2008); in the **Kabanga** deposit, in Tanzania (Maier et al. 2010; Maier & Barnes 2010); in the **Aguablanca** deposit, in Spain (Casquet et al. 2001; Ganino et al. 2014). Also in many komatiite-hosted sulfide ores, carbonaceous sulfidic sediments are observed in contact with the ores, and considered instrumental for sulfide segregation (e.g. Gresham and Loftus-Hills 1981; Huppert et al. 1984; Lesher 2017 and references therein). In the northern limb of the Bushveld Complex, the carbonaceous rocks of the Duitschland Formation are proposed to represent a reducing agent in the formation of the Platreef contact-style mineralization (Yudovskaya et al. 2018). The presence of abundant shale and calcsilicate xenoliths of extremely variable size in the ore-bearing igneous rocks corroborates this hypothesis (Maier et al. 2008).

A petrogenetic role of the interaction of Siberian Trap mafic magmas with coal or argillite-bearing sedimentary host rocks is also proposed for the exceptional sulfide ore of the **Noril'sk-Talnakh region** in Russia. These ores exceed all other magmatic deposits in the amounts of economically valuable metals per ton of ore (Naldrett, 2004 and references therein). This unique characteristic results from both the high abundance of sulfide mineralization in the three ore-bearing intrusions and the high metal contents of sulfide mineralization. The extremely high sulfide contents of these intrusions, up to 7 wt% of the whole intrusion (Zen'ko and Czamanske 1994) is mainly due to the occurrence of massive sulfide layers, up to 45 m thick, which accompany disseminated sulfide mineralization (Zen'ko and Czamanske 1994; Czamanske et al. 1995; Naldrett 2004). These high sulfide concentrations are ascribed to the important S enrichment of the magma, due to the assimilation of sulfate rocks (see section 3.1.5), whereas carbonaceous rocks are likely to represent the reducing agent that triggered the segregation of the sulfide melt forming the disseminated and the massive ores (Naldrett 2004; Arndt et al. 2005; Jugo and Lesher 2005; Jugo 2007, 2014; Li et al. 2009b; Ripley et al. 2010; Iacono-Marziano et al. 2014, 2017; Ryabov et al. 2018). The elevated metal contents of the ores are in contradiction with the high sulfide proportions in the intrusions, and are classically interpreted to derive from the interaction of the sulfide melt with large amounts of metal-rich silicate melt, i.e. undepleted magma. The estimated mass ratio of silicate to sulfide liquid (R; Campbell and Naldrett 1979) is about 3000 for massive ores and 10000 for disseminated ores (Barnes et al. 1997; Barnes and

Lightfoot 2005; Barnes and Ripley 2016). However, a different mechanism for metal enrichment of the sulfide melt can be deduced from magma-coal interaction experiments and will be discussed in the next section.

4.4.1 Association between sulfide melt and fluid phase: implications for sulfide melt mobility and metal enrichment (ongoing work in collaboration with Margaux Le Vaillant and Steve Barnes)

Several experimental studies show that, when a fluid phase is present in experimental charges, the sulfide melt is always associated with it (Mungall and Su 2005; Mungall and Brenan 2014; Mungall et al. 2015; Ferraina 2018). In experiments investigating interaction between mafic magmas and coal, the sulfide melt is spatially associated with the fluid phase (Fig.4.1) generated by both coal destabilization and degassing of the silicate melt. Micro CT investigations reveal that every gas bubble is attached to several sulfide globules, the biggest globules being generally associated to the biggest bubbles (Fig.4.7a). This suggests that the sulfide blebs and the gas bubbles grew simultaneously during the degassing of the silicate melt.

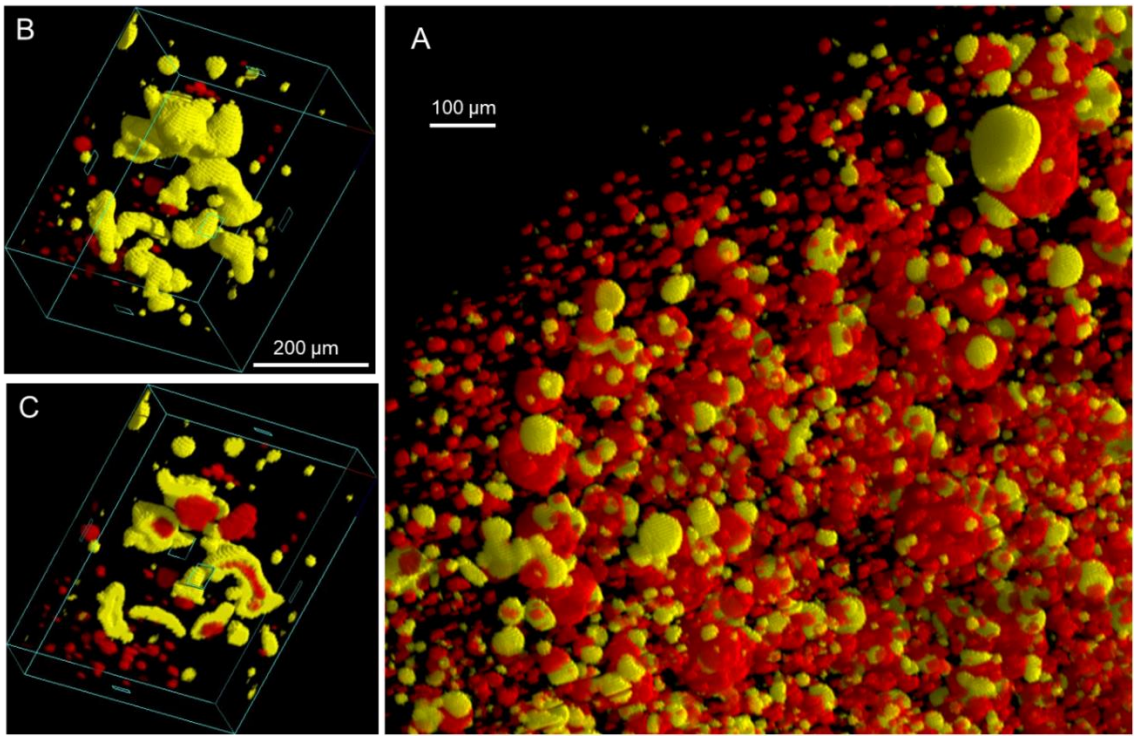

Fig.4.7 3D distribution of sulfide droplets (in yellow) and gas bubbles (in red) revealed by micro CT renderings, in an experimental sample that experienced interaction with coal. (a) General distribution of sulfide droplets and gas bubbles. (b) 3D shape of the largest sulfide bleb. The gas bubbles are also shown in red, with the same segmented volume as the sulfide blebs (shown by the white lines). (c) The segmented volume of sulfide blebs is smaller than the one of gas bubbles, in order to hide the upper

part of the sulfide blebs and to show the bubbles occurring at their interior. From Iacono-Marziano et al. submitted.

The association of sulfide blebs with gas bubbles is also observed in the magmatic sulfide deposits of the Noril'sk-Talnakh intrusions (Le Vaillant et al. 2017; Barnes et al. 2019). In these rocks the gas bubbles consist of subspherical spaces within the olivine and plagioclase crystal framework, partially or completely filled with late-crystallizing silicate minerals (silicate caps in Fig. 4.8). This suggests that a fluid phase was present during the crystallization of these rocks and possibly played a role in the formation of the ores (Barnes et al. 2019).

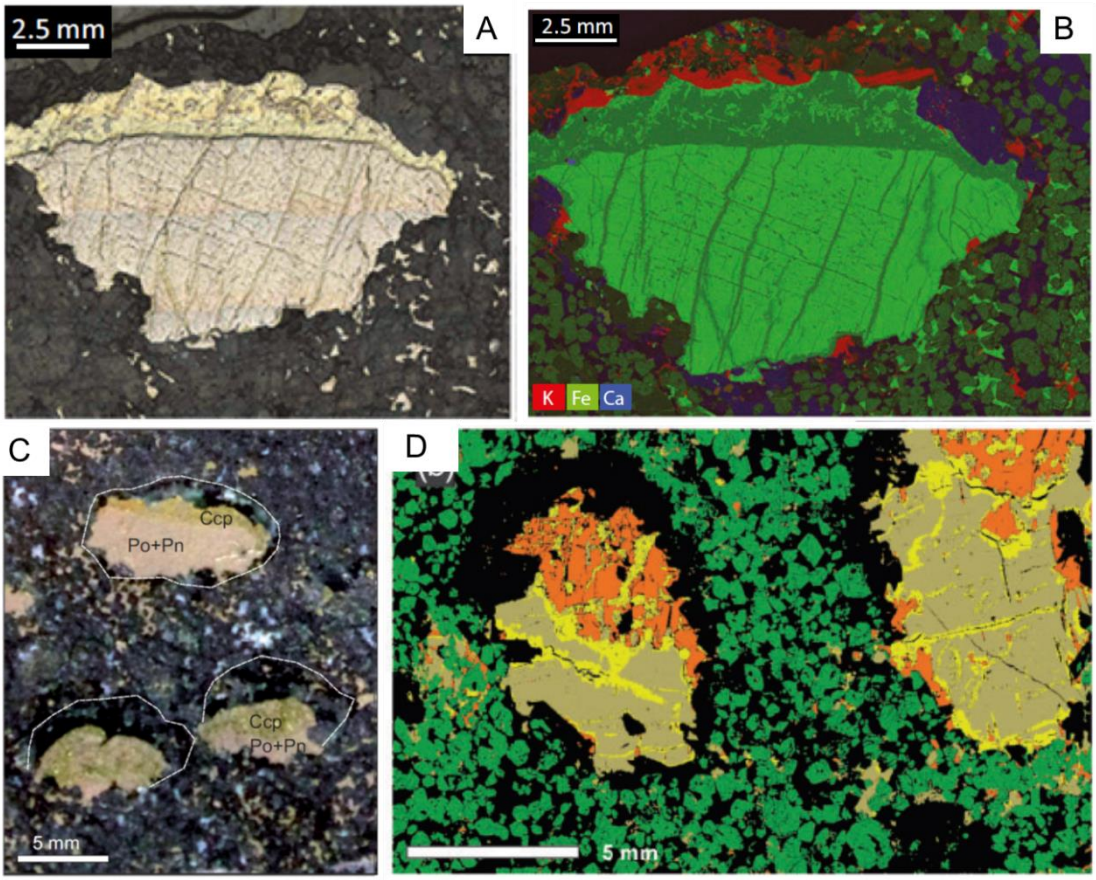

Fig.4.8 Sulfide-bubble associations in the Noril'sk-Talnakh sulfide ores, from Le Vaillant et al. 2017 (A and B) and Barnes et al. 2019 (C and D). (A) Photograph of a capped sulfide globule in a matrix of olivine and plagioclase containing disseminated sulfides. (B) Three elemental maps of the capped sulfide globule in (A), produced by synchrotron light micro-XRF. (C) Photograph of sulfide globules with outlines of silicate caps shown in white, in a matrix of picritic gabbrodolerite. (D) Tornado XRF map showing olivine crystal framework in green, and sulfide globules inside the olivine-free spaces (chalcopyrite in orange, phyrrhotite in military green and pentlandite in yellow).

The association between sulfide melt and gas bubbles seems to represent an efficient coalescence mechanism for sulfide blebs: this is suggested by the shape of the sulfide blebs in Figures 4.9a, and clearly showed by the sulfide bleb in Figures 4.9a and b, which is constituted of four coalesced sulfide droplets. Moreover, Figures 4.7b and c show 3D images of one of the largest sulfide accumulation observed in experimental samples: also in this case its shape is clearly due to the coalescence of several sulfide droplets. The coalescence most likely operates on the sulfide droplets that are connected to the same gas bubble, as illustrated by Figures 4.9b and c. The morphology of the sulfide-bubble compound, and probably the efficiency of the coalescence, depends on the surface tensions of the sulfide melt, the silicate melt and the fluid (Mungall et al. 2015), which in turn probably depend on oxygen fugacity. Interaction experiments between mafic magmas and coal suggest that the coalescence of sulfide droplets is extremely efficient at these reducing conditions, to the point of entrapping gas bubbles in the growing sulfide blebs (Fig.4.7c). This coalescence mechanism is potentially important in the genesis of massive sulfide deposits, as Robertson et al. (2015b) estimated that droplet break-up, rather than coalescence, is the dominant mechanism during magma flow.

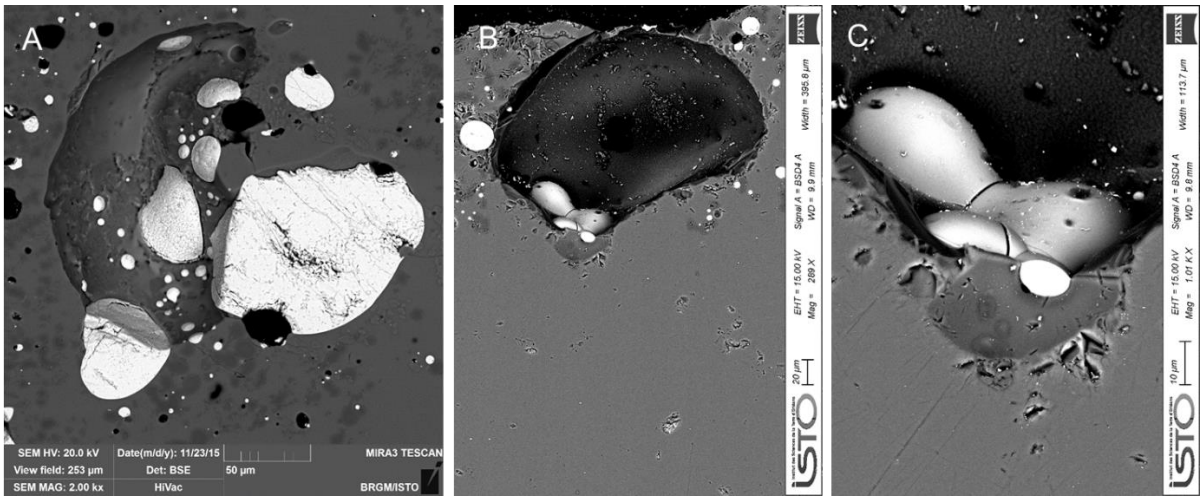

Fig.4.9 Sulfide blebs associated to gas bubbles in experimental samples. (a) Large sulfide blebs with irregular shapes suggesting coalescence of the sulfide droplets connected to the same bubble. (b) and (c) sulfide droplets that clearly coalesced at the interface between the silicate melt and the gas bubble. An additional droplet has been removed by polishing, leaving a pit in the centre of image.

Moreover, the association between sulfide melt and fluid phase seems to have another important implication in the metal enrichment of the sulfide melt. Sulfur degassing related to the interaction of the magma with carbonaceous material is likely to involve both the silicate and the sulfide melts. The sulfide melt of the experimental samples that interacted with coal show sulfur depletion with respect to the sulfide melt of coal-free samples. Figure 4.10 shows that (Ni+Cu)/S ratios in sulfides of coal-free

samples are inversely correlated to Fe/S ratios and to the proportion of sulfide melt. Despite the large proportions of sulfide melt, the sulfide droplets of coal-bearing samples can have high (Ni+Cu)/S and Fe/S ratios, suggesting S-loss during coal-induced degassing. By this mechanism, (i) the proportion of sulfide melt decreases, therefore (ii) the silicate melt/ sulfide melt ratio (R factor) increases, and (iii) the sulfide melt becomes enriched in metal elements. Metal elements are indeed more compatible with the sulfide melt than with the fluid phase, whereas sulfur preferentially degasses in the presence of a fluid phase. Analyses of massive sulfides from the Noril'sk-Talnakh intrusions (Zientek et al. 1994; Duran et al. 2017) show (Ni+Cu)/S and Fe/S ratios similar to those of coal-bearing experimental samples (Fig.4.10). This could corroborates the hypothesis that the sulfide ores of these intrusions owe their high metal contents to sulfur degassing triggered by the interaction of the magma with carbonaceous rocks. According to this hypothesis, the decreasing proportion of sulfides from the Kharaelakh to the Talnakh and to the Noril'sk 1 intrusion (Zen'ko and Czamanske 1994), would be the consequence of an increasing rate of degassing. An extreme degassing would lead to the total consumption of the sulfide melt and the crystallization of platinum-group minerals (PGM), associated with iron oxides (magnetite or chromite).

Low-sulfide PGE ores occur in the Upper Gabbroic Series of the Noril'sk 1, Talnakh and Kharaelakh intrusions (Sluzhenikin et al. in press). These ores are significantly different from both the massive and disseminated sulfides observed at the base and in the lower layers of the intrusions, and their occurrence suggests a fluid-controlled crystallization (Sluzhenikin et al. in press). If the hypothesis of extreme degassing is right, the widespread Pt-Fe alloys in the low sulfide ores of Noril'sk 1 and their absence in Talnakh and Kharaelak (Sluzhenikin et al. in press) would suggest higher degassing rate for Noril'sk 1 intrusion. This could be due to both the depth of the intrusion decreasing from Kharaelakh to Talnakh and to Norilsk 1 (Fig.3.6c), and the nature of the carbonaceous rocks: coal in Noril'sk and Talnakh and argillites in Kharaelakh (Fig.3.6c; Zen'ko and Czamanske 1994; Czamanske et al. 1995).

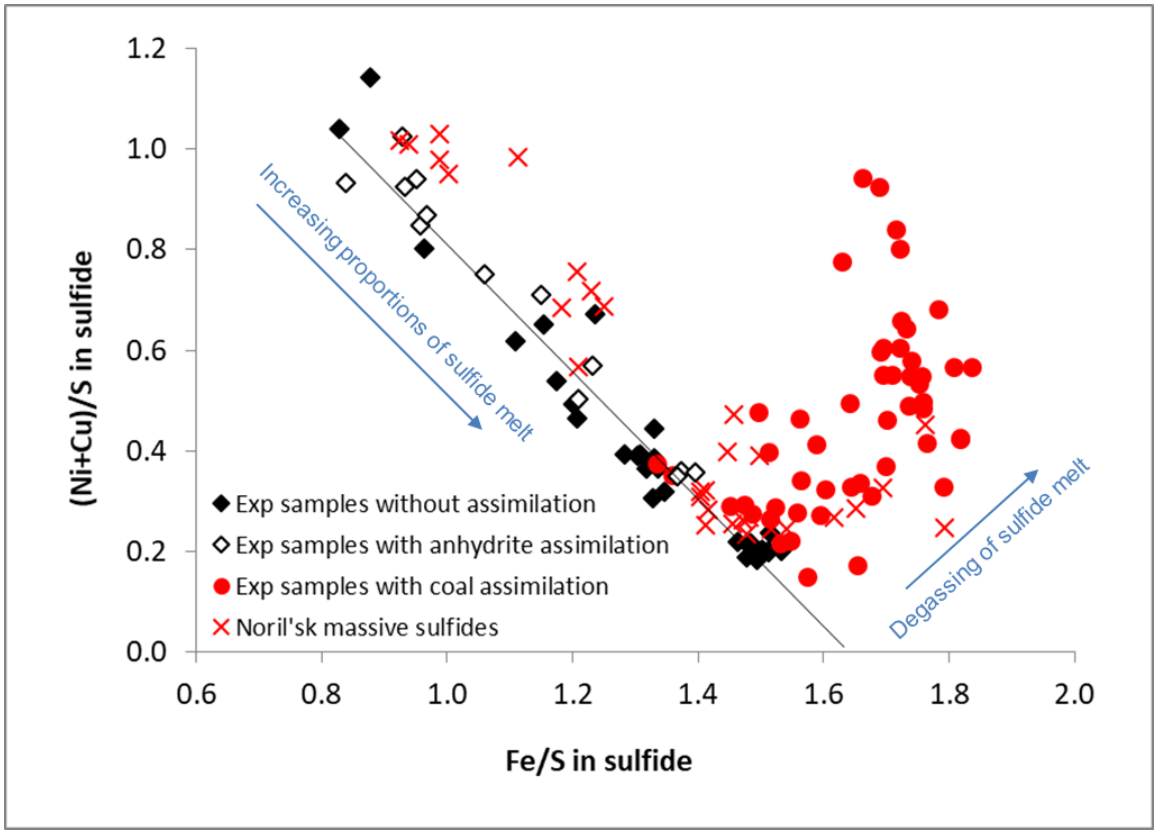

Fig.4.10 (Ni+Cu)/S versus Fe/S (both from wt% contents) in the sulfide melts of the experimental samples. Each symbol represents a single EMP analysis. The black line is the regression curve of the data obtained for the samples that did not experience any assimilation. For these samples, and those that experienced anhydrite assimilation, (Ni+Cu)/S ratios are inversely correlated to Fe/S ratios and only depend on the amount of sulfide melt. In coal-bearing samples, both (Ni+Cu)/S and Fe/S ratios can reach high values, despite the large proportions of sulfide melt, suggesting S-loss during degassing. The red crosses are whole rock compositions of massive sulfides from Noril'sk I, Kharaelakh and Talnakh intrusions from Zientek et al. (1994) and Duran et al. (2017).

This metal-enrichment process could be relevant to all the contexts in which a fluid phase coexists with the magma. Among the numerous examples discussed in the previous section, the **Noril'sk-Talnakh** intrusions and the **Duluth Complex** are probably the clearest cases: in both contexts the sulfide mineralization generally appears to have formed in a primary magmatic environment, but in the presence of a fluid phase (Ripley 1981; Barnes et al. 2019). Figure 4.11 illustrates that these two deposits are intermediate between the sulfide-poor type that cluster close to the PGE apex and the sulfide-rich type that cluster close to the Ni+Co apex and for which Ni and Cu together constitute the metals of major economic interest (Naldrett 2004). These two deposits are also Cu-richer with respect to all the others (Fig.4.11).

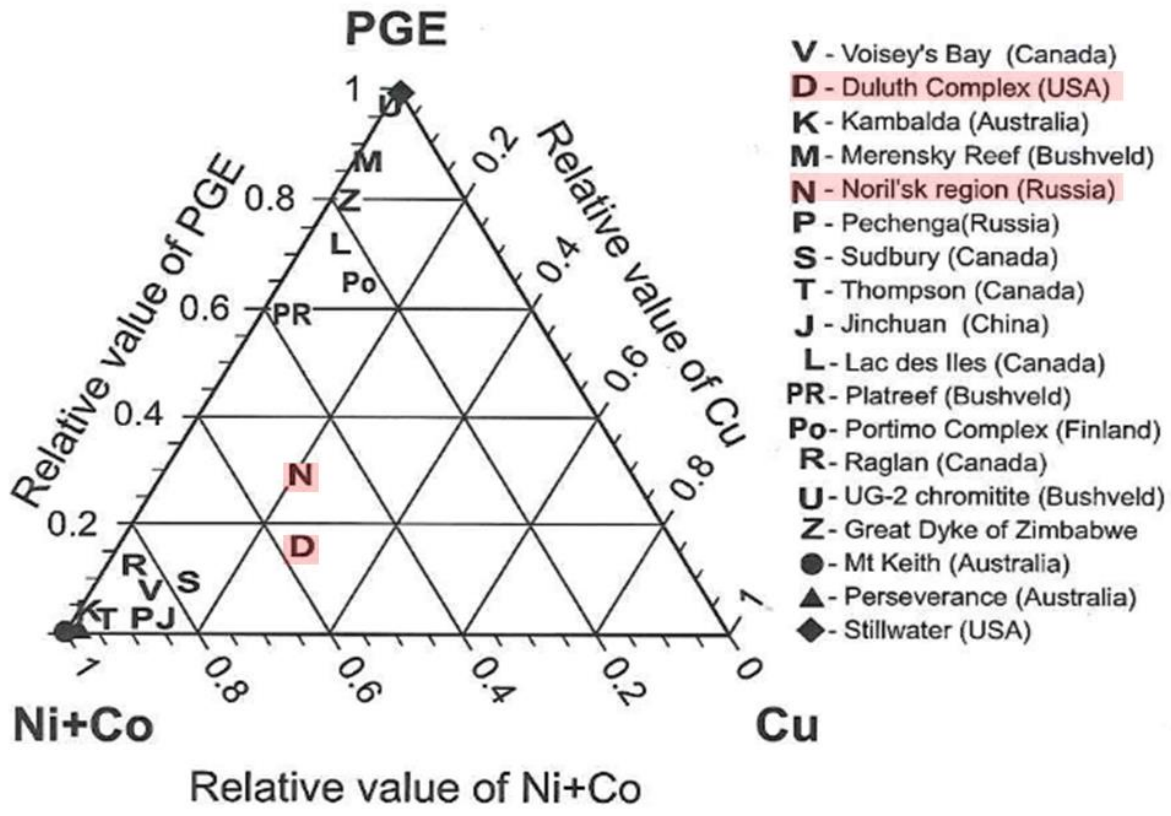

Fig.4.11 Relative value of the contributions of Ni+Co, Cu and PGE to the listed magmatic sulfide deposits. From Naldrett (2004).

By this degassing-driven mechanism, the R-factor could increase, due to the consumption of the sulfide melt. It is probably incorrect, however, to apply the R factor equation (Campbell and Naldrett 1979) in this case, because the assimilation of carbonaceous material and the related degassing are likely to be disequilibrium processes, and the partition coefficients of metals might not be valid anymore. Kinetics effects could prevail leading to element fractionation, as a consequence of their preferential partitioning into the fluid phase. This has been already proposed for the **Platreef** contact-style mineralization of the Bushveld Complex: Maier et al. (2008) suggested that the Pt/Pd ratios of these ore bodies, different from those of the western and eastern reefs, could have varied as a consequence of floor rock devolatilization, Pd being mobilized by fluids more easily than Pt.

4.5 Assimilation markers and tracers

Carbon-bearing xenoliths or magmatic crystals are the only distinct markers of the assimilation of organic matter. Organic matter-rich xenoliths are commonly observed in the magmatic rocks that experienced assimilation in Greenland and the Siberian Platform (e.g. Melson and Switzer 1966;

Mainwaring and Naldrett 1977; Pedersen, 1978, 1979a,b, 1981; Medenbach and El Goresi 1982; Ulff-Møller 1985; Pedersen and Ronsbo 1987; Pedersen and Larsen 2006; Ryabov & Lapkovsky 2010 and references therein). Likewise, the occurrence of magmatic (often difficult to distinguish from the residual) graphite and carbides is a clear indicator of the interaction of the magma with carbonaceous rocks (e.g. Mainwaring and Naldrett 1977; Ulff-Møller 1985; Ryabov and Lapkovsky 2010; Samalens et al. 2017). The abundant presence of other reduced phases, such as native iron, copper or lead, sulfides, wüstite, or ulvöspinel (Fig.4.3; e.g. Medenbach and El Goresi 1982; Ulff-Møller 1985; Ryabov & Lapkovsky 2010) is also a common consequence of the strong reduction experienced by the magma during assimilation.

When the carbonaceous rocks contain sedimentary sulfides, the sulfur isotopic signature can be a clear marker of the assimilation. For instance, sulfur isotopic compositions of magmatic sulfide ores of the **Duluth Complex** (USA) show that a large portion of the involved sulfur is derived from the metasedimentary footwall rocks: magmatic sulfides have $\delta^{34}S$ between 0.2 and 15.5 ‰, with an average value near 7.5 ‰, while sedimentary sulfides in the host rocks have $\delta^{34}S$ between 7.4 and 20 ‰ (Mainwaring and Naldrett 1977; Ripley et al. 1981; Queffurus and Barnes 2014). The high variability of the S isotopic composition strongly suggests the introduction of both isotopically and spatially variable country rock sulfur into the crystallizing magma (Ripley 1981).

Other isotopic tracer are used to detect magma contamination by carbonaceous sediments. Larsen and Pedersen (2009) showed a clear mixing trend between the uncontaminated picritic magma and the shales of the **Nuussuaq Basin** (Greenland), in a ^{143}Nd-^{144}Nd versus $^{87}Sr/^{86}Sr$ diagram (Fig.4.4b). This is a typical contamination trend by crustal rocks, which is not univocally linked to the carbonaceous nature of the contaminant. Similarly, the $^{187}Os/^{188}Os$ ratio of mafic rocks is also observed to increase with the assimilation of the carbonaceous sediments, due to the higher Re/Os ratio and therefore $^{187}Os/^{188}Os$ ratio of the crustal rocks, with respect to the magma (Pernet-Fisher et al. 2017).

Te, As, Bi and Sb (TABS) concentrations in magmas have also been used to model crustal contamination, as upper crust rocks are generally 10 to 100 times richer on average than mantle-derived magmas (Mansur and Barnes 2020). In particular, Sb and As concentrations can be used to trace crustal contamination also in sulfide-bearing magmas, as they are only marginally affected by the segregation of a sulfide melt (Mansur and Barnes 2020). The S/Se ratio of magmatic sulfides is also effectively used to determine if country rock assimilation has played a role in the genesis of the mineralization, due to the general selenium depletion of the sedimentary rocks relative to mantle-derived magmas (Thériault and Barnes 1998; Ripley et al. 2002; Queffurus & Barnes 2014, 2015).

However, both TABS contents, and S/Se ratios do not help discriminating if the crustal contaminant has a carbonaceous composition or not.

As organic matter is mainly composed of volatile elements (C, H, N), during magmatic assimilation it produces an abundant fluid phase coexisting with, or escaping from, the magma. These fluids can leave broad evidence of their occurrence, especially when they are associated with magmas that are dry or volatile-poor. In particular, assimilation-derived fluids can generate extended metamorphic/ metasomatic aureoles around magmatic intrusions. This is the case of the ore bearing intrusions of the **Noril'sk-Talnakh region** that are surrounded by metamorphic aureoles as thick as the intrusions themselves (up to 450 m; Czamanske et al. 1995; Naldrett 2004 and references therein). Inside these metamorphic aureoles, calcite mineralizations have strongly negative $\delta^{13}C$ signatures reaching -19.4‰ PDB, and indicating an organic source of carbon (Pokrovskii et al., 2005).

More generally, thick contact aureoles are always observed when dolerite sills intrude carbonaceous shales (Fig.4.12).

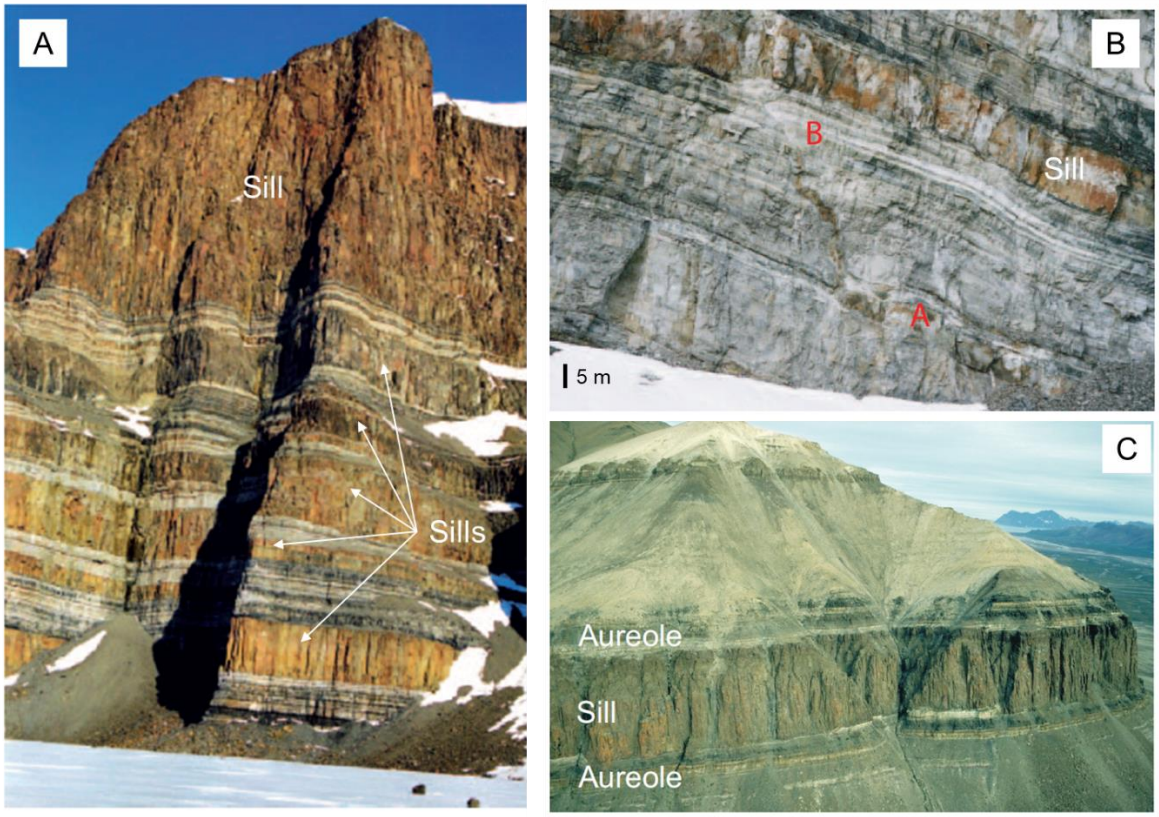

Fig.4.12 Typical sill exposures in the Theron Mountains, Antarctica (a), (b), and in Northern Jameson Land, East Greenland (c). (a) The sub-vertical cliff is approximately 700 m high. The sills intrude Permian sandstones, siltstones, and shales. From Hutton 2009. c) A 60 meter sill and the associated contact aureole in shales. In Horsedal, from Svensen et al. 2015.

Numerous examples are observed in other parts the **Tunguska Basin** (Russia), in **the Karoo Basin** (South Africa), in the **Amazonas and Solimoes Basins** (Brasil), and in the **East Greenland Basin** (Svensen et al. 2015; Heimdal et al. 2018). The thickness of the contact aureole varies within 30 and 250% of the intrusion thickness, depending on the type of host rock and the intrusion depth (Aarnes et al. 2010).

The abundant fluids produced by the assimilation of carbonaceous rocks can also generate magmatic breccias. In the ore-bearing Noril'sk-Talnakh intrusions, an intrusive breccia, up to 25 m thick, is observed in some localities at the roof of the intrusions (Naldrett 2004), and locally contains abundant coal fragments (Sluzhenikin et al. in press).

5. General considerations and conclusions

Several large igneous provinces (LIPs) were emplaced through sedimentary basins. They consist of flood basalts and numerous intrusions, commonly sill-like and dike-like, injected in the sedimentary rocks of the upper crust (Fig.4.12). They are therefore called “volcanic basins” and generally occur along rifted continental margins and on lithospheric cratons. Figure 5.1 (from Svensen et al. 2015) shows the distribution of large igneous provinces and major volcanic basins.

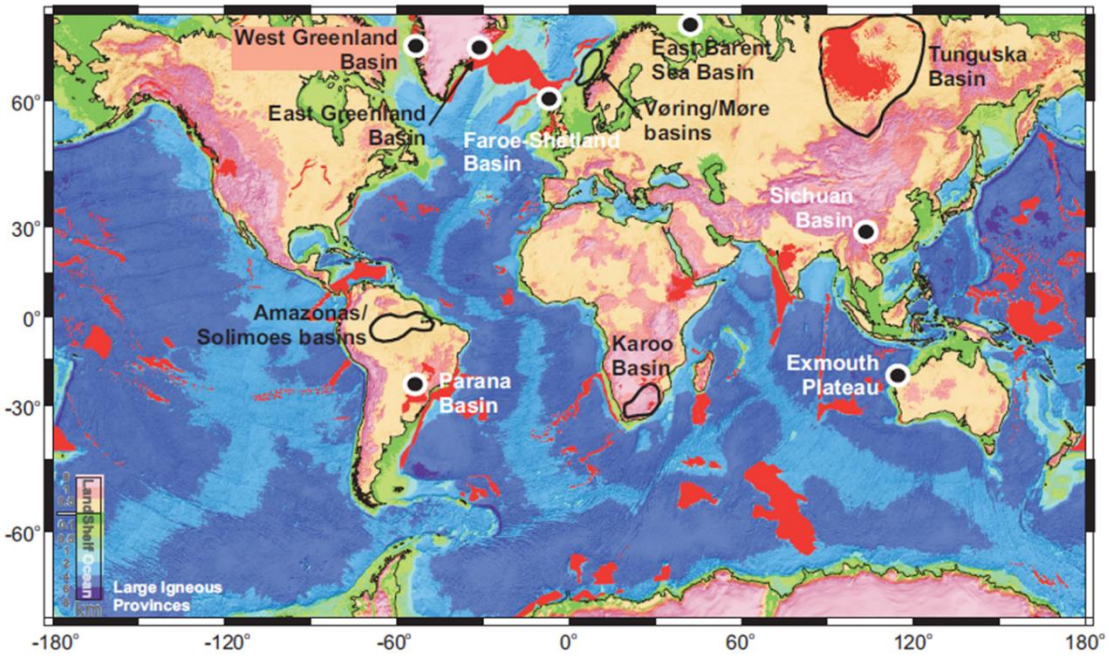

Fig.5.1 Distribution of large igneous provinces (in red). Major volcanic basins are either outlined with black lines or indicated by black filled circles.

The nature of the sedimentary rocks is likely to play a role in the formation and propagation of sill-like structures (e.g. Hutton 2009; Schofield et al. 2014). The main escarpment of the **Theron Mountains** in Antarctica offers one of the best exposures of sill complexes in the world: tholeiitic magmas belonging to the Ferrar sub-province of the Karoo-Ferrar magmatic province intrude a sedimentary sequence dominated by sandstones and siltstones with subordinate shales and coal seams (Fig. 4.12a,b). Sill thickness vary between 1 m and 160 m, the thickest sills being commonly composite. Hutton (2009) propose that the thicker sills are created by many smaller sills merging, with the first very thin proto-sills propagating along the planes of weakness, like for instance coal and shale horizons in the stratigraphy. This inference is corroborated by the common occurrence of coal seams at the immediate contact of the dolerite sills, sometimes at both the top and the bottom of the same sill (Fig. 4.12b). This process allows sills to intrude multiple coal beds or to jump between them. Similarly, hydrous salts are observed to represent the preferential horizons in a salt sequence that control the lateral intrusion

of magma in a sedimentary basin, switching form dyke to sill geometries (Fig. 3.5; Schofield et al. 2014). The preferential injection is probably related to several chemical and physical properties of the sedimentary rocks: (i) their lower density and mechanical weak behaviour, (ii) their fluidization caused by heating and dehydration (occurring at particularly low temperatures in coals and hydrous salts; Ogden and Sleep 2012; Schofield et al. 2014), and (iii) the creation of a secondary porosity by devolatilization/dissolution/melting. Altogether, these processes facilitate the lateral propagation of the intrusions, but also promote the assimilation by the creation of new interfaces between the magma and the host rock. Similarly, sedimentary rocks can constitute preferential intrusion horizons for rising magmas, at the scale of the magma chamber of single volcanoes. This is probably the case of Italian quaternary volcanoes and particularly of **Mt. Vesuvius**, where basaltic magmas seem to be horizontally channelled at the discontinuity between the crystalline basement and the Mesozoic sequences of sedimentary carbonates (De Natale et al. 2006; Iacono-Marziano et al. 2009). Seismic data are consistent with a sill-shaped zone at ~8-10 km b.s.l. constituted by magma interspersed in a densely fractured rock, favouring interactions between magma and host rock (Auger et al., 2001).

The most important implication of magma intrusion in volcanic basins is the generation of important amounts of greenhouse gases (in the range of 1000 to 10000 Gt for each basin) in the contact aureoles of the intrusions (Svensen et al. 2015). The nature of the gases generated by thermal metamorphism and assimilation depends on the types of sedimentary rocks intruded by the magma. Contact metamorphism of carbonaceous rocks can potentially produce the highest volumes of gases, because the cracking of organic matter occurs at much lower temperatures than those required for decarbonation, melting or assimilation (e.g. Ganino & Arndt 2009). This process mainly releases CH_4 and CO_2-rich gases (e.g. Svensen et al. 2004; Aarnes et al. 2010, 2011a, b), while the high-temperature interaction of carbonaceous material with magma liberates significantly lower amounts of CO-H_2-dominated gases (Iacono-Marziano et al. 2012a,b). Thermal breakdown and assimilation of carbonate rocks release relatively similar amounts of CO_2-dominated gases at similar temperatures, but thermal decarbonation of dolomitic rocks can start at temperatures as low as 600°C (Carter & Dasgupta 2018). Calc-silicate formation from impure carbonates can occur at lower temperatures (between 450 and 500°C) and contribute a significant, possibly larger than decarbonation, amount of liberated CO_2 (Ganino & Arndt 2009). Less information is available on thermal decomposition of evaporitic rocks, nevertheless suggesting that petroleum-bearing salts can release sulfur dioxide and halocarbons at low temperatures (<275°C; Svensen et al. 2009). Assimilation and desulfatation of sulfates produces SO_2-rich gases, and the minimum temperature at which desulfatation occurs probably depends on the presence of impurities in the rock (615 to 1400°C; Ganino & Arndt 2009).

Produced gases are released to the atmosphere via basin seepage processes, or vertical pipe structures. Basin seepage is generally associated to magmatic intrusions accompanied by lava flows, while vertical pipes and vent structures may be associated with explosive eruptions, due to pressure build-up during devolatilization of sedimentary rocks. In the **Southern Tunguska Basin** (Russia), for instance, hundreds of explosion pipes are associated with pyroclastic rocks, while, in the Northern part of the Siberian Traps, lavas largely dominate and no magnetite pipes are observed (Fig.3.6a). The distribution of tephra and magnetite pipes at the surface rigorously coincides with the occurrence of Cambrian evaporites at depths in the sedimentary basement (Svensen et al. 2009; Jerram et al. 2016). This suggests that the nature of the sedimentary rocks intruded by magmas not only controls the composition and the amount of the gases coexisting with the magma, but can also affect its eruptive behaviour and therefore the dispersion of the gases into the atmosphere. Explosive eruptions are indeed more effective than effusive eruptions in injecting sulfur, carbon, and, in this case, halogen-rich gases into the stratosphere, although additional processes such as coal combustion could play a role (Ogden and Sleeps 2012).

Due to (i) the large volumes of emplaced magmas and therefore of produced gases, (ii) the nature of produced greenhouse gases, (iii) the rapidity of the gas release to the atmosphere, and (iv) the possible injection into the stratosphere, the environmental consequences are generally important, e.g. breakdown of the ozone layer, rapid global warming and mass extinction (Svensen et al. 2015 and references therein). Table 5.1 summarizes the LIPs that were emplaced in sedimentary basins and are therefore associated to environmental crises (modified from Svensen et al. 2015).

Table 5.1: Large Igneous Provinces emplaced in sedimentary basins and related environmental crisis

LIP	**Sedimentary basins**	**Age**	**Mass extinction**	**C isotope excursion**	**Sedimentary rocks involved**
Emeishan Traps	Sichuan (China)	End-Guadalupian	major	yes	carbonaceous+ carbonates
Siberian Traps	Tunguska (Russia)	Permian-Triassic boundary	major	yes	evaporites+ carbonaceous+ carbonates
Central Atlantic	Amazonas, Solimoes (Brasil)	Triassic-Jurassic boundary	major	yes	evaporites+ carbonaceous+ carbonates
Karoo-Ferrar	Karoo (South Africa)	Toarcian	minor	yes	carbonaceous
North Atlantic	West and East Greenland, Faeroe-Shetland	Palaeocene	minor	yes	carbonaceous
North East Atlantic	Vøring, Møre (Norway)	Palaeocene-Eocene	minor	yes	carbonaceous

Modified after Svensen et al. 2015.

In all cases a carbon isotopic excursion is observed in the sedimentary record (Table 5.1), suggesting that carbonaceous rocks are likely to have interacted with the mafic magmas, as already discussed in section 4.3 for the Siberian and Emeishan Traps. The occurrence of carbonaceous rocks indeed sensibly enhances the production of ^{12}C-enriched gases, likely CH_4-rich (e.g. Svensen et al. 2004; Retallack and Jahren 2008).

At the scale of a single volcano, the interactions between magma and host sedimentary rocks can sensibly boost gas emissions, explaining the high heterogeneity in volatile fluxes released by volcanoes worldwide, particularly observed for CO_2 (e.g. Kerrick 2001; Aiuppa et al. 2017; Mason et al. 2017). The increase in magma volatile content most likely implies an increase in magma explosivity, as proposed for **Merapi volcano** in Indonesia (and particularly for the 2006 and 2010 eruptions; Borisova et al. 2013; Carr et al. 2018), but also for **Mt. Vesuvius** (Jolis et al. 2013; Blyth et al. 2015), and **Mt. Etna** in Italy (Chiodini et al. 2011).

The contribution of assimilation of volatile-rich sedimentary rocks in the formation of magmatic ores is relatively well studied, although the actual processes operating are still largely debated (e.g. Thériault & Barnes 1998; Ripley and Li 2003; Naldrett 2004; Ganino et al. 2008; Samalens et al. 2017; Iacono-Marziano 2017; Yudovskaya et al. 2018). The three effects of assimilation that appear to be crucial for ore processes are: (1) the release of abundant fluids, (2) the modification of the redox conditions of the magma induced by the fluids, and (3) the input of external elements to the magma (mainly sulfur). The first and the second processes together seem to be at the origin of several types of ores, above all skarn deposits that are generally associated with carbonate rocks (Meinert et al. 2005). Moreover, the magnetite deposits of the Middle and Lower Yangtze metallogenic belt and the Tunguska Basin pipes seem to be related with strongly oxidizing, high salinity brines deriving from magma-evaporite interactions (Mazurov et al. 2007; Svensen et al. 2009; Li et al. 2015; Neumann et al. 2017), while graphite mineralizations of the Borrowdale and Huelma deposits and probably of the Bushveld Complex are associated with reduced C-O-H-S fluids produced by the interaction with carbonaceous rocks (Ballhaus and Stumpfl 1985; Barrenechea et al. 1997, 2009; Luque et al. 1998, 2009; Ortega et al. 2009, 2010). The variations in the redox conditions of the magma are also instrumental to the formation of three types of magmatic deposits: (i) oxide deposits like those of the Panzhihua intrusion (Ganino et al. 2008; Tang et al. 2017) and the Lac Doré intrusions (Mathieu 2019); (ii) native iron deposits, described at Disko, Bühl, and in several intrusions in the Siberian Platform (e.g. Steenstrup 1884; Pedersen 1979a,b; Medenbach and ElGoresy 1982; Ulff-Møller 1985; Ryabov and Lapkovsky 2010; Iacono-Marziano et al. 2012a); (iii) magmatic sulfide deposits. For the latter type of deposits, the input of external sulfur is also recognized to be essential, like proposed for Duluth (Mainwaring & Naldrett 1977; Ripley 1981; Thériault & Barnes 1998; Thériault et al. 2000; Queffurus

& Barnes 2014; Samalens et al. 2017), Eagle (Ding et al. 2012), Voisey's Bay (Ripley et al. 2002), Hangshandong (Gao et al. 2013; Mao et al. 2017), and Noril'sk-Talnakh deposits (e.g Naldrett 2004; Arndt et al. 2005; Jugo and Lesher 2005; Li et al. 2009b; Ripley et al. 2010; Iacono-Marziano et al. 2014, 2017). For magmatic sulfide deposits in general, the interaction with carbonaceous rocks ensures magma reduction necessary to segregate large amounts of sulfide melt and external fluids that may play a role in its metal enrichment (sections 4.4 and 4.4.1).

In conclusion, the interaction with volatile-rich sedimentary rocks leads the magma to coexist with possibly important amounts of fluid phase and may engender the formation of either "volatile-assisted" magmatic deposits, or magmatic-hydrothermal deposits. My future projects will be devoted to explore this magmatic-hydrothermal transition.

6. Future projects

My current and future projects are geared towards the magmatic-hydrothermal transition, which is a relatively poorly explored field. Only recent insights were obtained into the speciation and transport of economic metals in low-density vapour and fluid phases typical of hydrothermal-magmatic deposits (Pokrovski et al. 2013), but very few are relevant for mafic magmas. Most of the studies are focussed on low-temperature fluids in equilibrium with felsic magmas, probably because mafic magmas are generally considered volatile-poor, or at least volatile-poorer than felsic ones. As discussed above, mafic magmas have however a higher capacity of assimilating host rocks and can therefore coexist with abundant fluid phases. These "sedimentary-doped" fluid phases significantly extend the compositional field and the redox conditions of purely magmatic fluids. For instance we saw above that the assimilation of evaporitic rocks can produce highly salinity oxydizing fluids coexisting with mafic magmas (Li et al. 2015; Iacono-Marziano et al. submitted). This kind of fluids are generally not expected to be produced by mafic magmas. Similarly, the interaction with carbonaceous rocks can release C-rich reduced fluids (e.g. Barrenechea et al. 1997; Ortega et al. 2010; Iacono-Marziano et al. 2017) that are normally unusual in magmatic contexts. I'm interested in the role of this "sedimentary-doped" fluid phase in transporting and/or concentrating metals and metalloids both in magmatic and hydrothermal contextes.

Following the PhD of Clément Ferraina on the partitioning of Ni, Cu, Co, and Pd between the sulfide liquid and the silicate melt, the ongoing project presented in section 4.4.1 is now exploring the effects of assimilation and degassing on this partitioning. Volatile degassing may indeed enrich the sulfide melt in metals due to sulfur exsolution to the fluid phase. We are trying to provide experimental constraints on this process by means of the interaction experiments presented in section 4.4.1 and additional decompression experiments simulating sulfur degassing and sulfide melt consumption. Trace element composition of the sulfide melt, sulfide melt/silicate melt partition coefficients, and $\delta^{34}S$ composition of the sulfide melt will be analysed in both undecompressed and decompressed samples to characterize the effect of sulfur degassing.

Depending on metal partitioning between sulfide melt, silicate melt and fluid phase, a part of the metals initially incorporated in the sulfide melt could be released into the fluid phase, especially if sulfide consumption by degassing is complete (Mungall et al. 2015). If reaching the atmosphere, this metal-enriched fluids may have important environmental consequences (Le Vaillant et al. 2017). Otherwise they can redistribute/transport the metals together wit the sulfur and possibly form hydrothermal sulfides. PGE-enriched hydrothermal sulfides are proposed to accompany magmatic

sulfides, to my knowledge only within the magmatic body or in its proximity (e.g. Ballhaus & Stumpfl 1985; Holwell et al. 2013; Sluzhenikin et al. in press).

The role of magmatic (including sedimentary-doped) fluids in the genesis of hydrothermal deposits is another main goal of my future projects. Fluid circulation associated with magmatic processes is indeed considered to be at the origin of large hydrothermal metalliferous systems (e.g. Hedenquist & Lowenstern 1994; Jensen & Barton 2000; Lang & Baker 2001; Harris et al. 2003). The exsolution of a fluid phase from a magma has been shown to be able to extract and concentrate metals to constitute a source of metalliferous fluids. Nevertheless, systematic studies on metal and metalloid mobility at magmatic conditions are rare and too frequently focussed on porphyric systems (Ulrich et al. 1999; Kamenetsky et al. 1999; Halter et al. 2002). Moreover, the few experimental data available on the partitioning of metals between silicate melts and fluid phases are all for felsic magma compositions (e.g. Candela & Holland 1984; Keppler and Wyllie 1991; Frank et al. 2002; Simon et al. 2005, 2007, 2009; Zajacz et al. 2011).

To partially fill the gap, I will supervise a PhD project funded by the Labex VOLTAIRE on metal and metalloid extraction from the magma during high temperature degassing. The main goal of this project is to evaluate if magma degassing can produce metal and metalloid-enriched fluids at the origin of certain hydrothermal mineralization, like Sb(-Hg-As-W-Au-Ag) deposits. Experiments at magmatic conditions will be employed to study the behaviour of Sb, Hg, As, W, Au, Ag, and possibly Zn, Mo, Pb, Bi, Cu, Se, Te and PGE. These elements are likely to be transported in the fluid phase of the magma and generally have an incompatible behaviour in the principal magmatic minerals. The proposed approach involves classical experiments in internally heated pressure vessels and *in-situ* experiments in a pressure vessel equipped with a sapphire window and coupled with a Raman probe (recently developed in the PLANEX platform at ISTO). The challenges of this project are therefore (i) the assessment of silicate melt-fluid phase partition coefficients for the selected metals and metalloids, and (ii) the study of volatile species-metal complexes in the fluid phase. The final target is the role of the major element composition (C-H-O-S-Cl) of the fluids in the partitioning of metals and metalloids between silicate melt and fluid phase.

This experimental study is integrated in the ERA-MIN2 project “AUREOLE” (*tArgeting eU cRitical mEtals (Sb, W) and predictibility of Sb-As-Hg envirOnmentaL issuEs*, coordinated by E. Gloaguen, BRGM-ISTO), which aims to improve the efficiency for Sb and W mining exploration in EU and assess the potential environmental risk at a large scale. In particular, the PhD project is conceived in the frame of WP1 of AUREOLE, devoted to develop new regional-scale fully-integrated metallogenical models for Sb ± W ore deposits in high potential areas illustrated by the Variscan massifs of Iberia and France. A spatial

and genetic link has been indeed recently proposed for the Central Armorican Belt between a 360 Ma old mafic event and numerous occurrences of Sb mineralisation (e.g. Pochon et al. 2016, 2018). Similarly, Sb and Hg mineralisations, including the Almaden world-class deposit (Higueras et al. 2013), are spatially associated with mafic events in the Central Iberian Zone (Gumiel & Arribas 1987). Besides spatial and temporal correspondences, metal sources and extraction processes are generally unknown in these two zones.

References:

Aarnes I., Svensen H., Connolly J.A.D., Podladchikov Y.Y., 2010. How contact metamorphism can trigger global climate changes: Modeling gas generation around igneous sills in sedimentary basins. Geochimica et Cosmochimica Acta, 74(24), 7179-7195.

Aarnes I., Svensen H., Polteau S., Planke S., 2011a. Contact metamorphism devolatilization of shales in the Karoo Basin, South Africa, and the effects of multiple sill intrusions. Chemical Geology 281, 181-194.

Aarnes I., Svensen H., Polteau S., Planke S., 2011b. The impact of host-rock composition on devolatilization of sedimentary rocks during contact metamorphism around mafic sheet intrusions. Geochemistry, Geophysics, Geosystems 12, Q10019, doi:10.1029/2011GC003636.

Aiuppa A., Fischer T.P., Plank T., Robidoux P., Di Napoli R. 2017. Along-arc, inter-arc and arc-to-arc variations in volcanic gas CO2/ST ratios reveal dual source of carbon in arc volcanism. Earth-Science Reviews 168, 24-47.

Arndt N.T., Czamanske G.K., Walker R.J., Chauvel C., Fedorenko V.A., 2003. Geochemistry and origin of the intrusive hosts of the Noril'sk–Talnakh Cu–Ni–PGE sulfide deposits. Economic Geology and the Bulletin of the Society of Economic Geologists 98, 495–515.

Arndt N.T., Lesher C.M., Czamanske G.K., 2005. Mantle derived magmas and magmatic Ni–Cu–PGE deposits. Economic Geology 100th Anniversary Volume, 5–24.

Auger E., Gasparini P., Virieux J., and Zollo A., 2001. Seismic evidence of an extended magmatic sill under Mt. Vesuvius. Science 294, 1510–1512, doi: 10.1126/science.1064893.

Ayuso R.A., De Vivo B., Rolandi G., Seal R.R., Paone A., 1998. Geochemical and isotopic (Nd–Pb–Sr–O) variations bearing on the genesis of volcanic rocks from Vesuvius, Italy. J. Volcanol. Geotherm. Res. 82, 53–78.

Bacon K. L., Belcher C. M., Haworth M., McElwain J. C., 2013. Increased atmospheric SO2 detected from changes in leaf physiognomy across the Triassic–Jurassic boundary interval of East Greenland. PloS ONE 8(4), e60614. doi:10.1371/journal.pone.0060614.

Baker C.K., Black P.M., 1980. Assimilation and metamorphism at a basalt-limestone contact, Tokatoka, New Zealand. Mineral Mag 43, 797–807.

Ballhaus, C.G., Stumpfl, E.F., 1985. Occurrence and petrological significance of graphite in the Upper Critical Zone, western Bushveld Complex, South Africa. Earth and Planetary Science Letters 74, 58-68.

Barberi F., Buonasorte G., Cioni R., Fiordelisi A., Foresi L., Iaccarino S., Laurenzi M. A., Sbrana A., Vernia L., Villa I.M., 1994. PlioPleistocene geological evolution of the geothermal area of Tuscany and Latium. Memorie Descrittive Carta Geologica d'Italia XLIX, 77–134.

Barnes S-J., Zientek M., Severson M.J., 1997. Ni, Cu, Au and platinum group element contents of sulfides associated with intraplate magmatism: A synthesis. Canadian Journal of Earth Science 34, 337-351.

Barnes S-J., Lightfoot P.C., 2005. Formation of magmatic nickel-sulfide ore deposits and processses affecting their copper and platinum-group element contents. In Hedenquist, J.W., Thompson, J.F.H., Goldfarb, R.J. and Richards, J.P. (eds.) Economic Geology 100th Anniversary Volume, 179-213.

Barnes S.-J., Ripley E.M., 2016. Highly siderophile and strongly chalcophile elements in magmatic ore deposits. Reviews in Mineralogy and Geochemistry 81, 725-774.

Barnes C.G., Prestvik T., Sundvoll B., Surratt D., 2005. Pervasive assimilation of carbonate and silicate rocks in the Hortavær igneous complex, North-Central Norway. Lithos 80, 179–199.

Barnes S. J., Robertson J. C., 2019. Time scales and length scales in magma flow pathways and the origin of magmatic Ni-Cu-PGE ore deposits. *Geoscience Frontiers* 10, 77-87.

Barnes S. J., Le Vaillant M., Godel B., Lesher C.M., 2019. Droplets and bubbles: solidification of sulphide-rich vapour-saturated orthocumulates in the Norilsk-Talnakh Ni-Cu-PGE ore-bearing intrusions. Journal of Petrology 60, 269-300.

Barrenechea J.F., Luque F.J., Rodas M., Pasteris J.D., 1997. Vein-type graphite mineralization in Jurassic volcanic rocks of the External Zone of the Betic Cordillera (southern Spain). Canadian Mineralogist 35, 1379-1390.

Barrenechea J.F., Luque F.J., Millward D., Ortega L., Beyssac O., Rodas M., 2009. Graphite morphologies from the Borrowdale deposit (NW England, UK): Raman and SIMS data. Contributions to Mineralogy and Petrology 158, 37-51.

Barton M.D., Johnson D.A., 1996. Evaporitic source model for igneous-related Fe oxide-(REE-Cu-Au-U) mineralization. Geology 24, 259-262.

Barton M.D., 2014. Iron oxide (-Cu-Au-REE-P-Ag-U-Co) systems. In: Scott, S.D. (Ed.), Geochemistry of Mineral Deposits. Treatise on Geochemistry, 2nd ed, 515-541.

Bazarkina E.F., Pokrovski G.S., Hazemann J-L., 2014. Structure, stability and geochemical role of palladium chloride complexes in hydrothermal fluids. Geochimica et Cosmochimica Acta 146, 107-131.

Bezard R., Davidson J.P., Turner S., Macpherson C.G., Lindsay J.M., Boyce A.J., 2014. Assimilation of sediments embedded in the oceanic arc crust: myth or reality? Earth and Planetary Science Letters 395, 51–60.

Black B.A., Elkins-Tanton L.T., Rowe M.C., Peate I.U., 2012. Magnitude and consequences of volatile release from the Siberian traps. Earth and Planetary Science Letters 317, 363-373.

Blažić L., Moreau J., 2016. Discovery of Lower Cretaceous hydrothermal vent complexes in a late rifting setting, southern North Sea: insight from 3D imaging. Journal of the Geological Society 174, 233-241.

Blythe L.S., Deegan F.M., Freda C., Jolis E.M., Masotta M., Misiti V., Taddeucci J., Troll V.R., 2015. CO2 bubble generation and migration during magma-carbonate interaction. Contribution to Mineralogy and Petrology 169, 42.

Bohrson W. A., Spera F. J., 2001. Energy-constrained open-system magmatic processes II: application of energy-constrained assimilation–fractional crystallisation (EC-AFC) model to magmatic systems. Journal of Petrology 42, 1019–1041.

Bohrson W. A., Spera F. J., 2003. Energy-constrained open system magmatic processes IV: geochemical, thermal and mass consequences of energy-constrained recharge, assimilation and fractional crystallisation (EC-RAFC). Geochemistry, Geophysics, Geosystems 4, doi: 10.1029/2002GC00316.

Bohrson W. A., Spera F. J., Ghiorso M.S., Brown G.A., Creamer J.B., Mayfield A., 2014. Thermodynamic model for energy-constrained open-system evolution of crustal magma bodies undergoing simultaneous recharge, assimilation and crystallisation : the Magma Chamber Simulator. Journal of Petrology 55, 1685-1717.

Borisova A. Y., Martel C., Gouy S., Pratomo I., Sumarti S., Toutain J.P., Bindeman I.N., de Parseval P., Metaxian J-P., Surono, 2013. Highly explosive 2010 Merapi eruption: evidence for shallow-level crustal assimilation and hybrid fluid. Journal of Volcanology and Geothermal Research 261, 193–208.

Bouvier A.S., Deloule E., Métrich N., 2010. Fluid inputs to magma sources of St. Vincent and Grenada (Lesser Antilles): new insights from trace elements in olivine-hosted melt inclusions. Journal of Petrology 51 (8), 1597–1615.

Byrnes A.P., Wyllie P.J., 1981. Subsolidus and melting relations for the join CaCO3-MgCO3 at 10 kbar. Geochimica et Cosmochimica Acta 45, 321-328.

Caliro S., Chiodini G., Avino R., Cardellini C., Frondini F., 2005. Volcanic degassing at Somma–Vesuvio (Italy) inferred by chemical and isotopic signatures of groundwater. Applied Geochemistry 20, 1060–1076.

Campbell I. H., Naldrett A. J., 1979. The influence of silicate: sulfide ratios on the geochemistry of magmatic sulfides. Economic Geology 74, 1503-1506.

Campbell I. H., Barnes S. J., 1984. A model for the geochemistry of the platinum-group elements in magmatic sulfide deposits. Canadian Mineralogist 22, 151–160.

Candela P.A., Holland H.D., 1984. The partitioning of copper and molybdenum between silicate melts and aqueous fluids. Geochimica et Cosmochimica Acta 1984, 373-380.

Carr B. B., Clarke A. B., Vitturi M. D., 2018. Earthquake induced variations in extrusion rate: A numerical modeling approach to the 2006 eruption of Merapi Volcano (Indonesia). Earth and Planetary Science Letters 482, 377–387.

Carter L.B., Dasgupta R., 2015. Hydrous basalt–limestone interaction at crustal conditions: implications for generation of ultracalcic melts and outflux of CO2 at volcanic arcs. Earth and Planetary Science Letters 427, 202–214.

Carter L.B., Dasgupta R., 2016. Effect of melt composition on crustal carbonate assimilation: implications for the transition from calcite consumption to skarnification and associated CO2 degassing. Geochem. Geophys. Geosyst. 17, 3893–3916.

Carter L.B., Dasgupta R., 2018. Decarbonation in the Ca-Mg-Fe carbonate system at mid-crustal pressure as a function of temperature and assimilation with arc magmas – Implications for long-term climate. Chemical Geology 492, 30-48.

Casquet C., Galindo C., Tornos F., Velasco F., Canales A., 2001. The Aguablanca Cu-Ni ore deposit (Extremadura, Spain), a case of synorogenic orthomagmatic mineralization : age and isotope composition of magmas (Sr, Nd) and ore (S). Ore Geology Reviews 18, 237-250.

Chadwick J.P., Troll V.R., Ginibre C., Morgan D., Gertisser R., Waight T.E., Davidson J.P., 2007. Carbonate assimilation at Merapi Volcano, Java, Indonesia: Insights from crystal isotope stratigraphy. Journal of Petrology 48, 1793–1812.

Chiarabba C., Amato A., Delaney P.T. 1997. Crustal structure, evolution and volcanic unrest of the Alban Hills, Central Italy. Bulletin of Volcanology 59, 161-170.

Chiaradia M., Banks D., Cliff R., Marschik R., Haller A., 2006. Origin of fluids in iron oxide-copper-gold deposits: constraints from $\delta^{37}Cl$, $^{87}Sr/^{86}Sr$ and Cl/Br. Mineralium Deposita 41, 565-573.

Chiodini G., Marini L., Russo M., 2001. Geochemical evidence for the existence of high-temperature hydrothermal brines at Vesuvio volcano, Italy. Geochim. Cosmochim. Acta. 65, 2129–2147.

Chiodini G., Frondini F., 2001. Carbon dioxide degassing from the Albani Hills volcanic region, Central Italy. Chem. Geol. 177, 67-83.

Chiodini G., Cardellini C., Amato A., Boschi E., Caliro S., Frondini F., Ventura G., 2004. Carbon dioxide Earth degassing and seismogenesis in central and southern Italy. Geophys. Res. Lett. 31.

Chiodini G., Caliro S., Aiuppa A., Avino R., Granieri D., Moretti R., Parello F., 2011. First 13C/12C isotopic characterisation of volcanic plume CO2. Bulletin of Volcanology 73, 531-542.

Cioni R., 2000. Volatile content and degassing processes in the AD 79 magma chamber at Vesuvius (Italy). Contrib. Mineral. Petrol. 140, 40–54.

Cioni R., Marianelli P., Santacroce R., 1998. Thermal and compositional evolution of the shallow magma chambers of Vesuvius: evidence from pyroxene phenocrysts and melt inclusions. J. Geophys. Res. 103, 18277–18294.

Civetta L., D'Antonio M., de Lorenzo S., Di Renzo V., Gasparini P., 2004. Thermal and geochemical constraints on the 'deep' magmatic structure of Mt. Vesuvius. J. Volcanol. Geotherm. Res. 133, 1–12.

Claypool G.E., Holser W.T., Kaplan I.R., Sakai H., Zak I., 1980. The age curves of sulfur and oxygen isotopes in marine sulphate and their mutual interpretation. Chemical Geology 28, 199-260.

Conte A.M., Dolfi D., Gaeta M., Misiti V., Mollo S., Perinelli C., 2009. Experimental constraints on evolution of leucite-basanite magma at 1 and 10−4GPa: implications for parental compositions of Roman high-potassium magmas. Eur. J. Mineral.21, 763–782.

Costa F., Andreastuti S., Bouvet de Maisonneuve C., Pallister J.S., 2013. Petrological insights into storage conditions, and magmatic processes that yielded the centennial 2010 Merapi explosive eruption. Journal of Volcanology and Geothermal Research 261, 209-235.

Coulson I.M., Westphal M., Anderson R.G., Kyser T.K., 2007. Concomitant skarn and syenitic magma evolution at the margins of the Zippa Mountain pluton. Mineral Petrol 90, 199–221.

Courtillot V., Renne P.R., 2003. On the ages of fl ood basalt events: Comptes Rendus Geoscience, 335, 113–140.

Czamanske G.K., Zen'ko K.E., Fedorenko V., Calk L.C. Budahn J.R., Bullock J.H.J., Fries T.L., King B.S., Siems D.F., 1995. Petrographic and geochemical characterization of ore-bearing intrusions of the Noril'sk Type, Siberia; with discussion of their origin. Resource Geology Special Issue 18, 1–48.

Dallai L., Freda C., Gaeta M., 2004. Oxygen isotope geochemistry of pyroclastic clinopyroxene monitors carbonate contributions to Roman-type ultrapotassic magmas. Contrib. Mineral. Petrol. 148, 247–263.

Dallai L., Boschi C., D'Oriano C., Cioni R., 2007. Oxygene isotope composition of mafic magmas at Vesuvius. Geoitalia2007. Epitome.02.0433:126.

Daly R.A., 1910. Origin of the alkaline rocks. Geol Soc Am Bull 21, 87–118.

Deegan F.M., Troll V.R., Freda C., Misiti V., Chadwick J.P., McLeod C.L., Davidson J.P., 2010. Magma-carbonate interaction processes and associated CO2 release at Merapi Volcano, Indonesia: insight from experimental petrology. Journal of Petrology 51, 1027-1051.

Del Moro A., Fulignati P., Marianelli P., Sbrana A., 2001. Magma contamination by direct wall rock interaction: constraints from xenoliths from the walls of a carbonate-hosted magma chamber (Vesuvius 1944 eruption). J. Volcanol. Geotherm. Res. 112, 15–24.

De Natale G., Troise C., Pingue F., Mastrolorenzo G., Pappalardo L., 2006. The Somma–Vesuvius volcano (Southern Italy): Structure, dynamics and hazard evaluation. Earth-Science Reviews 74, 73–111, doi: 10.1016/j.earscirev.2005.08.001.

Di Battistini G., Montanini A., Vernia L., Venturelli G., Tonarini S., 2001. Petrology of melilite-bearing rocks from the Montefiascone Volcanic complex (Roman Magmatic Province): new insights into the ultrapotassic volcanism of Central Italy. Lithos 59, 1–24.

Ding X., Ripley E.M., Shirey S.B., Li C., 2012. Os, Nd, O and S isotope constraints on country rock contamination in the conduit-related Eagle Cu-Ni-(PGE) deposit, Midcontinental Rift System, Upper Michigan. Geochimica et Cosmochimica Acta 89, 10-30.

Di Renzo V., Di Vito M.A., Arienzo I., Carandente A., Civetta L., D'antonio M., Giordano F., Orsi G., Tonarini S., 2007. Magmatic history of Somma–Vesuvius on the basis of new geochemical and isotopic data from a deep Borehole (Camaldoli della Torre). J. Petrol. 48, 753–784.

Driesner T., Heinrich C.A., 2007. The system H_2O-NaCl. Part I: correlation formulae for phase relations in temperature-pressure-composition space from 0 to 1000°C, 0 to 5000 bar, and 0 to 1 X_{NaCl}. Geochimica et Cosmochimica Acta 71, 4880-4901.

Duran C. J., Barnes S.-J., Pleše P., Kudrna Prašek M., Zientek M. L., Pagé P., 2017. Fractional crystallization-induced variations in sulfides from the Noril'sk-Talnakh mining district (polar Siberia, Russia). *Ore Geol. Rev.* 90, 326–351.

Eiler J.M., 2001. Oxygen isotope variation in basaltic lavas and upper mantle rocks. In: Valley JW, Cole DR (eds) Stable isotope geochemistry. Rev. Mineral. Geochem. 43, 319–364.

Elliott-Kingston C., Haworth M., McElwain J. C., 2014. Damage structures in leaf epidermis and cuticle as an indicator of elevated atmospheric sulphur dioxide in early Mesozoic floras. Review of Palaeobotany and Palynology 208, 25–42.

Federico M., Peccerillo A., Barbieri M., Wu T.W., 1994. Mineralogical and geochemical study of granular xenoliths from the Alban Hills volcano, Central Italy: bearing on evolutionary processes in potassic magma chambers. Contrib. Mineral. Petrol. 115, 384– 401.

Ferraina C., 2018. Partage des métaux entre liquid sulfuré et liquid silicate : experimentation, modélisation et applications aux gisements de sulfures magmatiques. PhD Université d'Orléans, 244 p.

Feuillet N., Nostro C., Chiarabba C., Cocco M., 2004. Coupling between earthquake swarms and volcanic unrest at the Alban Hills Volcano (central Italy) modeled through elastic stress transfer. J. Geophys. Res. 109, B02308. doi: 10.1029/2003JB002419.

Fowler S.J., Bohrson W.A., Spera F.J., 2004. Magmatic evolution of the Skye igneous centre, Western Scotland: modelling of assimilation, recharge and fractional crystallization. Journal of Petrology 45, 2481-2505.

Frank M.R., Candela P.A., Piccoli P.M., Glascock M.D., 2002. Gold solubility, speciation, and partitioning as a function of HCl in the brine-silicate melt-metallic gold system at 800°C and 100 MPa. Geochimica et Cosmochimica Acta 66, 3719-3732.

Freda C., Gaeta M., Misiti V., Mollo S., Dolfi D., Scarlato P., 2008. Magma–carbonate interaction: an experimental study on ultrapotassic rocks from Alban Hills (Central Italy). Lithos 101, 397–415.

Frezzotti M.L., De Astis G., Dallai L., Ghezzo C., 2007. Coexisting calcalkaline and ultrapotassic magmatism at Monti Ernici, Mid Latina Valley (Latium, central Italy). Eur. J. Mineral. 19, 479–497.

Frondini F., Chiodini G., Caliro S., Cardellini C., Granieri D., 2004. Diffuse CO2 soil degassing at Vesuvio, Italy. Bulletin of Volcanology 66, 642–651.

Fulignati P., Marianelli P., Santacroce R., Sbrana A., 2000. The skarn shell of the 1944 Vesuvius magma chamber: Genesis and P–T–X conditions from melt and fluid inclusion data. Eur. J. Mineral. 12, 1025–1039.

Fulignati P., Marianelli P., Métrich N., Santacroce R., Sbrana A., 2004. Towards a reconstruction of the magmatic feeding system of the 1944 eruption of Mt Vesuvius. J. Volcanol. Geotherm. Res. 133:13–22.

Gambardella B., Cardellini C. Chiodini G, Frondini F, Marini L., Ottonello G., Vetuschi Zuccolini M., 2004. Fluxes of deep CO2 in the volcanic areas of central-southern Italy. Journal of Volcanology and Geothermal Research 136, 31-52.

Ganino C., Arndt N.T., Zhou M-F., Gaillard F., Chauvel C., 2008. Interaction of magma with sedimentary wall rock and magnetite ore genesis in the Panzhihua mafic intrusion, SW China. Mineralium Deposita 43, 677-694.

Ganino C., Harris C., Arndt N.T., Prevec S.A., Howarth G.H., 2013a. Assimilation of carbonate country rock by the parent magma of the Panzhihua Fe-Ti-V deposit (SW China): evidence from stable isotopes. Geosciences Frontiers 4, 547-554.

Ganino C., Arndt N.T., Chauvel C., Jean A., Arthurion C., 2013b. Melting of carbonate wall rocks and formation of the heterogeneous aureole of the Panzhihua intrusion, China. Geosciences Frontiers 4, 535-546.

Ganino C., Arndt N.T., Chauvel C., Tornos F., 2014. Metamorphic degassing of carbonates in the contact aureole of the Aguablanca Cu-Ni-PGE deposit, Spain. Contribution to Mineralogy and Petrology 168, 1053.

Gao J-F., Zhou M-F., Lightfoot P.C., Wang C.Y., Qi L., Sun M., 2013. Sulfide saturation and magma emplacement in the formation of the Permian Huangshandong NI-Cu sulphide deposit, Xinjiang, Northwestern China. Economic Geology 108, 1833-1848.

Gilg H.A., Lima A., Somma R., Ayuso R.A., Belkin H.E., De Vivo B., 2001. Isotope geochemistry and fluid inclusion study of skarns from Vesuvius. Mineral. Petrol. 73, 145–176.

Goff F., Janik C.J., Delgado H., Werner C., Counce D., Stimac J.A., Siebe C., Love S.P., Williams S.N., Fischer T., Johnson L., 1998. Geochemical surveillance of magmatic volatiles at Popocatepetl Volcano, Mexico. Geol. Soc. Am. ´ Bull. 110, 695–710.

Goff F., Love S.P., Warren R.G., Counce D., Obenholzner J., Siebe C., Schmidt S.C., 2001. Passive infrared remote sensing evidence for large, intermittent CO2 emissions at Popocatepetl volcano, Mexico. Chemical Geology 177, 133–156.

Grasby E.E., Hamed S., Beauchamp B., 2011. Catastrophic dispersion of coal fly ash into oceans during the latest Permian extinction. Nature Geoscience 4, 104-107.

Gresham J.J., Loftus-Hills G.D., 1981, The geology of the Kambalda nickel field, Western Australia: Economic Geology, v. 76, p. 1373–1416.

Grinenko L.N., 1985. Sources of sulfur of the nickeliferous and barren gabbro-dolerite intrusions of the northwest Siberian platform. International Geology Review 28, 695–708.

Gumiel P., Arribas A., 1987. Antimony deposits in the Iberian Peninsula. Economic Geology 82, 1453–1463.

Halter W.E., Pettke T., Heinrich A., 2002. The origin of Cu/Au ratios in porphyry-type ore deposits. Science 296, 1844-1846.

Harris, A.C., Kamenetsky, V.S., White, N.C., van Achterbergh, Ryan, C.G., 2003. Melt inclusions in veins: linking magmas and porphyry Cu deposits. Science 302, 2109–2111.

Harris A., Steffke A., Calvari S., Spampinato L., 2011. Thirty years of satellite-derived lava discharge rates at Etna: Implications for steady volumetric output. J. Geophys. Res., 116, B08204, doi:10.1029/2011JB008237.

Hedenquist, J.W., Lowenstern, J.B., 1994. The role of magmas in the formation of hydrothermal ore deposits. Nature 370, 519–527.

Heimdal T.H., Svensen H.H., Ramezani J., Iyer K., Pereira E., Rodrigues R., Jones M.T., Callegaro S., 2018. Large-scale sill emplacement in Brazil as a trigger for the end-Triassic crisis. Scientific Reports 8, DOI:10.1038/s41598-017-18629-8.

Heimdal T.H., Callegaro S., Svensen H.H., Jones M.T., Pereira E., Planke S., 2019. Evidence for magma-evaporite interactions during the emplacement of the Central Atlantic Magmatic Province (CAMP) in Brazil. Earth and Planetary Science Letters 506, 476-492.

Higueras P., Oyarzun R., Lillo J., Morata D., 2013. Intraplate mafic magmatism, degasification, and deposition of mercury: the giant Almadén mercury deposit (Spain) revisited. Ore Geology Reviews 51, 93-102.

Hoefs J., 1987. Stable isotope geochemistry. Springer, Berlin.

Holwell D.A., Jones A., Smith JW, Boyce A.J., 2013. New mineralogical and isotopic constraints on Main Zone-hosted PGE mineralisation at Moorddrift, northern Bushveld Complex. Mineralium Deposita 48, 675-686.

Holm P.M., Munskgaard N.C., 1982. Evidence for mantle metasomatism: an oxygen and strontium isotope study of the Vulsinian district, Central Italy. Earth Planet. Sci. Lett. 60, 376–388.

Holness M.B., 1997. Geochemical self-organization of olivine-grade contact metamorphosed chert nodules in dolomite marble, Kilchrist, Skye. J. Metamorph. Geol. 15, 765–775.

Holness M.B., 2000. Metasomatism and self-organization of dolerite dyke-marble contacts: Beinn an Dubhaich, Skye. J. Metamorph. Geol. 18, 103-118.

Huppert, H.E., Sparks, R.S.J., Turner, J.S., Arndt, N.T., 1984. Emplacement and cooling of komatiite lavas. Nature 309, 19–22.

Hutton D.H.W., 2009. Insights into magmatism in volcanic margins: bridge structures and a new mechanism of basic sill emplacement – Theron Mountains, Antarctica. Petroleum Geoscience 15, 269-278.

Iacono Marziano G., Gaillard F., Pichavant M., 2007. Limestone assimilation and the origin of CO_2 emissions at the Alban Hills (Central Italy): constraints from experimental petrology. J. Volcanol. Geotherm. Res. 166, 91–105.

Iacono-Marziano, G., Gaillard F., Pichavant M., 2008. Limestone assimilation by basaltic magmas: an experimental re-assessment and application to Italian volcanoes. Contributions to Mineralogy and Petrology 155, 719-738.

Iacono-Marziano G., Gaillard F., Scaillet B., Pichavant M., Chiodini G., 2009. Role of non-mantle CO_2 in the dynamics of volcano degassing: the Mount Vesuvius example. Geology 37, 319-322.

Iacono-Marziano G., Gaillard F., Scaillet B., Polozov A.G., Marecal V., Pirre M., Arndt N., 2012 a. Extremely reducing conditions reached during basaltic intrusion in organic matter-bearing sediments. Earth and Planetary Science Letters 357-358, 319-326.

Iacono-Marziano G., Marecal V., Pirre M., Gaillard F., Scaillet B., Arndt N.T., 2012 b. Gas emissions due to magma-sediment interactions during flood magmatism at the Siberian Traps: gas dispersion and environmental consequences. Earth and Planetary Science Letters 357, 308-318.

Iacono-Marziano G., Morizet Y., Le Trong E., Gaillard F., 2012 c. New experimental data and semi-empirical parametrization of H_2O-CO_2 solubility in mafic melts. Geochimica et Cosmochimica Acta 97, 1-23.

Iacono-Marziano G., Gaillard F., Arndt N.T., 2014. The effect of magma-sediment interactions on the redox state and volatile content of the magma and their implications for ore genesis. 12th International Platinum Symposium Abstract Volume, 32-33.

Iacono-Marziano G., Ferraina C., Gaillard F., Di Carlo I., Arndt N.T., 2017. Assimilation of sulfate and carbonaceous rocks: Experimental study, thermodynamic modeling and application to the Noril'sk-Talnakh region (Russia). Ore Geology Reviews 90, 399-413.

Iacono-Marziano G., Ferraina C., Gaillard F., Di Carlo I., Le Vaillant M., Barnes S.J., Arbaret A., Ryan C.G., Thieme J., Williams G.J., Arndt N.T. Mechanisms of assimilation of evaporitic and carbonaceous rocks by mafic magmas deduced from experiments at magmatic conditions. Submitted to Lithos.

Jensen E.P., Barton M.D., 2000. Gold deposits related to alkaline magmatism, in: Hagemann, S.G., Brown, P.E. (Eds.), Gold in 2000. Society of Economic Geology, Inc, Boulder, 279-314.

Jerram D.A., Svensen H.H., Planke S., Polozov A.G., Torsvik T.H., 2016. The onset of flood volcanism in the north-western part of the Siberian Traps: explosive volcanism versus effusive lava flows. Paleogeography, Paleoclimatology, Paleoecology 441, 38-50.

Joesten R., 1977. Mineralogical and chemical evolution of contaminated igneous rocks at a gabbro-limestone contact, Christmas Mountains, Big Bend region, Texas. Geol. Soc. Am. Bull. 88, 1515-1529.

Jolis E.M., Freda C., Troll V.R., Deegan F.M., Blythe L.S., McLeod C.L., Davidson J.P. 2013. Experimental simulation of magma-carbonate interaction beneath Mt.Vesuvius, Italy. Contributions to Mineralogy and Petrology 166, 1335-1353.

Jolis E.M., Troll V.R., Harris C., Freda C., Gaeta M., Orsi G., Siebe C. 2015. Skarn xenolith record crustal CO2 liberation during Pompeii and Pollena eruptions, Vesuvius volcanic system, central Italy. Chemical Geology 415, 17-36.

Joron J.l., Metrich N., Rosi M., Santacroce R., Sbrana A., 1987. Chemistry and petrography. In: Santacroce R (ed) Somma– Vesuvius. Quaderni de la ricerca scientifica, CNR Roma 8, 105–171.

Jugo P.J., Lesher C.M., 2005. Redox changes caused by evaporite and carbon assimilation at Noril'sk and their role in sulfide precipitation. Geological Society of America Abstracts with Programs 39, 360.

Jugo P.J., 2007. Redox changes caused by evaporite and carbon assimilation at Noril'sk and their role in sulfide precipitation. GSA Denver Annual Meeting.

Jugo P.J., 2014. Refinement of the model for sulfur content at sulfide saturation (SCSS) in basalts as function of oxygen fugacity (fO_2). 12th International Platinum Symposium Abstract Volume, 105-106.

Jugo P. J., Luth R. W., Richards J. P., 2005. An experimental study of the sulfur content in basaltic melts saturated with immiscible sulfide or sulfate liquids at 1300°C and 1.0 GPa. Journal of Petrology 46, 783–798.

Jugo P.J., 2009. Sulfur content at sulfide saturation in oxidized magmas. Geology 37, 415-418.

Kamenetsky V., Wolfe R.C, Eggins S.M., Mernagh T.P., Bastrakov E., 1999. Volatile exsolution at the Dinkidi Cu-Au porphyry deposit, Philippines: a melt-inclusion record of the initial ore-forming process. Geology 27, 691-694.

Keays E.R., Lightfoot P.C., 2010. Crustal sulfur is required to form magmatic Ni-Cu sulfide deposits: evidence from chalcophile element signatures of Siberan and Deccan Trap basalts. Mineralium Deposita 45, 241-257.

Keppler, H., Wyllie, J.W., 1991. Partitioning of Cu, Sn, Mo, W, U and Th between melt and aqueous fluid in the systems haplogranite–H2O–HCl and haplogranite–H2O–HF. Contrib. Mineralog. Petrol. 109, 139–150.

Kerr R. C., 1994. Dissolving driven by vigorous compositional convection. Journal of Fluid Mechanics 280, 287-302.

Kerrick D.M., 2001. Present and past nonantrhropogenic CO2 degassing from the solid Earth. Reviews of Geophysics 34, 565-585.

Kogiso T., Hirschmann M.M., 2001. Experimental study of clinopyroxenite par-tial melting and the origin of ultra-calcic melt inclusions. Contrib. Mineral. Petrol.142, 347–360.

Labidi J., Cartigny P., Birck J.L., Assayag N., Bourrand J.J., 2012. Determination of multiple sulfur isotopes in glasses: a reappraisal of the MORB $\delta^{34}S$. Chemical Geology 334, 189-198.

Lang J.R., Baker T., 2001. Intrusion-related gold systems: the present level of understanding. Mineralium Deposita 36, 477-489.

Larsen L.M., Pedersen A.K., 2009. Petrology of Paleocene picrites and flood basalts on Disko and Nuussuaq, West Greenland. Journal of Petrology 9, 1667-1711.

Lehmann J., Arndt N., Windley B., Zhou M-F., Wang C., Harris C., 2007. Field relationships and geochemical constraints on the emplacement of the Jinchuan intrusion and its Ni-Cu-PGE sulphide deposit, Gansu, China. Economic Geology 102, 75-94.

Lentz D.R, 1999. Carbonatite genesis: a re-examination of the role of intrusion-related pneumatolytic skarn processes in limestone melting. Geology 27, 335-338.

Lesher C.M., 2017. Roles of xenomelts, xenoliths, xenocrysts, xenovolatiles, residues, and skarns in the genesis, transport, and localization of magmatic Fe-Ni-Cu-PGE sulfides and chromite. Ore Geology Reviews 90, 465-484.

Le Vaillant M., Barnes S.J., Mungall J.E., Mungall E.L., 2017. Role of degassing of the Noril'sk nickel deposits in the Permian-Triassic mass extinction event. Proceedings of the National Academy of Sciences of the United States of America 114, 2485-2490.

Li C., Ripley E.M., Naldrett A.J., 2003. Compositional variations of olivine and sulfur isotopes in the Noril'sk and Talnakh intrusions, Siberia: Implications for ore-forming processes in dynamic magma conduits. Economic Geology 98, 69–86.

Li C., Ripley E.M., Naldrett A.J., Schmitt A.K., Moore C.H., 2009a. Magmatic anhydrite-sulfide assemblages in the plumbing system of the Siberian traps. Geology 37, 259-262.

Li C., Ripley E.M., Naldrett A.J., 2009b. A new genetic model for the giant Ni–Cu–PGE sulfide deposits associated with the Siberian flood basalts. Economic Geology and the Bulletin of the Society of Economic Geologists 104, 291–301.

Li W., Audétat A., Zhang J., 2015. The role of evaporites in the formation of magnetite-apatite deposits along the Middle and Lower Yangtze River, China: Evidence from LA-ICP-MS analysis of fluid inclusions. Ore Geology Reviews 67, 264-278.

Lickhachev A.P., 1994. Ore-bearing intrusions of the Noril'sk region. In: Lightfoot, P.C., Nadrett, A.J. (Eds.). Proceedings of the Sudbury-Noril'sk Symposium, Ontario Geological Survey special publication issue 5. Ontario Geological Survey, Greater Sudbury, 185-201.

Liotta M., Rizzo A., Paonita A., Caracausi A., Martelli M., 2012. Sulfur isotopic composition of fumarolic and plume gases at Mount Etna (Italy) and inferences on their magmatic source. Geochemistry Geophysics Geosystems 13 (5), Q05015, doi:10.1029/2012GC004118.

Luque F.J., Pasteris J.D., Wopenka B., Rodas M., Barrenechea J.F., 1998. Natural fluid-deposited graphite: mineralogical characteristics and mechanisms of formation. American Journal of Science, 298, 471-498.

Luque F.J., Ortega L., Barrenechea J.F., Huizenga J.-M., Millward D., 2012. Key factors controlling massive graphite deposition in volcanic settings: an exemple of a Self-Organized Critical System. Journal of the Geological Society 169, 269-277.

Maier W.D., de Klerk L., Blaine J., Manyeruke T., Barnes S.-J., Stevens M.V.A., Mavrogenes J.A., 2008. Petrogenesis of contact-style PGE mineralisation in the northern lobe of the Bushveld Complex: comparison of data from the farms Rooipoort, Townlands, Drenthe and Nonnenwerth. Mineralium Deposita, 43, 255–280.

Maier W.D., Barnes S-J., Sarkar A., Ripley E., Li C., Livesey T., 2010. The Kabanga Ni sulfide deposit, Tanzania: I. Geology, petrography, silicate rock geochemistry, and sulfur and oxygen isotopes. Mineralium Deposita 45, 419-441.

Maier W.D., Barnes S-J., 2010. The Kabanga Ni sulfide deposit, Tanzania: II. Chalcophile and siderophile element geochemistry. Mineralium Deposita 45, 443-460.

Mainwaring P.R., Naldrett A.J., 1977. Country rock assimilation and genesis of Cu-Ni sulfides in the Water Hen intrusion, Duluth Complex, Minnesota. Economic Geology 72, 1269–1284.

Malich N.S., Tazihin N.N., Tuganova E.V., Bunzen E.A., Kulikova N.G., Safonova Ivapoa, V.B., Baskov E.A., Galabala P.O., Gavrikov S.I., Golovanova M.P., Gogina N.I., Gorshkova N.I., Grozdilov A.L., Gromova A.I., Egorov L.S., Ivanova A.M., Isaeva L.L., Kljuchanskyi N.G., Kolobova N.I., Kutejnikov E.S., Leonov B.N., Ledneva V.P., Mironjuk E.P., Mihajlov M.V., Mishnin V.M., Stavtsev A.L., Stulov A.T., Shahotko L.I., Schtein L.F., Tsekhomskyi A.M., Yanova E.N., 1974. Map of geological formations of the Siberian platform cover (1:1 500 000). In: Malich, N.S. (Ed.), All-Union Research Geologic Institute (VSEGEI), Leningrad.

Malitch K.N., Latypov R.M., Badanina I.Yu., Sluzhenikin S.F., 2014. Insights into ore genesis of Ni-Cu-PGE sulfide deposits of the Noril'sk Province (Russia): evidence from copper and sulfur isotopes. Lithos 204, 172-187.

Mao Y-J., Qin K-Z., Barnes S.J., Ferraina C., Iacono-Marziano G., Verrall, M., Tang D., Xue S., 2017. A revised oxygen barometry in sulphide-saturated magmas and application to the Permian magmatic Ni-Cu deposits in the southern Central Asian Orogenic Belt. Mineralium Deposita https://doi.org/10.1007/s00126-017-0771-3.

Marianelli P., Metrich N., Santacroce R., Sbrana A., 1995. Mafic magma batches at Vesuvius: a glass inclusion approach to the modalities of feeding potassic strato-volcanoes. Contrib. Mineral. Petrol. 120, 159–169.

Marianelli P., Sbrana A., Metrich N., Cecchetti A., 2005. The deep feeding system of Vesuvius involved in recent violent strombolian eruptions. Geophys. Res. Lett. 32 doi: 10.1029/2004GL021667.

Mason E., Edmonds M., Turchyn A.V. 2017. Remobilization of crustal carbon may dominate volcanic arc emissions. Science 357, 290-294.

Mathieu L. 2019. Origin of the vanadiferous serpentine-magnetite rocks of the Mt. Sorcerer area, Lac DOré layered intrusion, Chibougamau, Quebec. Geosciences 9, 110; doi:10.3390/geosciences9030110.

Mazurov M.P., Grishina S.N., Istomin V.E., Titov A.T., 2007. Metasomatism and ore formation at contacts of dolerite with saliferous rocks in the sedimentary cover of the southern Siberian platform. Geol. Ore Depos. 49, 271-284.

Mazzotti A., Stucchi E., Fradelizi G.L., Zanzi L., Scandone P., 2000. Seismic exploration in complex terrains: a processing experience in the Southern Apennines. Geophysics 65, 1402–1417.

McElwain J., Wade-Murphy J., Hesselbo S.P., 2005. Changes in carbon dioxide during an oceanic anoxic event linked to intrusion into Gondwana coals. Nature 435, 479-482.

Medenbach O., El Goresy A., 1982. Ulvöspinel in native iron-bearing assemblages and the origin of these assemblages in basalts from Ovifak, Greenland, and Bühl, Federal Republic of Germany. Contribution to Mineralogy and Petrology 80, 358-366.

Meinert L.D., Dipple G.M., Nicolescu S., 2005. World skarn deposits. Economic Geology 100th Anniversary Volume, 299-366.

Métrich N., Mandeville C. W., 2010. Sulfur in magmas, Elements, 6, 81-86.

Michaud V., 1995. Crustal xenoliths in recent hawaiites from Mount Etna, Italy: evidence for alkali exchanges during magma-wall rock interaction. Chemical Geology 122, 21–42.

Mitchell R.H., Kjarsgaard B.A., 2008. Experimental studies of the system Na2Ca(CO3)2-NaCl-KCl at 0.1 GPa: implications for the differentiation and low-temperature crystallization of natrocarbonatite. Canadian Mineralogist 46 (4), 971-980.

Mollo S., Gaeta M., Freda C., Di Rocco T., Misiti V., Scarlato P., 2010. Carbonate assimilation in magmas: a reappraisal based on experimental petrology. Lithos 114, 503-514.

Monteiro L.V., Xavier R.P., de Carvalho E.R., Hitzman M.W., Johnson C.A., de Souza Filho C.R., Torresi I., 2008. Spatial and temporal zoning of hydrothermal alteration and mineralization in the Sossego iron oxide-copper-gold deposit, Carajas Mineral Province, Brazil: paragenesis and stable isotope constraints. Mineralium Deposita 43, 129-159.

Mungall J.E., Su S., 2005. Interfacial tension between magmatic sulphide and silicate liquids: Constraints on kinetics of sulphide liquation and sulphide migration through silicate rocks. Earth Planet. Sci. Lett. 234, 135–149.

Mungall J.E., Brenan J.M., 2014. Partitioning of platinum-group elements and Au between sulphide liquid and basalt and the origins of mantle–crust fractionation of the chalcophile elements. Geochim. Cosmochim. Acta 125, 265–289.

Mungall J.E., Brenan J.M., Godel B., Barnes S.J., Gaillard F., 2015. Transport of S, Cu and Au in magmas by flotation of sulphide melt on vapour bubbles. Nature Geoscience, 8, 216-219.

Naldrett A.J., Lightfoot P.C., Fedorenko V., Doherty W., Gorbachev N.S., 1992. Geology and geochemistry of intrusions and flood basalts of the Noril'sk region, USSR, with implications for the origin of the Ni–Cu ores. Economic Geology 87, 975–1004.

Naldrett A.J., Fedorenko V.A., Lightfoot P.C., Kunilov V.I., Gorbachev N.S., Doherty W., Johan Z., 1996. Controls on the composition of Ni-Cu sulfide deposits as illustrated by those at Noril'sk, Siberia. Economic Geology 91, 751–773.

Naldrett A.J., 2004. Magmatic Sulfide Deposits: Geology, Geochemistry and Exploration. Springer, Heidelberg.

Nappi G., Renzulli A., Santi P., Gillot P.Y., 1995. Geological evolution and geochronology of the Vulsini Volcanic District (central Italy). Boll. Soc. Geol. It. 114, 599–613.

Naumov G.B., Ryzhenko B.N., Khodakovsky I.L., 1974. Handbook of thermodynamic data. Menlo Park, California, U.S. Geological Survey, 328 p.

Neri M., Acocella V., Behncke B., Maiolino V., Ursino A., Velardita R., 2005. Contrasting triggering mechanisms of the 2001 and 2002–2003 eruptions of Mount Etna (Italy). J. Volcanol. Geotherm. Res. 144, 235– 255.

Neumann E.-R., Svensen H.H., Polozov A.G., Hammer Ø., 2017. Formation of Si-Al-Mg-Ca-rich zoned magnetite in an end-Permian phreatomagmatic pipe in the Tunguska Basin, East Siberia. Mineralium Deposita 52, 1205-1222.

Nordenskjöld A. E., 1871. Redogörelse för en ekspedition till Grönland ar 1870. Öfversikt af kungliga Vetenskabeliga Akademiens Förhandlingar Stockholm 27(10), 923-1082.

Obenholzner J.H., Schroettner H., Golob P., Delgado H., 2003. Particles from the plume of Popocatépetl volcano, Mexico—The FESEM/EDS approach, in Oppenheimer, C., et al., eds., Volcanic degassing. Geological Society of London Special Publication 213, 123–148.

Ogden D.E., Sleep N.H., 2012. Explosive eruption of coal and basalt and the end-Permian mass extinction. PNAS 109, 59-62.

Ortega L., Luque F.J., Barrenechea J.F., Rodas M., Millward D., Beyssac O., 2009. Assimilation, hydrothermal alteration and graphite mineralization in the Borrowdale deposit (UK). In: Williams PJ et al., editors. Smart Science for Exploration and Mining, vol. 1, 257-259.

Ortega L., Millward D., Luque F.J., Barrenechea J.F., Beyssac O., Huizenga J-M., Rodas M., Clarke S.M. 2010. The graphite deposit at Borrowdale (UK): A catastrophic mineralizing event associated with Ordovician magmatism. Geochimica et Cosmochimica Acta, 74, 2429-2449.

Owens B.E., 2000. High-temperature contact metamorphism of calc-silicate xenoliths in the Kiglapait Intrusion, Labrador. Am. Miner. 85, 1595-1605.

Pang K.-N., Arndt N.T., Svensen H., Planke S., Polozov A., Polteau S., Iizuka Y., Chung S.-L., 2013. A petrologic, geochemical and Sr-Nd isotopic study on contact metamorphism and degassing of Devonian evaporites in the Norilsk aureoles, Siberia. Contribution to Mineralogy and Petrology 165, 683-704.

Peccerillo A., 1998. Relationships between ultrapotassic and carbonate-rich volcanic rocks in central Italy: petrogenetic and geodynamic implications. Lithos 43, 267–279.

Peccerillo A., 2005. Plio-quaternary volcanism in Italy. Springer, Berlin, pp 727.

Pedersen A.K., 1978. Non-stoichiometric magnesian spinels in shale xe- noliths from a native iron-bearing andesite at Asuk, Disko, central West Greenland. Contrib. Mineral. Petrol. 67, 331-340.

Pedersen A.K., 1979a. A shale buchite xenolith with Al–Armalcolite and native iron in a lava from Asuk, Disko, Central West Greenland. Contribution to Mineralogy and Petrology 69, 83–94.

Pedersen A.K. 1979b. Basaltic glass with high-temperature equilibrated immiscible sulphide bodies with native iron from Disko, central West Greenland. Contribution to Mineralogy and Petrology 69, 397– 407.

Pedersen A.K., 1981. Almalcolite-bearing Fe-Ti oxide assemblages in graphite-equilibrated salic volcanis rocks with native iron from Disko, central West Greenland. Contribution to Mineralogy and Petrology 77, 307-324.

Pedersen A.K., Rønsbo J.G., 1987. Oxygen deficient Ti oxides (natural magnéli phases) from mudstone xenoliths with native iron from Disko, central West Greenland. Contribution to Mineralogy and Petrology 96, 35-46.

Pedersen A.K., Larsen L.M., 2006. The Ilugissoq graphite andesite volcano, Nuussuaq, central West Greenland. Lithos 92, 1–19.

Pernet-Fisher J.F., Day J.M.D, Howarth G.H., Ryabov V.V., 2017. Atmospheric outgassing and native-iron formation during carbonaceous sediment-basalt melt interactions. Earth and Planetary Science Letters 460, 201-212.

Peters S.T.M., Alibabaie N., Pack A., McKibbin S.J., Raeisi D., Nayebi N., Torab F., Ireland T., Lehmann B., 2019. Triple oxygen isotope variations in magnetite from iron-oxide deposits, central Iran, record magmatic fluid interaction with evaporite and carbonate host rocks. Geology 48, 211-215.

Petrychenko O.Y., Peryt T.M., Chechel E.I., 2005. Early Cambrian seawater chemistry from fluid inclusions in halite from Siberian evaporites. Chem. Geol. 219, 149–161.

Pichavant M., Scaillet B., Pommier A., Iacono-Marziano G., Cioni R., 2014. Nature and evolution of primitive Vesuvius magmas: an experimental study. Journal of Petrology 55, 2281-2310.

Piochi M., Ayuso R.A., De Vivo B., Somma R., 2006. Crustal contamination and crystal entrapment during polybaric magma evolution at Mt. Somma–Vesuvius volcano, Italy: geochemical and Sr isotope evidence. Lithos 86, 303–329.

Pochon A., Gapais D., Gloaguen E., Gumiaux C., Branquet Y., Cagnard F., Martelet G., 2016. Antimony deposits in the Variscan Armorican belt, a link with mafic intrusives? Terra Nova 28, 138–145.

Pochon A., Gloaguen E., Branquet Y., Poujol M., Ruffet G., Boiron M.-C., Boulvais P., Gumiaux C., Cagnard F., Gouazou F., Gapais D., 2018. Variscan Sb-Au mineralization in Central Brittany (France): A new metallogenic model derived from the Le Semnon district. Ore Geology Reviews 97, 109–142.

Pokrovskii B.G., Sluzhenikin S.F., Krivolutskaya N.A., 2005. Interaction conditions of Noril'sk Trap Intrusions with their host rocks: isotopic (O, H, and C) evidence. Petrology 13, 49-72.

Pokrovski G.S., Borisova A.Y., Bychkov A.Y., 2013. Speciation and transport of metals and metalloids in geological vapors. Reviews in Mineralogy and Geochemistry 76, 165-218.

Pronost J., Harris C., Pin C., 2008. Relationship between footwall composition, crustal contamination, and fluid-rock interaction in the Platreef, Bushveld Complex, South Africa. Mineralium Deposita 43, 825-848.

Queffurus M., Barnes S-J., 2014. Selenium and sulfur concentrations in country rocks from the Duluth Complex, Minnesota, USA: implication for formation of the Cu-Ni-PGE sulfides. Economic Geology 109, 785-794.

Queffurus M., Barnes S-J., 2015. A review of sulfur to selenium ratios in magmatic nickel-copper and platinum-group element deposits. Ore Geology Reviews 69, 301-324.

Retallack G.J., Jahren A.H., 2008. Methane release from igneous intrusion of coal during Late Permian extinction events. The Journal of Geology 116, 1-20.

Rice J.M., 1977. Contact metamorphism of impure dolomitic limestone in the Boulder Aureole, Montana. Contribution to Mineralogy and Petrology 59, 237-259.

Ripley E.M., 1981. Sulfur isotopic studies of the Dunka Road Cu-Ni deposit, Duluth Complex, Minnesota. Economic Geology 76, 610–620.

Ripley E.M., Li C., Shin D., 2002. Paragneiss assimilation in the genesis of magmatic Ni-Cu-Co sulfide mineralization at Voisey's Bay, Labrador; $\delta^{34}S$, $\delta^{13}C$, and Se/S evidence: Economic Geology 97, 1307–1318.

Ripley E.M., Li C.S., 2003. Sulfur isotope exchange and metal enrichment in the formation of magmatic Cu–Ni–(PGE) deposits. Economic Geology and the Bulletin of the Society of Economic Geologists 98, 635–641.

Ripley E.M., Li C., Moore C.H., Schmitt A.K., 2010. Micro-scale S isotope studies of the Kharaelakh intrusion, Noril'sk region, Siberia: Constraints on the genesis of coexisting anhydrite and sulfide minerals. Geochimica et Cosmochimica Acta 74, 634–644.

Ripley E.M., Li C., 2013. Sulfide saturation in mafic magmas; is external sulfur required for magmatic Ni-Cu-(PGE) ore genesis? Economic Geology 108, 45-58.

Rittmann A. , 1933. Die geologisch bedingte evolution und differentiation des Soma–Vesuv magmas. Zeitsch fur Vulkanol 15.

Roberge J., Delgado-Granados H., Wallace P. J., 2009. Mafic magma recharge supplies high CO2 and SO2 gas fluxes from Popocatepetl volcano, Mexico. Geology, 37(2), 107–110.

Robertson J.C., Ripley E.M., Barnes S.J., Li C., 2015a. Sulfur liberation from country rocks and incorporation in mafic magmas. Economic Geology 110, 1111–1123.

Robertson J.C., Barnes S.J., Le Vaillant M., 2015b. Dynamics of magmatic sulphide droplets during transport in silicate melts and implications for magmatic sulphide ore formation. Journal of Petrology 56, 2445-2472.

Rosi M., Santacroce R., Sheridan M.F., 1987. Volcanic hazard. In Santacroce , R., ed., Somma-Vesuvius. Quaderni de la ricerca scientifi ca, CNR, Roma, 8, 197–220.

Ryabov V.V., Lapkovsky A.A., 2010. Native iron (-platinum) ores from the Siberian Platform trap intrusions. Australian Journal of Earth Sciences 57, 707–736.

Ryabov, V.V., Simonov, O.N., Snisar, S.G., Borovikov, A.A., 2018. The source of sulfur in sulfide deposits in the Siberian Platform traps (from isotope data). Russian Geology and Geophysics 59, 945-961.

Salem L.C., Edmonds M., Corsaro R.A., Maclennan J., 2019. Carbon dioxide in geochemically heterogeneous melt inclusions from Mount Etna, Italy. Geochemistry, Geophysics, Geosystems 20, 3150-3169.

Sakai H., Marais D., Ueda A., Moore J., 1984. Concentrations and isotope ratios of carbon, nitrogen and sulfur in ocean-floor basalts. Geochimica et Cosmochimica Acta 48 (12), 2433–2441.

Samalens N., Barnes S.-J., Sawyer E.J., 2017. The role of black shales as a source of sulfur and semimetals in magmatic nickel copper deposits: example from the Partridge River Intrusion, Duluth Complex, Minnesota, USA. Ore Geology Reviews 81, 173–187.

Sano Y., Marty B., 1995. Origin of carbon in fumarolic gas from island arcs. Chemical Geology 119, 265–274, doi: 10.1016/0009–2541(94) 00097-R.

Schiano P., Eiler J.M., Hutcheon I.D., Stolper E.M., 2000. Primitive CaO-rich, silica-undersaturated melts in island arcs: evidence for the involvement of clinopyroxene-rich lithologies in the petrogenesis of arc magmas. Geochem. Geophys. Geosyst.1, 1–33

Schofield N., Alsop I., Warren J., Underhill J.R, Lehné R., Beer W., Lukas V., 2014. Mobilizing salt: Magma-salt interactions. Geology 42, 599-602.

Shand S.J., 1945. The present status of Daly's hypothesis of the alkaline rocks. Am J Sci 23, 495–507.

Simon A.C., Frank M.R, Pettke T., Candela P.A., Piccoli P.M., Heinrich C.A., 2005. Gold partitioning in melt-vapor-brine systems. Geochimica et Cosmochimica Acta 69, 3321-3335.

Simon A.C., Pettke T., Candela P.A., Piccoli P.M., Heinrich C.A., 2007. The partitioning behavior of As and Au in S-free and S-bearing magmatic assemblages. Geochimica et Cosmochimica Acta 71, 1764-1782.

Simon A.C., Pettke T., Candela P.A., Piccoli P.M., 2009. The partitioning behavior of silver in a vapor-brine-rhyolite melt assemblage. Geochimica et Cosmochimica Acta 72, 1638-1659.

Sluzhenikin S.F., Yudovskaya M.A., Barnes S.J., Abramova V.D., Le Vaillant M., Petrenko D.B., Grigor'eva A. V., Brovchenko V.D., in press. Low-sulfide PGE ores of the Noril'sk-Talnakh ore cluster. Economic Geology.

Sobolev A.V., Krivolutskaya N.A., Kuzmin D.V., 2009. Petrology of the parental melts and mantle sources of Siberian tap magmatism. Petrology 17 (3), 253-286.

Solovova I.P., Ryabchikov I.D., Girnis A.V., Pedersen A., Hansteen T., 2002. Reduced magmatic fluids in basalt from the island of Disko, central West Greenland. Chemical Geology 183, 365-371.

Spera F. J., Bohrson W. A., 2001. Energy-constrained open-system magmatic processes I: general model and energy-constrained assimilation–fractional crystallisation (EC-AFC) formulation. Journal of Petrology 42, 999–1018.

Spera F. J., Bohrson W. A., 2002. Energy-constrained open-system magmatic processes III: energy-constrained recharge, assimilation, and fractional crystallisation (EC-RAFC). Geochemistry, Geophysics, Geosystems 3, doi: 10.1029/2002GC00315.

Steenstrup K.J.V., 1884. On the Existence of Nickel-iron with Wid- mannstS.tten's Figures in the Basalt of North Greenland. Mineralogical Magazine 6 (27), 1- 13.

Stoppa F., Woolley A.R., 1997. The Italian carbonatites: field occurrence, petrology and regional significance. Mineral Petrol 59, 43–67.

Svensen H., Planke S., Malthe-Sørenssen A., Jamtveit B., Myklebust R., Eldem T.R., Rey S.S., 2004. Release of methane from a volcanic basin as a mechanism for initial Eocene global warming. Nature 429(6991), 542-545

Svensen, H. Planke S., Chevallier L., Malthe-Sørenssen A., Corfu F., Jamtveit B., 2007. Hydrothermal venting of greenhouse gases triggering Early Jurassic global warming. Earth and Planetary Science Letters 256, 554-566.

Svensen H., Planke S., Polozov A.G., Schmidbauer N., Corfu F., Podladchikov Y.Y., Jamtveit B., 2009. Siberian gas venting and the end-Permian environmental crisis. Earth and Planetary Science Letters 277, 490–500.

Svensen H., Fristad K.E., Polozov A.G., Planke S., 2015. Volatile generation and release from continental large igneous provinces. In A. Schmidt, K. Fristad, & L. Elkins-Tanton (Eds.), Volcanism and Global Environmental Change (pp 177-192). Cambridge University Press.

Tang Q., Li C., Tao Y., Ripley E.M., Xiong F., 2017. Association of Mg-rich olivine with magnetite as a result of brucite marble assimilation by basaltic magma in the Emeishan Large Igneous Province, SW China. Journal of Petrology 58, 699-714.

Taylor H.P., Turi B., Cundari A., 1984. 18-O/16-O and chemical relationships K-rich volcanic rocks from Australia, East Africa, Antarctica, and San Venanzo–Cupaello, Italy. Earth Planet. Sci. Lett. 69, 263–276.

Tedesco D., Nagao K., Scarsi P., 1998. Noble gas isotopic ratios from historical lavas and fumaroles at Mount Vesuvius (southern Italy): Constraints for current and future volcanic activity. Earth and Planetary Science Letters 164, 61–78, doi: 10.1016/S0012–821X(98)00167–8.

Thakurta J., Ripley E.M., Li C., 2008. Geochemical constraints on the origin of sulphide mineralization in the Duke Island Complex, southeastern Alaska. Geochemistry Geophysics Geosystems 9, doi: 10.1029/2008GC001982.

Thériault R.D., Barnes S.-J., 1998. Compositional variations in Cu-Ni-PGE sulfides of the Dunka Road deposit, Duluth Complex, Minnesota: the importance of combined assimilation and magmatic processes. Canadian Mineralogist 36, 869–886.

Thériault R.D., Barnes S.-J., Severson M.J., 2000. Origin of Cu-Ni-PGE sulfide mineralization in the Partridge River intrusion, Duluth Complex, Minnesota. Economic Geology 95, 929-943.

Tilley C.E., 1952. Some trends of basaltic magma in limestone syntexis. American Journal of Science 250A, 529-545.

Toplis M.J., Carroll M.R., 1995. An experimental study of the influence of oxygen fugacity on Fe–Ti oxide stability, phase relations, and mineral-melt equilibria in ferro-basaltic systems. J. Petrol. 36, 1137–1170.

Tracy R.J., 1991. Ba-rich micas from the Franklin Marble, Lime Crest and Sterling Hill, New Jersey. American Mineralogist 76, 1683-1693.

Troll V. R., Hilton D.R., Jolis E.M., Harris C., Chadwick J.P., Blythe L.S., Deegan F.M., Schwarzkopf L.M., Zimmer M., 2012. Crustal CO2 liberation during the 2006 eruption and earthquake events at Merapi volcano, Indonesia. Geophysical Research Letters 39, L11302, doi: 10.1029/2012GL051307.

Troll V. R., Deegan F.M., Jolis E.M., Harris C., Chadwick J.P., Gertisser R., Schwarzkopf L.M., Borisova A.Y., Bindeman I.N., Sumarti S., Preece K., 2013. Magmatic differentiation processes at Merapi Volcano: inclusion petrology and oxygen isotopes. J. Volcanol. Geotherm. Res. 261, 38–49.

Ulff-Møller F., 1985. Solidification history of the Kitdlidt lens: immiscible metal and sulphide liquids from a basaltic dyke on Disko, central West Greenland. Journal of Petrology 26, 64–91.

Ulrich, T., Gunther, D., Heinrich, C.A., 1999. Gold concentration of magmatic brines and the metal budget of porphyry copper deposits. Nature 399, 676–679.

van der Sluis M.L., 2010. Melting relations in the anhydrite-dolomite system. Unpublished Master thesis, Universiteit Utrecht. (http://igitur-archive. library.uu.nl/student-theses/2010-0828-200201/UUindex.html).

Wang K.Y., Pyle J.A., Shallcross D.E., Larry D.J., 2001. Formulation and evaluation of IMS, an interactive three-dimensional tropospheric chemical transport model, 2. Model chemistry and comparison of modeled CH4, CO and O3 with surface measurements. J. Atmos. Chem. 38, 31–71.

Watkinson D.H., Wyllie P.J., 1969. Phase equilibrium studies bearing on the limestone assimilation hypotheses. Geol. Soc. Am. Bull. 80, 1565–1576.

Wenzel T., Baumgartner L.P., Brügmann G.E., Konnikov E.G., Kislov E.V., Orsoev D.A., 2001. Contamination of mafic magma by partial melting of dolomitic xenoliths. Terra Nova 13, 197-202.

Wenzel T., Baumgartner L.P., Brügmann G.E., Konnikov E.G., Kislov E.V., Orsoev D.A., 2002. Partial melting and assimilation of dolomitic xenoliths by mafic magma: the Ioko-Dovyren intrusion (north Baikal region, Russia). J. Petrol. 43, 2049–2074.

Werner, C., and Brantley, S., 2003. CO2 emissions from the Yellowstone volcanic system. Geochemistry, Geophysics, Geosystems 4, 1061, doi: 10.1029/2002GC000473.

Williams T.J., Candela P.A., Piccoli P.M., 1995. The partitioning of copper between silicate melts and two-phase aqueous fluids: an experimental investigation at 1 kbar, 800°C and 0.5 kbar, 850°C. Contribution to Mineralogy and Petrology 121, 388-399.

Wyllie P.J., 1965. Melting relationships in the system CaO-MgO-CO2-H2O, with petrological applications. Journal of Petrology 6, 101-123.

Wyllie P.J., 1974. Limestone assimilation. In: Sorensen H (ed) The Alkaline Rocks, pp 459–473.

Xavier, R.P., Wiedenbeck, M., Trumbull, R.B., Dreher, A.M., Monteiro I.V., Rhede D., De Araujo, C.E., Torresi, I., 2008. Tourmaline B-isotopes fingerprint marine evaporites as the source of high-salinity ore fluids in iron oxide-copper-gold deposits, Carajas Mineral Province (Brazil). Geology 36, 743-746.

Yallup C., Edmonds M., Turchyn A.V., 2013. Sulfur degassing due to contact metamorphism during flood basalt eruptions. Geochimica et Cosmochimica Acta 120, 263-279.

Yudovskaya, M.A., Sluzhenikin, S.F., Costin G., Shatagin, K.N., Dubinina E.O., Grobler D.F., Ueckermann H., Kinnaird J., 2018. Anhydrite assimilation by ultramafic melts of the Bushveld Complex, and its consequence to petrology and mineralization. Society of Economic Geologists 21, 177-206.

Zajacz Z., Seo J.H., Candela P.A., Piccoli P.M., Tossell J.A., 2011. The solubility of copper in high-temperature magmatic vapors: a quest for the significance of various chloride and sulfide complexes. Geochimica et Cosmochimica Acta 75, 2811-2827.

Zharkov M.A., 1984. Paleozoic Salt Bearing Formations of the World. Springer-Verlag, Berlin, Heidelberg, New York & Tokyo.

Zen'ko T.E., Czamanske G.K., 1994. Tectonic controls on ore-bearing intrusions of the Talnakh ore junction: Position, morphology and ore distribution. International Geology Review 36, 1033–1057.

Zientek M. L., Likhachev A. P., Kunilov V. E., Barnes S.-J., Meier A. L., Carlson R. R., Briggs P. H., Fries T. L., Adrian B. M., 1994. Cumulus processes and the composition of magmatic ore deposits : examples from the Talnakh district, Russia. In *Proceedings of the Sudbury - Noril'sk Symposium Special volume 5* Ministry of Northern Development and Mines, Ontario. 373–392.